VIETNAM
JOURNAL OF HYDRO - METEOROLOGY

ISSN 2525 - 2208

VIETNAM METEOROLOGICAL AND HYDROLOGICAL ADMINISTRATION

No 05
08-2020

Publishing licence
No: 166/GP-BTTTT - Ministry of Information and Communication dated 17/04/2018

Editorial office
No 8 Phao Dai Lang, Dong Da, Ha Noi
TEL: 04.39364963; Fax: 04.39362711
Email: tapchikttv@yahoo.com or tapchikttv@gmail.com

Engraving and printing
Thien Ha Joint Stock Company
Tel: 04.3990.3769 - 0912.565.222

VIETNAM JOURNAL OF HYDROMETEOROLOGY
Volume 05 - 08/2020

TABLE OF CONTENT

VIETNAM JOURNAL OF HYDROMETEOROLOGY

Preface

The Japan International Cooperation Agency (JICA) Project for Strengthening Capacity in Weather Forecasting and Flood Early Warning System in the Social Republic of Vietnam is a 3.5 year bilateral technical cooperation project between Japan and Vietnam which started in May 2018. This project is related to S-band radars that were installed at Hai Phong (Phu Lien) and Vinh in September 2017 by another grant aid project of Japan. Scopes of the JICA project are divided into four output targets: 1) surface meteorological observation, 2) radar maintenance and products, 3) weather forecasting, and 4) regional weather dissemination. The Japanese JICA project team members and staff of the Viet Nam Meteorological and Hydrological Administration (VNMHA) collaborated in above output activities. The project term is divided into two periods, Period 1 (June 2018 to March 2020) and Period 2 (April 2020 to December 2021), and in March 2020, the 4th meeting of the Joint Coordination Committee (JCC) was held in Hanoi to summarize the achievements in Period 1 and discuss the prospect of the project in Period 2.

This special issue of the Vietnam Journal of Hydrometeorology (VNJHM) covers research articles based on achievement reports submitted in the 4th JCC meeting and two invited papers relating to the scientific scopes of the JICA activities. The first is a review paper by Tonouchi et al. on the JICA project, and details of achievements in the projects are described by Mikami et al. (output 1), Kimpara et al. (output 2), Sasaki et al. (output 3), and Saito et al. (output 3). Based on the results in output 3, the National Center for Hydro-Meteorological Forecasting (NCHMF) of VNMHA started operational use of GSMaP data in October 2019 (Hung et al.). These six papers are all coauthored by the Japanese JICA team members and counterpart members of VNMHA. Two invited papers are on the start date of active storm season (Huong and Chinh), and on application of remote sensing techniques for analyzing operation of reservoirs (Phuong et al.).

We appreciate efforts made by the JICA members from Japan and Vietnam, and thank the Headquarters of JICA, the Aero-Meteorological Observatory and NCHMF of VNMHA, the Japan Meteorological Business Support Center, and the Japan Weather Association for their continuous support. We believe that this volume contributes to review and demonstrate achievements of the JICA project in Period 1 and becomes a good reference for further progress of the project in Period 2 and future technical cooperation between Japan and Vietnam.

August 2020

Kazuo Saito, Editor of VNJHM,

Quang Dzung Bach, Chief Editor of VNJHM

VIETNAM JOURNAL OF HYDROMETEOROLOGY

Research Article

Activities of JICA on disaster prevention and achievement of JICA project in Period 1

Michihiko Tonouchi[1*], Yasuhiro Kasuya[2], Yasuhiro Tanaka[3], Kunio Akatsu[4], Kenji Akaeda[5], Nguyen Vinh Thu[6]

[1] Japan Meteorological Business Support Center, Tokyo, 101–0054, Japan; tono@jmbsc.or.jp
[2] Japan International Cooperation Agency, Hanoi, Vietnam; kasuya.yasuhiro@jica.go.jp
[3] Vietnam Disaster Management Authority, Hanoi, Vietnam; yasuhirotanaka102@gmail.com
[4] Japan International Cooperation Agency, Narashino, Japan; akatsuk@aqua.ocn.ne.jp
[5] Japan International Cooperation Agency, Viet Nam Meteorological and Hydrological Administration, Hanoi, Vietnam; akaeda191@yahoo.co.jp
[6] Aero–Meteorological Observatory, Viet Nam Meteorological and Hydrological Administration, Hanoi, Vietnam; nvthu@monre.gov.vn
***** Correspondence: tono@jmbsc.or.jp; Tel.: +81–3–5577–2181

Received: 12 July 2020; Accepted: 20 August 2020; Published: 25 August 2020

Abstract: The Japan International Cooperation Agency (JICA) has supported various natural disaster prevention activities in Vietnam in accordance with the "Sendai Framework for Disaster Risk Reduction 2015–2030". From 2007 to 2017, around 90 percent of the total damages in Vietnam were accounted by water–related natural disasters. JICA implemented several grants and technical cooperation programs for reducing water–related disaster risks, and as a part of these activities, the "Project for Strengthening Capacity in Weather Forecasting and Flood Early Warning System" by the Vietnam Meteorological and Hydrological Administration (VNMHA) and JICA started in May 2018 as a 3.5 year project. In the Period 1 (June 2018 to March 2019), Automatic Weather Station (AWS) inspection and maintenance manuals were prepared and through trainings at Phu Lien and Vinh radar sites, practical radar maintenance knowledges were shared. Fifteen Automatic Rain Gauges (ARGs) were newly installed in Phu Lien and Vinh radar areas and radar composition started to cover whole Vietnam. For weather forecasting, temperature guidance for 63 cities by the Kalman Filter was developed, and precipitation products based on satellites were evaluated. Discussion on improvement of short–range precipitation forecasting up to 15 hours ahead also started.

Keywords: JICA; Disaster risk reduction; International cooperation; Meteorological observation; Forecasting.

1. Activities of JICA on disaster prevention

The Japan International Cooperation Agency (JICA) has supported various natural disaster prevention activities in Vietnam. Every year natural disasters occur frequently in Vietnam, and more than 100 people of deaths and missing are recorded. In 2019, 133 people were dead or missing, and the damage by natural disasters cost 304 million USD [1]. Floods and landslides caused by heavy rains and storms dominate in Vietnam. According to the record of deaths, missing and damages by natural disasters from 2007–2017, around 90

percent of the total damages were accounted by water–related natural disasters such as storms, floods, flashfloods, or landslides [2]. Other natural disasters such as coastal erosion, drought, salt damage, etc. also occur and suffer the land. According to the Law on Natural Disaster Prevention and Control (No:33/2013/QH13), 19 types of disasters are prescribed in the article 3: typhoon, tropical depression, whirlwind, lightning, heavy rain, flood, flashflood, inundation, landslide and land subsidence due to floods or water currents, water rise, salt intrusion, heat wave, drought, damaging coldness, hail, hoarfrost, earthquake, tsunami and other types of natural disaster. Adding snow damage and forest fires, the Vietnamese government copes with 21 natural disasters [3].

Although 133 of deaths and missing in 2019 are the lowest since 2014 and the damage cost decreased by 67% compared to 2018, Vietnam has suffered from great disasters in its history. For example, Typhoon Linda, which hit the Mekong Delta in November 1997, capsized many fishery boats, and brought great damage to coastal villages. This typhoon caused more than 3,000 deaths and missing people.

In November 1999, due to heavy rain in the central region, 2,500mm of precipitation was recorded at Thua Thien Hue Province and caused severe flood widely in the central region. This caused 567 deaths and missing and 66,038 ha of paddy fields were flooded and damaged. In recent years, several typhoons hit Vietnam in 2017 and heavy rain caused flood and landslide in central and northern areas. The disaster damage cost in 2017 was counted as 2,641 million USD, which is the largest in 30 years.

In 2019, flashflood hit Thanh Hoa Province in August, and severe flood occurred in Phu Quoc Island in Kien Giang Province in August and Vinh City in Nghe An Province in October.

In order to strengthen the capacity to cope with natural disasters in Vietnam, JICA has supported various activities in accordance with the “Sendai Framework for Disaster Risk Reduction 2015–2030” and the “2030 Agenda for Sustainable Development (SDGs)”. Especially, JICA emphasizes the importance of efforts for Disaster Risk Reduction (DRR) and puts the highest priority on prevention and mitigation, and encourages “disaster risk reduction investment to improve resilience”. For the achievement of DRR, promoting for understanding of disaster risks, pre–investment for disaster prevention, Build Back Better (BBB) concept are also important as well as formulating DRR plan at local level. Therefore, JICA takes an approach to support formulating regional disaster prevention plan in local by the following eight steps:

Step1. Collecting local hazard information

Step2. Understanding local disaster risks

Step3. Confirming DRR plans by national and other authorities

Step4. Identifying residual risks considering time–series

Step5. Listing all necessary DRR measures by local governments

Step6. The One–Year–Old

Step7. Arranging budget allocation in necessary levels

Step8. Implementing DRR measures and reviewing periodically

The recent increase of natural disasters gives us some concern that climate change would affect more severely and harshly in Vietnam with heavier rainfall and more powerful typhoons. In addition, the rise of sea level would detain smooth river flow into the ocean and it can result in flooding in wider areas.

For these reasons, JICA understands it is necessary to support sustainable investment in disaster prevention as climate change adaptation. For example, JICA supported the Vietnam Disaster Management Authority (MARD) to develop “Priority Programs for Disaster Risk Reduction in Vietnam” in 2018. In the programs a goal was set as establishment of disaster resilient society aiming at socioeconomic development, and six priority programs were

identified to strengthen investment in DRR in Vietnam in accordance with Sendai Framework.

As for strengthening DRR management in river, a grant aid project, "Emergency Reservoir Operation and Flood Effective Management Using Water Disaster Related Management Information System", was signed between MARD and JICA in 2017. This project focuses on establishment of an X–band radar rainfall observation equipment, water level gauges, and gate opening meters for dam in the Huong River basin to install the real–time observation network. In addition, CCTV cameras are utilized to monitor visually the downstream of the Huong river. These observed data are integrated into the information system and utilized for optimizing the operation of dams and monitoring the condition of river flow during the time of flooding.

In addition, in response to the frequent occurrence of flashfloods and landslides in the northern part of Vietnam in recent years, JICA's basic surveys have been carrying out to understand the risk of flashflood and landslide and to find out appropriate countermeasures in these areas from December 2019. During the survey, the JICA survey team will conduct on–site surveys where flashflood and landslide disasters occurred in the past in Yen Bai and Son La provinces, and investigate current situation and issues to be solved.

2. National Meteorological and Hydrological Services and Disaster Risk Reduction

The World Meteorological Organization (WMO) assists National Meteorological and Hydrological Services (NHMS), especially those of developing and least developed countries, in their efforts to contribute in the most effective manner to the national development and to become full partners in global collaborative efforts, especially when it pertains to:

- ✓ Protection of life and property
- ✓ Safeguarding the environment
- ✓ Contributing to sustainable development
- ✓ Promoting long–term observation and collection of meteorological, hydrological and climatological data, including related environmental data

NMHS covers observation, forecast, data communication, forecast/warning dissemination and so on, and has to be responsible for various scientific and technical fields to provide reliable meteorological information to the public [4].

Almost every NMHS has approximately the same meteorological service operation system such as (1) observation of meteorological phenomena, (2) obtaining domestic and international meteorological information, (3) data analysis, (4) weather forecasting and (5) dissemination of meteorological information to related organization and the public.

However, the contents of an operation system in each field such as from meteorological observation to dissemination of meteorological information has some differences in detail among NMHSs. These differences depend on the context of each country including the capacity of staff members and infrastructures of NMHS, and these situation gives influences in the quality of the final products of each NMHS.

NMHS in many developing countries recognize that they have problems or issues to be solved for better quality in the field such as (1) to (5) mentioned above. However, in many cases, they have difficulties to take concrete countermeasures against these problems or issues due to many circumstances.

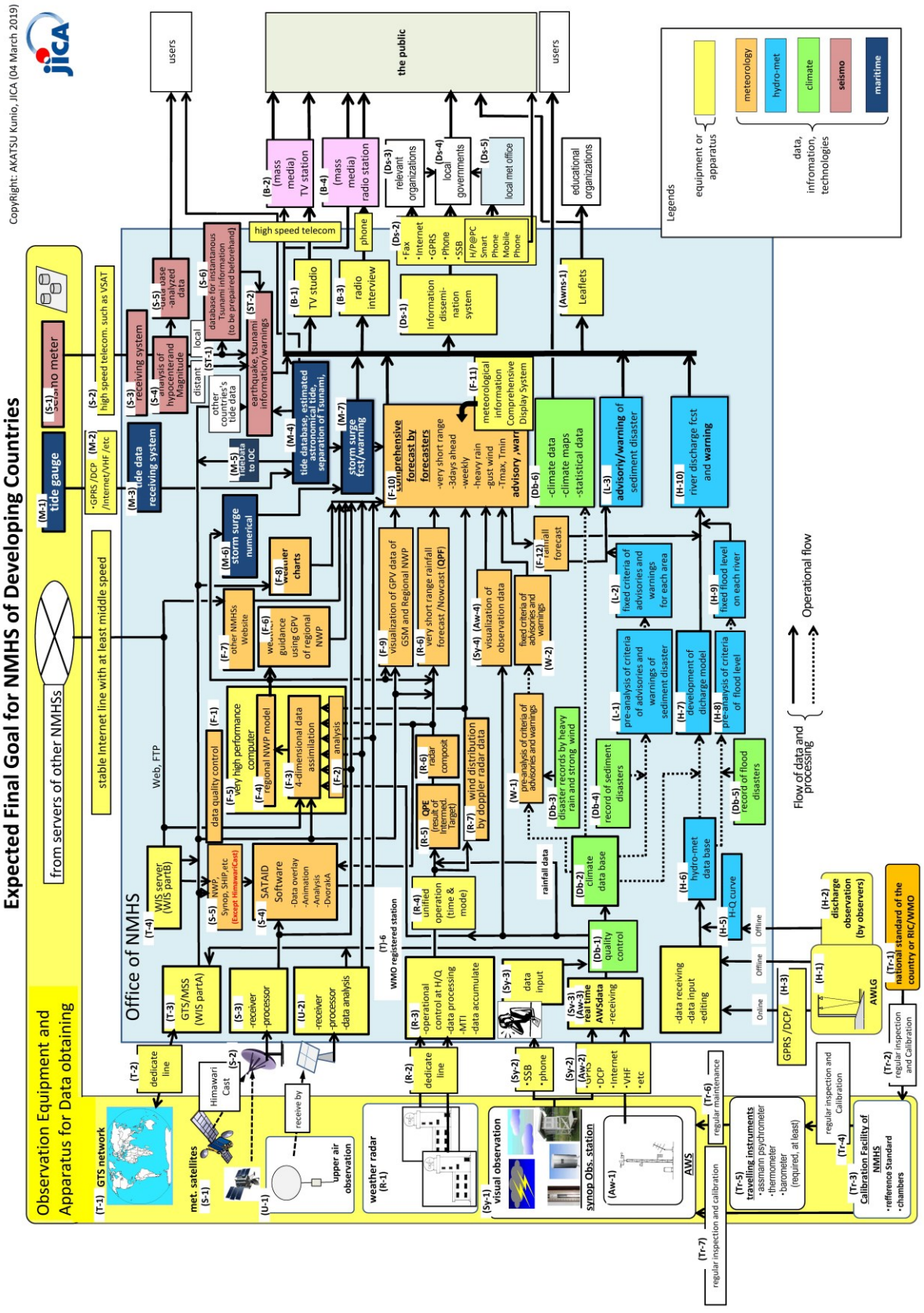

Figure 1. Expected Final Goal (AkatsuChart).

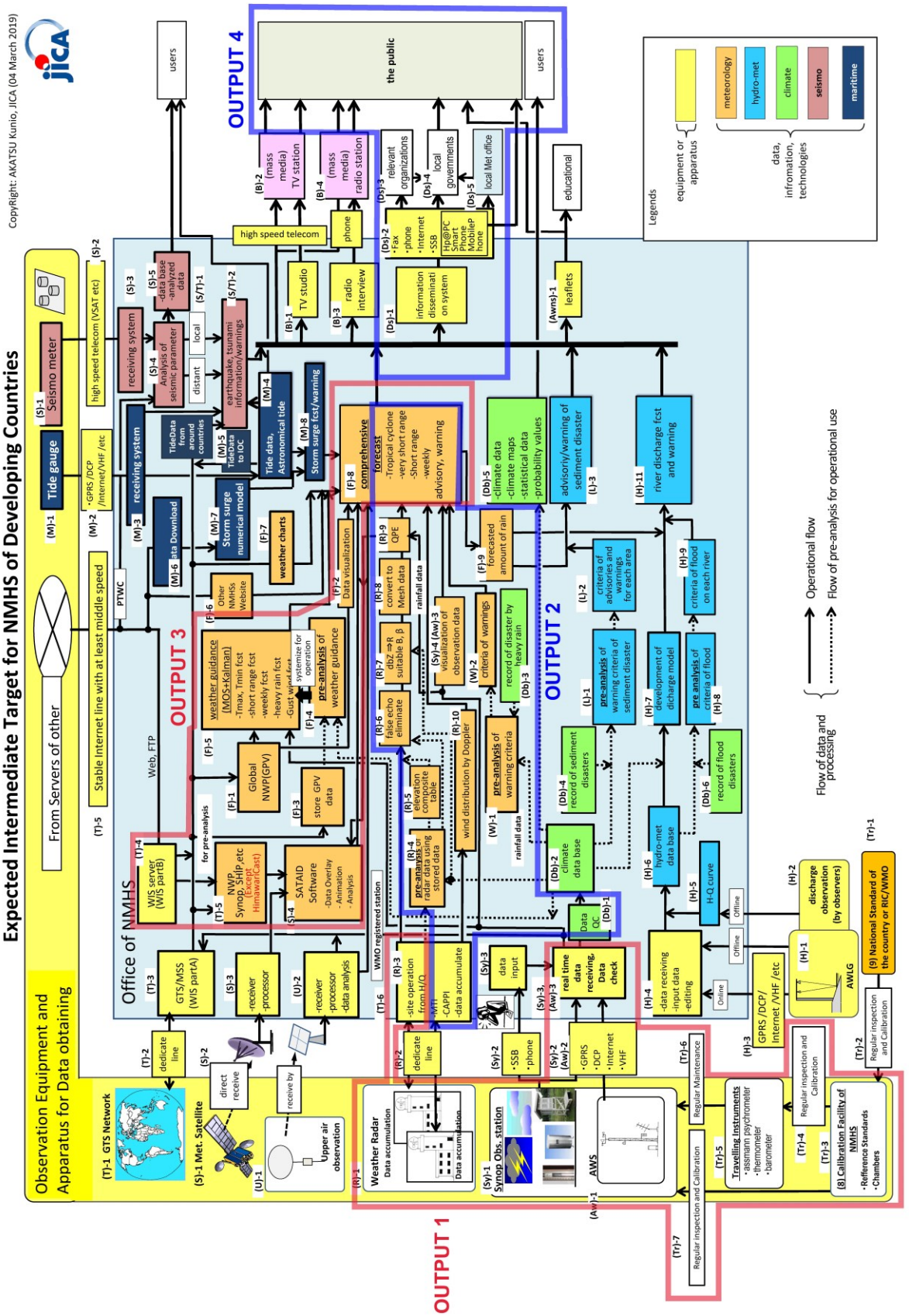

Figure 2. Expected Intermediate Target (AkatsuChart).

JICA has created the schematic charts which indicate the specific contents and concrete methods of every meteorological field (from observation to information dissemination) and total data flow network to be prepared among various fields of each NMHS (Figures 1–2).

Useful characteristics of these charts are that (1) it shows total operation system or data network required in every NMHS as birds–eye view, (2) every staff member of NMHSs can understand their duties or responsibilities clearly for total activities required to NMHSs and (3) everybody easily understands the order of priority fields to be improved in NMHSs. The charts are called as "AkatsuChart" among many developing NMHSs including international donors.

AkatsuCharts consist of 2 (two) versions, one is titled as "Expected Final Goal" and another is titled as "Expected Intermediate Target". The "Final Goal" chart (Figure 1) includes themes which seem difficult to be prepared for developing NMHSs, then the "Intermediate Target" chart (Figure 2) is designed to show expected achievements for every developing NMHSs. Items enclosed in rectangular box in the chart correspond to each "Activities" of the Project Design Matrix (PDM) which shows details of targets of JICA projects.

When JICA plans to prepare new meteorological project in some countries, JICA implements a preliminary survey composed of the JICA officials including JICA Senior Technical Advisor. AkatsuChart is utilized in the survey in the following manners. (1) JICA officials carry out a preliminary survey on outline of the operation situation of NMHS, (2) JICA explains JICA's recommendable future plans such as Final Goal and Intermediate Target by using AkatsuChart, (3) JICA explains the results on outline of preliminary survey and shows issues or challenges of each field, (4) discussions between NMHS and JICA are held on the issues or challenges, (5) finally, the results of discussions are summarized and these are utilized for JICA official project.

Through taking these processes, structures and components of the project (what, why, how) are clarified and gaps of understanding between both sides can be avoidable, furthermore the theme for next step–up after the project will be visualized. Additionally, by using AkatsuChart, the chart of standard developing model for technical support, JICA can avoid the occurrence of gaps of directivity among technical cooperation projects for NHMSs and JICA supports.

Vietnam is a vulnerable country against natural disasters and suffers from damages by high impact weather events. Therefore, enhancement of meteorological capacity/skill for more accurate information and for adequate dissemination are strongly required. Vietnam and Japan exchanged an agreement on "Programme for the Improvement of Capabilities to cope with Natural Disasters Caused by Climate Change" on 30th of June, 2010 and Vietnam requested the "Project for Strengthening Capacity in Weather Forecasting and Flood early warning system".

JICA implemented the Detailed Design Survey for the request from 8th to 23rd of June 2017. JICA experts visited the Vietnam Meteorological and Hydrological Administration (VNMHA), implemented assessment of VNMHA observation/forecasting/dissemination services, including North central Regional Hydro–Meteorological Center. Based on results of detailed design survey the both sides discussed details of the project with, referring Akatsu Charts and results were summarized as the Project Design Matrix (PDM) and the Plan of Operation (PO), and the Both sides exchanged the Record of Discussion (R/D) for the project for enhancement of capacity in weather forecasting and flood early warning system on 17th of November 2017.

As a part of JICA cooperation for DRR activities, a technical cooperation project "Project for Strengthening Capacity in Weather Forecasting and Flood Early Warning System" (hereafter, described as 'the Project') was started in June 2018 as a part of JICA

activities and enhancing NMHS abilities for disaster risk reduction. Scopes of activities for each output 1 to 4 of the VNMHS project are overlaid on Figure 2.

3. Project Design and Operation Plan

This project is designed to strengthen capacity for (1) maintenance and traceability of meteorological observation equipment, (2) analysis and quality control ability for radar, (3) forecasting/warning ability regarding heavy rain and typhoon and (4) dissemination ability of meteorological information. Through enhancing these abilities, more accurate meteorological information should be provided to related agencies and to the public and meteorological/hydrological information from VNMHA would contribute to disaster prevention activities by related agencies and the people.

On the PDM of the project, the outline is described as follows,

=Overall Goal=

Weather information disseminated from VNMHA is well utilized by the public and disaster related organizations.

=Project Purpose=

More accurate and timely meteorological information is disseminated to the public and the disaster related organizations.

=Output=

Output1: Capacity on maintenance and calibration of ground meteorological observation equipment is improved.

Output2: Capacity on weather observation, radar data analysis and quality management are improved.

Output3: Capacity on monitoring and forecasting of heavy rainfall and typhoon is improved.

Output4: Quality, contents and accessibility of Regional weather forecasts in North East (Phu Lien) and North Central (Vinh) are improved.

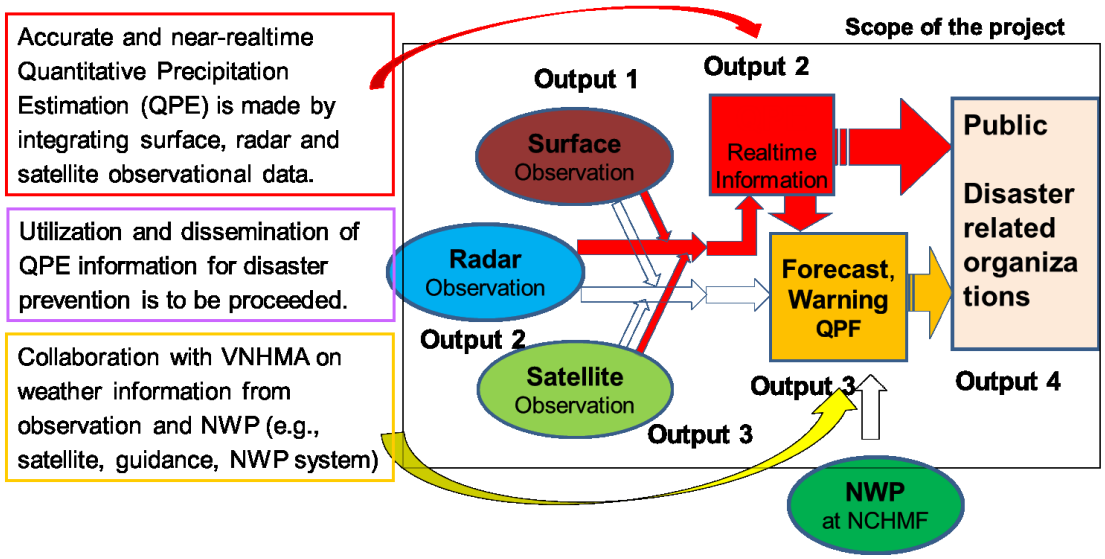

Figure 3. Structure of the project.

The project is designed as a 3.5 year project and is divided into periods, Period 1 (May 2018 to March 2020) and Period 2 (April 2020 to October 2021) shown in Figure 4. For the implementation of the project, Technical Working Groups are organized for each output and Working Group (WG) member, several officers from VNMHA and JICA experts, are assigned and project activities are mainly implemented and lead by these WGs.

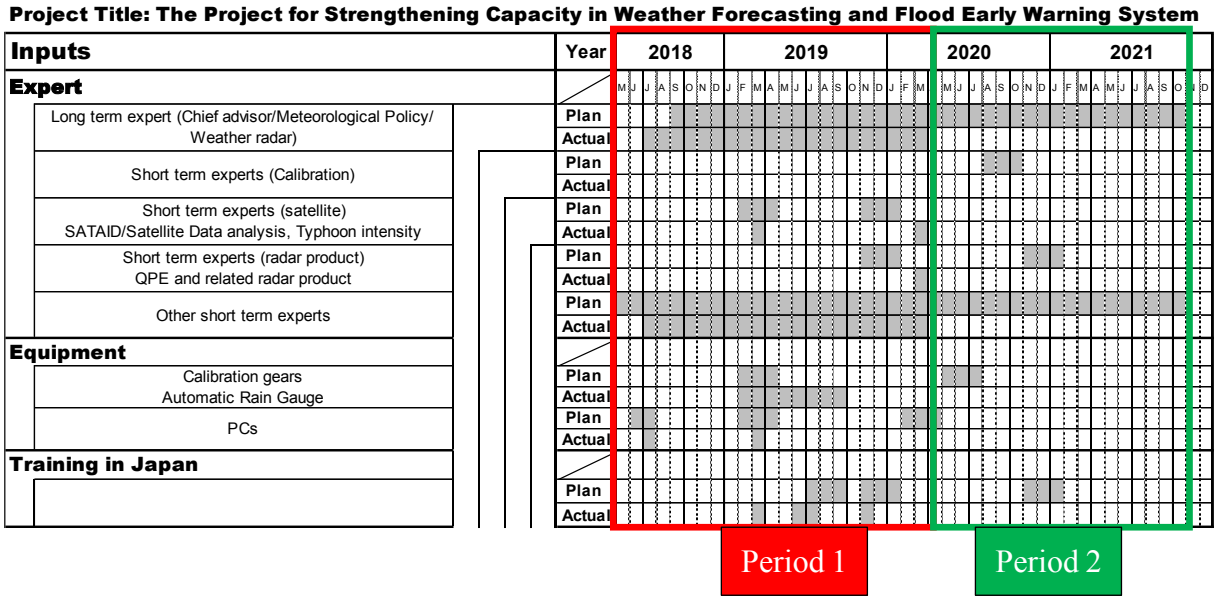

Figure 4. Project operation chart.

4. Summary of Activities in Period 1

As shown in Figure 3, the project consists of four outputs, namely Output1 (observation), Output2 (radar), Output3 (forecasting) and Output 4 (dissemination). The project is reviewed by the Joint Coordination Committee (JCC) held in every six months and VNMHA and JICA discussed matters, countermeasures and activity plans. Besides activities on the four outputs, the project was held on site special trainings/seminars by (former) Japan Meteorological Agency (JMA) experts for one week on satellite usage (March 2019), radar product and advanced satellite usage (March 2020) respectively. Activities during Period 1 are summarised as follows.

4.1. Output 1 (observation)

In VNMHA, traceability and maintenance of surface observation instruments are handled by the Hydrological Meteorology and Environment Observation Station Network Center, and for evaluation of instrument accuracy periodical calibration is also carried out. In the Synop manned observation, almost common equipments are used, but Automatic Weather Stations (AWSs) use different equipments by donors, and instruments were calibrated by the Headquarters at the time of shipment to districts. At present, there are 338 AWSs and 74 anemometers, and the development plan states that VNMHA will shift from manned observation (Synop) to automatic observation by AWS. For the calibration/maintenance of AWSs, WG drafted AWS inspection and a maintenance manual and based on the manual, WG carried out AWS maintenance at six AWS (three in Vinh region and three in Hai Phong region) sites.

For maintenance of radars, WG confirmed that daily/monthly maintenance has been implemented by Phu Lien and Vinh staff members continuously and recorded on maintenance reports. JICA experts attended JRC maintenance activities in September 2018 and shared information with JRC engineers, Phu Lien and Vinh radar staff members. Additionally, on site trainings at Phu Lien and Vinh radar sites, “maintenance of tower and radome”, “electric power supply”, “inspection of transmitter”, “inspection of DRSP”, “measurement of an antenna angle accuracy”, “training of measurement equipment”, “lectures of trouble shooting” and so on, were implemented in November to December 2018. And annual maintenances at Phu Lien and Vinh radar sites were implemented from May

2019 with experts and partly with a JRC local staff member. Additionally, scan angles for Phu Lien and Vinh radar were discussed a plan of new scan sequence was proposed. The details of Output 1 activities are given by [5].

4.2. Output 2 (radar)

JMA implements an international project "South–east Asia radar composite program" based on the WMO–WIGOS (WMO Integrated Global Observing System) project. So far, JMA shared a radar Quality Control/ Quantitative Precipitation Estimate (QC/QPE) package to NMHSs of Thailand, Malaysia and Indonesia and supported radar composition in these countries. VNMHA requested JMA to share the package and JMA implemented trainings for VNMHA trainees (two trainees) to explain the package in Japan in May 2019.

The shared JMA QC/QPE package was installed to a PC server set in AMO. The QC/QPE package was modified to VNMHA radars: at first Phu Lien, Vinh (JRC), and then Tam Ky, Dong Ha, Nha Be (Single–polarization radar, Vaisala), Pha Din, Pleiku, Quy Nhon (Dual–polarization radar, Vaisala) were calibrated with AWS data in May and June 2019. An experimental composition and QPE started in the PC server from September 2019 and WG confirmed composite radar data were overlay on cloud images using SATAID, a satellite data visualization and manipulation system developed by JMA. The radar composite techniques for Vaisala and JRC radars were improved, i.e. improvement of QPE processes (PPI composition tables, exact site location of radar/AWS), and lectures for QPE process and programs were implemented in November 2019. Modified QPE package to avoid over calibration by far rain gauges were corrected and adapted in February 2020. A detailed description on PQE conducted in Output 2 is given by [6].

4.3. Output 3 (forecast)

For development of temperature guidance, WG carried out verification of maximum and minimum temperatures of city forecasts for 63 major cities issued by VNMHA and Kalman filter (KF) guidance with JMA's global model data (GMS–KF guidance), and confirmed KF guidance mostly showed more accurate results than NWP itself and operational city forecasts. Based on the results, WG started an experimental operation of KF guidance for 63 cities up to 3 days ahead. In December 2019, WG developed another KF guidance, based on the ECMWF's global model (IFS) data up to 9 days ahead using 00UTC and 12 UTC initial grid point values (GPVs) and conducted a trial operation of it [7].

VNMHA had temporary used a relationship between cloud top temperature (TBB) and rain amount [8] to estimate rainfall amount from satellite data. Since the heavy rainfall event in December 2018 was not brought by deep convection but by the warm rain process, rainfall intensity around central Vietnam was significantly underestimated. To improve the precipitation analysis, WG examined GSMaP rainfall produced by JAXA EORC [9], i.e. standard product (GSMaP_MVK; 3–hours delay) and real–time product (GSMaP_NOW; updated every half hour by extrapolation using cloud motion vectors). Threat scores of GSMaP_MVK are apparently better than GSMaP_NOW and rain estimation using TBB [10]. VNMHA started operational use of GSMaP data for their precipitation analysis in October 2019 [11].

Additionally, Training on utilization of satellite, radar and GPV data for monitoring heavy rainfall was provided. Post–analyses of heavy rain events including tropical cyclones in 2018 were carried out. Presentation/Practice for "weather guidance" and "case study analysis for heavy rain" at the regional forecasting centers were implemented in July and followed–up in November 2019.

4.4. Output 4 (dissemination)

Questionnaires to grasp customer needs were prepared and distributed to municipal disaster prevention authorities, the People's Committee, mass media and related private sectors in June 2018. On–site interviews to forecasters were conducted and copies of forecast manual/warning logs were collected in the North East Regional Center in December 2018.

Pre–site surveys (for 20 candidate rain gauge sites) were implemented to decide appropriate sites for Automatic Rain Gauge (ARG) installation for radar data calibration in Phu Lien and Vinh areas. Based on the survey result, 18 sites were recommended for ARG installation in 2018. Basement and stand for Fifteen ARG systems were set in April and May 2019. 15 ARG system were transported, calibrated and set in 15 sites in September and October 2019, data collection and monitoring were started from the middle of October 2019.

5. Conclusion and Suggestion (for Activities in Period 2)

During Period 1, the project concentrated to enhance abilities of VNMHA for observations and forecasts and achieved various outputs, however, in Period 2, the project aims to disseminate weather products aggressively and utilize them for DRR activities. In Period 2, the project targets further technical skill developments of VNMHA and WG tackles to weather information dissemination and utilization.

For Output 1, activities for maintaining AWS equipment and traceability are scheduled. Regarding radar maintenance, maintenance activities at sites have been steadily implemented and annual maintenance works by AMO also have been implemented regularly. Though, there remain outstanding matters, (i) radar maintenance contract with manufacturers for further stable operation, (ii) preparation of spare parts for AWS and (iii) quality check of AWS observation data.

For Output 2, radar composition products, not only for JRC radars but for those covering whole Vietnam country were succeeded and QPE using composite radar and AWS data experimentally started. However, for accurate and reliable QPE, there remain lots of matters to be tackled, i.e. modification of scan angles, improvement of composite table, quality check/control of AWS data, evaluation of QPE and improvement of QPE based on these activities. Additional next challenges are usage of doppler velocity, trial to Quantitative Precipitation Forecast (QPF).

For Output 3, Kalman–filter temperature guidance developed for major cities, could be used operationally, however, guidance for precipitation and improvement of numerical weather prediction, with VNHMA's great expectations, are under discussion through investigating and discussion by VNMHA and JICA. These terms are one of the most important targets in Period 2.

For Output 4, transportation of procurement items for calibration gears and three additional AWSs started in May 2020. WG would tackle for improvement of web site and dissemination of weather products.

For developing more accurate and timely meteorological information, VNMHA and JICA continuously challenges to clear matters step by step steadily. And meteorological information developed through the project will be disseminated aggressively mainly through mobile web sites to achieve the project purpose.

Author Contributions: This article is written by experts for each component. "Activities of JICA on disaster prevention" is written by Y. Kasuya (outline of JICA activity) and Y. Tanaka (DRR projects in Vietnam). "National Meteorological and Hydrological Services and Disaster Risk Reduction" is written by Mr. K. Akatsu based on his experiences as JICA experts more than 10 countries. "Outline, activities and plan of the project" is written by Mr. K. Akaeda and Mr. M. Tonouchi based on the progressive report of the project. Finally, the article was commented by Mr. N.V. Thu.

Acknowledgments: This JICA technical cooperation project was supported by the people of Japan as JICA projects and technical assistances by JMA as DRR technical cooperation of WMO international cooperation frame for southeast Asian countries. We express our special thanks to JICA Tokyo experts who supported the project and staff members of the Vietnam Meteorological and Hydrological Administration who have joined the JICA Project for Strengthening Capacity in Weather Forecasting and Flood Early Warning System in the Social Republic of Vietnam.

References

1. Central Steering Committee for Disaster Prevention and Control, Natural Disaster in Vietnam in 2019, 2019.
2. VNDMA, MARD and JICA. Leaflet of Priority Programs for Disaster Risk Reduction in Vietnam, 2018.
3. Japan International Cooperation Agency. Data Collection Survey on Strategy Development of Disaster Risk Reduction and Management in The Socialist Republic of Vietnam, 2018.
4. World Metrological Organization. National Meteorological and Hydrological Services. Available online: https://public.wmo.int/en/our–mandate/how–we–do–it/role–and–operation–of–nmhss
5. Mikami, M.; Ichijo, H.; Matsubara, M.; Nguyen, H.A.; Duc, L.X. A proposal of AWS maintenance and periodic calibration tools and installation of ARGs for Radar QPE calibration. *VN J. Hydrometeorol.* **2020**, *5*, 13–35.
6. Kimpara, C.; Tonouchi, M; Hoa, B.T.K.; Hung, N.V.; Cuong, N.M.; Akaeda, K. Quantitative precipitation estimation by combining rain gauge and meteorological radar network in Vietnam. *VN J. Hydrometeorol.* **2020**, *5*, 36–50.
7. Sasaki, K.; Anh, V.T.; Han, N.T.; Trang, T. Development of maximum and minimum temperature guidance with Kalman filter for 63 cities in Vietnam up to 10 days ahead. 2020, *VN J. Hydrometeorol.* **2020**, *5*, 51–64.

8. Vicente, G.; Scofield, R.A.; Mensel, W.P. The operational GOES infrared rainfall estimation technique. *Bull. Amer. Meteor. Soc.* **1998**, *79*, 1881–1898. https://doi.org/10.1175/1520–0477(1998)079<1883:TOGIRE>2.0.CO;2
9. Japan Aerospace Exploration Agency Earth Observation Research Center: *JAXA global rainfall watch*. Available online: https://sharaku.eorc.jaxa.jp/GSMaP/index.htm
10. Saito, K.; Hung, M.K.; Hung, N.V.; Vinh, N.Q.; Tien, D.D. Heavy rainfall in central Viet Nam in December 2018 and modification of precipitation nowcasting at VNMHA. *VN J. Hydrometeorol.* **2020**, *5*, 65–79.
11. Hung, M.K.; Saito, K.; Khiem, M.V.; Tien, D.D.; Hung, N.V. Application of GSMaP Satellite data in precipitation estimation and nowcasting: evaluations for October 2019 to January 2020 period for Vietnam. *VN J. Hydrometeorol.* **2020**, *5*, 80–94.

VIETNAM JOURNAL OF HYDROMETEOROLOGY

Research Article

A proposal of AWS maintenance and periodic calibration tools and installation of ARGs for Radar QPE calibration

Masao Mikami[1*], Hiroyuki Ichijo[1], Koji Matsubara[1], Le Xuan Duc[2], Hoang Anh Nguyen[2]

[1] Japan Meteorological Business Support Center; mikami@jmbsc.or.jp; ichijo@jmbsc.or.jp; koth_matsubara@nifty.com
[2] Viet Nam Meteorological and Hydrological Administration, lexuanduc@gmail.com; hoanganhck@gmail.com
***** Correspondence: mikami@jmbsc.or.jp; Tel.: +81–3–5281–0440

Received: 5 July 2020; Accepted: 21 August 2020; Published: 25 August 2020

Abstract: Automatic weather station (AWS) can automatically observe surface weather elements and can transmit the data to data center through internet or mobile phone lines. Therefore, it is suitable to monitor mesoscale disturbances and precipitation, in particular. Viet Nam Meteorological and Hydrological Administration (VNMHA) currently operates AWS and Automatic Rain Gauge (ARG) networks by multi–national donors. However, the instruments were not calibrated after installation, and it was difficult to perform maintenance on a regular basis, so technical problems often occurred in their observation accuracy and reliable operation. Japan–Vietnam joint technical project between Japan International Cooperation Agency (JICA) and VNMHA started in May 2018. As part of this project, the introduction of AWS maintenance and traceability technology, and ARG network for the calibration of radar rainfall quantitative estimation (QPE) were proposed. In this paper, we discuss the current situation of AWS and ARG network in VNMHA. Next, we will explain the maintenance and cyclic calibration of the instrument proposed in this project. Furthermore, we will explain the installation plan of the ARGs to calibrate two radar data in Phu Lien and Vinh for the development of QPE. Installation of ARGs has been achieved with cooperative works of VNMHA staffs and JICA experts. So, we introduce their activities for each step from site survey to pre–operational evaluation. Furthermore, we will discuss future issues for stable and accurate observations of AWS and ARG networks.

Keywords: Automatic Weather Station; Automatic Rain Gauge; Traceability; Calibration.

1. Introduction

With the invention of telegraph technology and the development of ground meteorological instruments, modern meteorological observations were started in various countries since the latter half of the 19th century. As a result, quantitative surface meteorological observation data using hygrometers, barometers, and rain gauges with guaranteed traceability have been distributed to the world in near real time base.

The meteorological stations in each country simultaneously observe the surface meteorological elements every 3 to 6 hours and deliver them to each country. The establishment of a global simultaneous meteorological observation network made it possible to observe synoptic–scale meteorological disturbances with horizontal scales of 1,000 to

10,000 km. For this reason, this surface meteorological observation is called "SYNOP surface observation" [1]. For better accuracy and more reliable SYNOP surface observation, World Meteorological Organization (WMO) has established the guideline of the observation environment of the observatory for synoptic meteorological observation [1]. As an example, Figure 1 shows the guideline of the layout of the observation station shown in [1]. In this way, by satisfying the standards set by WMO for the ground meteorological observations of each country in the world, it is possible to simultaneously perform world meteorological observations based on the same standard and the same accuracy.

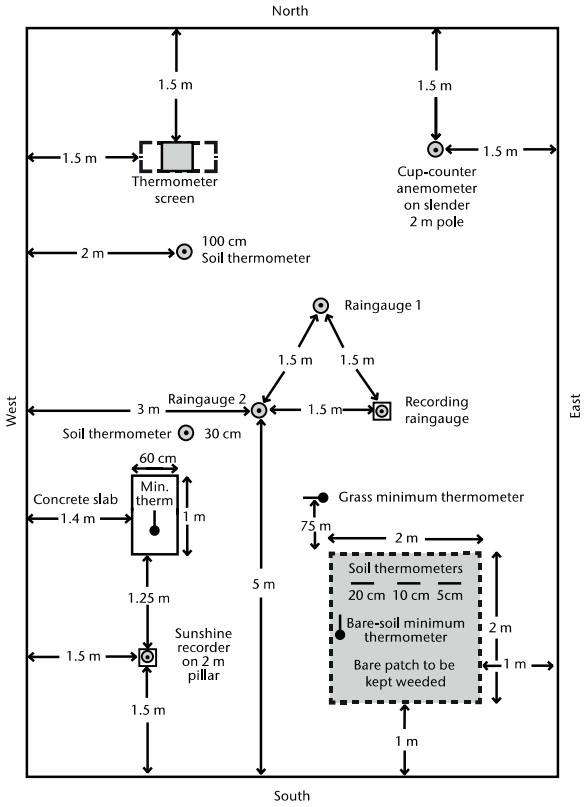

Figure 1. WMO layout design of surface observing station in [2].

The Vietnam Hydrometeorological service has a history of development for over 120 years. The first meteorological station was established in Nam Dinh Province on April 18, 1891. VNHMA has been conducted SYNOP observations based on WMO's surface meteorological observation guideline. Currently, 183 surface meteorological observation sites are operated by VNMHA in Vietnam. However, until recently, most of the surface observation was manned SYNOP observation. In recent years, technological innovations in measuring instruments have made it possible to automatically measure surface meteorological elements that were previously measured by observers. In addition, due to the progress of digital technology, Automatic Weather Station (AWS) has become popular. AWS collects data obtained by automatic measuring instruments and distribute them through mobile phones and/or internet. With the progress of these technologies, AWS has been rapidly introduced in many countries. In VNMHA, 191 sites of the AWS observation have been operated up to now. Figure 2 shows the site location map of AWSs in VNMHA.

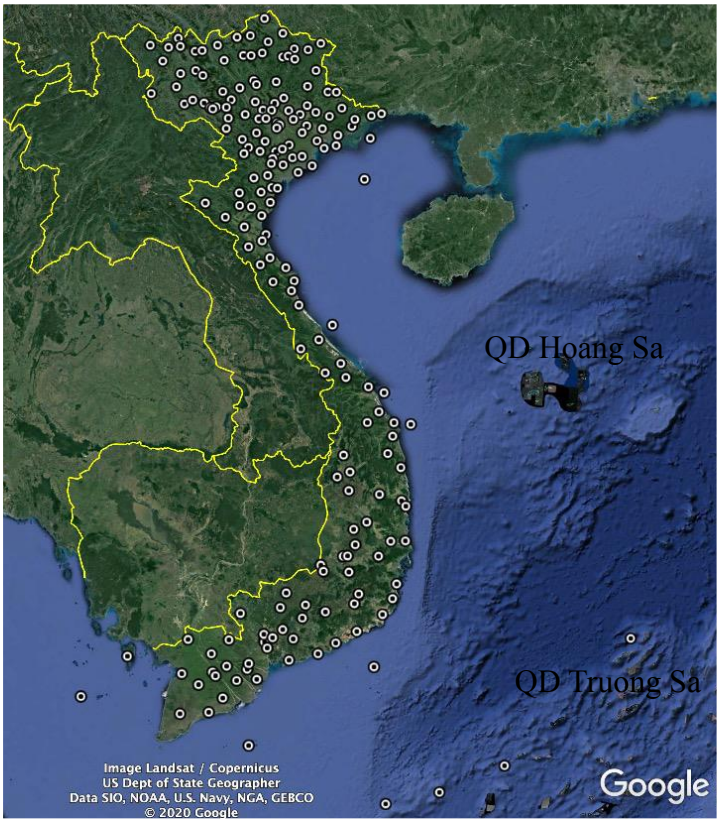

Figure 2. VNMHA AWS site location map.

The advantage of AWS observation can be summarized as follows: (1) Near real–time observation is possible. This enables to use AWS data for disaster early warning information such as heavy rainfall. (2) Frequent observation is possible. SYNOP observations are every 3 hours, but most AWS can operate at time intervals of 1 to 20 minutes. (3) Operation is automatically done. Therefore, it can be installed at many sites with fewer human resources. As a result, observations with higher spatial density than SYNOP observations are possible. And the observation information of high spatial density with short time intervals gives a great advantage in monitoring mesoscale disturbances such as heavy rainfall. (4) In terms of operation, the initial cost is high, but the operation cost is relatively low. (5) Even if there is a communication failure at the observation site, the data can be archived in AWS itself, and there is little risk of data loss. (6) Since AWS data are digital data, it is easy to process and analyze the AWS data and develop applications for various weather information. In summary, AWS observations have a great advantage over SYNOP observations in monitoring heavy rainfall associated with mesoscale disturbances.

On the other hand, the disadvantages of AWS observation are as follows: (1) Since AWS has unmanned observations installed at many sites, it is not easy to secure traceability by periodic verification by standard instrument. It is required to make periodical calibration of AWS instruments to maintain measurement accuracy. (2) Even though the operation of AWS is automatic, if maintenance of AWS system cannot be performed regularly, long–term stable operation will be difficult. (3) Since data transmission depends on the reliability of the network, data transmission is often interrupted in remote areas where the communication

infrastructure is weak. (4) Data transmission from AWS is automatically delivered, so Quality Control (QC) by human check and Automatic Quality Control (AQC) at RHMC data center and IDC are required.

Thus, the stable and reliable operation of AWS requires (1) periodic maintenance of AWS system and calibration of AWS instruments and (2) QC at the observation site and AQC system at RHMC data center and Information and Data Center (IDC) in VNHMA.

Vietnam is a vulnerable country against natural disasters and has been suffered from damages by meteorological events especially for heavy rainfall. Typhoons and monsoons bring heavy/torrential rains to plains and steep mountain areas which bring about serious damage to Vietnam's society and economy. Based on this background, JICA and VNMHA started "the project for Strengthening Capacity in Weather Forecasting and Flood early warning system" (hereafter this project) on 31th of May 2017.

Output 1 activity of this project aims to improve the maintenance and calibration capabilities of surface meteorological observation equipment, AWS rainfall information is used as (1) disaster prevention information such as warnings by monitoring the real-time rainfall distribution. In addition (2) it is also used to improve the accuracy and reliability of QPE by using rainfall data as ground truth to calibrate the rainfall estimated by the radar signal intensity from the Z–R relationship. Therefore, improving the reliability and maintaining capacity of the rain gauge in AWS and ARG systems are a key issue for Output 1 and 2 of this project.

Based on the above consideration, the purposes of this paper are (1) to review the current situation of VNMHA's AWS network system, (2) to discuss the technical issues for operation of AWS and ARG systems with high accuracy and reliability that can be used for monitoring of heavy rainfall and for development of application such as QPE and (3) to propose a maintenance and calibration tools for AWS to improve the maintenance and calibration capabilities of AWSs in VNMHA.

2. AWS systems in VNMHA

2.1. Current status of AWS systems in VNMHA

In this project, in order to identify the current situation and issues to address for the output goals, first, a Base Line Survey (BLS) was conducted from June 4 to 29 in 2018. For this, the site survey was conducted at Mid–Central Regional Hydro–Met. Center (RHMC) in Da Nang as well as North–East RHMC in Hai Phong and North–Central RHMC in Vinh. Among them, North–East and North–Central RHMCs are the target regions in this project.

In Vietnam, the data of each AWS site are collected by IDC in VNMHA and then distributed to the forecast section. In BLS, field survey on the current situation of AWS observation was conducted at the three RHMCs.

It was found that different AWS systems are installed by different donors in each of the three RHMCs. In Mid–Central RHMC, AWSs made in Italy has been operated. In North–Central RHMC, AWSs made in Germany by World Bank (WB) donor are used. And in the North–East RHMC, AWSs made in Korea by Korean donors are used. At the time of the survey, AWSs of the WB were still in the long–term trial operation before the handover, and they were not used in the operation yet. Each AWS network is deployed only in their RHMC

region with the exception of the WB donored AWSs in North–Central RHMC. All the AWSs data are sent to IDC in VNMHA via the data center in each of RHMCs. Currently, AWS data are mainly used only by each RHMC. For this reason, the management and operation of each AWS is carried out by each RHMC. However, after the defect warranty period by the donor is over, the cost of maintenance and repair of any AWS systems are not account for. Therefore, there remain problems in stable operation over a long period of time.

2.2. Overview of AWS for each donor

The AWS systems used in the three RHMCs we inspected in the BLS have different specifications. An outline of each AWS system is shown below.

2.2.1. Korean AWS

In North–East Region, AWS system made in Korea, which was donated by Korean International Cooperation Agency, has been operating since September 2015, and the 2–year warranty period has expired. AWSs are located at 25 sites within this region. Observation data are distributed to IDC via the data center of the RHMC in Hai Phong in real time basis. The specifications of the instruments used for observation of atmospheric pressure, air temperature, humidity, wind speed and direction, and precipitation are shown in Table 1.

Figure 3 also shows AWS system installed at Phu Lien meteorological station in North–East Region. Many AWSs in VNMHA are installed within the observation field of the SYNOP observatory. AWS in North–East Region sends the 10–minute average of atmospheric pressure, air temperature, relative humidity, wind direction, wind speed, and precipitation to IDC every 10 minutes.

Table 1. Specifications of Korea AWS instruments in North–East RHMC.

Element	Model Number	Range	Accuracy	Comment
Atmospheric Pressure	JYB400	500 – 1080 hPa	±0.4 hPa, 25°C	Long term stability: ±0.5 hPa/year
Air Temperature	JY100829	–40°C to 60°C	±0.3°C	
Humidity	Vaisala HMP110	0 –100% RH	±1.7% RH (0 – 90% RH), ±2.5% RH (90 – 100% RH)	
Wind Direction	JY–WD160C	0 – 360°	< ±3°	Resolution 2.8°
Wind Speed	JY–WS161D	0 – 75 m/s	±0.15 m/s	
Precipitation	JY100097-2	0 – 700 mm/h	±0.5 mm (0 – 20 mm/h), ±3% (>20 mm/h)	Diameter 20.32 cm, Resolution 0.5 mm

Figure 3. An appearance of Korea AWS observation station (Phu Lien Meteorological Radar Station).

The anemometer is a 3–cup anemometer type sensor with a wind speed range of up to 75 m/s and an accuracy of ± 0.15 m/s. The wind vane has a resolution of 2.8 ℃ and the accuracy of the wind direction is within ± 3 ℃. The thermometer is a Pt 100Ω type sensor, whose resolution is 0.1 ℃, and accuracy is within ± 0.3 ℃. The hygrometer uses Humicap (Vaisala, Type HMP110). The thermometer and hygrometer are contained in a natural ventilation type radiation shield (Figure 4a). For this reason, air temperature of AWS during calm to weak wind condition in sunny days may tends to be higher than the temperature of SYNOP observation, which is measured in a Stevenson screen box. Therefore, it is necessary to be careful when using daytime AWS temperature data [2]. The barometer is a digital barometer using a non–mercury type silicon sensor with microprocessor–based signal compensation process (Figure 4b). The accuracy is ±0.4 hPa at 25 ℃ and long–term stability is ± 0.5 hPa/Year. The rain gauge is a tipping bucket type sensor with an opening diameter of 200 mm, which has a measuring range up to 700 mm of hourly rainfall, and has a resolution of 0.5 mm (Figure 4c). It should be noted that the rain gauge sensor does not use windshield to prevent the reduction of rain capture rate due to wind, so rainfall data may tend to be affected by strong wind. For this, we need to be careful with precipitation data by this sensor when wind speed is high [3].

All sensor signals are logged to the data logger every 10 seconds, the data logger calculates the 10 minutes average value, and then transmits the averaged data to IDC every 10 minutes.

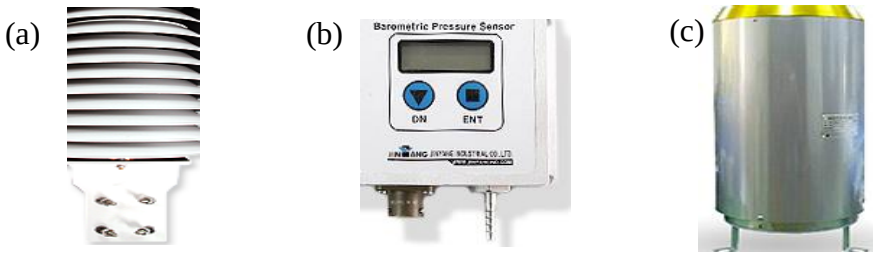

Figure 4. Sensors used in the Korean AWS: (a) air temperature and hygrometer sensors with radiation shield; (b) Ditigal barometeer and (c) rain gauge.

2.2.2. World Bank AWS

In North–Central RHMC, AWS system designed in Germany, which was donated by WB, has been used. Totally 22 AWS sites are located in this RHMC. There are also 43 ARGs installed by WB's donor in this RHMC. Installation of the AWS and ARG systems were completed in 2017. However, at the time of the BLS (March 2019), these AWS systems were before handover and were in the field trial operation period. Nevertheless, observation data are distributed to IDC through mobile phone line every 10 minutes.

The specifications of the observation elements and instruments are shown in Table 2. And Figure 5a shows AWS system installed at Vinh meteorological station in North–Central Region.

Table 2. Specifications of World Bank AWS instruments.

Element	Type	Range	Accuracy	Comment
	5600–0120–3A/OTT Hydromet.	500 – 1100 hPa	0.2 hPa at 20 °C and 0.1 hPa outside the heat range	Resolution: 0.01 hPa
Air Temperature	OTT TRH	–40°C – +80°C	±0.1 °C at 20 °C, ±0.5°C at –40 °C, 80°C linearity	Resolution: 0.01 °C
Humidity	OTT TRH	0 – 100 %RH	max. ±2% RH (0–90% RH); max. ±3% RH (90–100% RH)	Resolution: 0.1 %
Wind Direction	Lufft V200A–UMB	0 – 360°	< 3°	Resolution: 0.1°
Wind Speed	Lufft V200A–UMB	0.3 – 90 m/s	±0.2 m/s or ± 2 %	Resolution: 0.1 m/s
Precipitation	Adon RG–Pro	0 – 8mm/min.	±2 % with adjustable rainfall intensity	Orifice 200 cm^2, diameter 15.96 cm, Res. 0.1 mm

(a) (b)

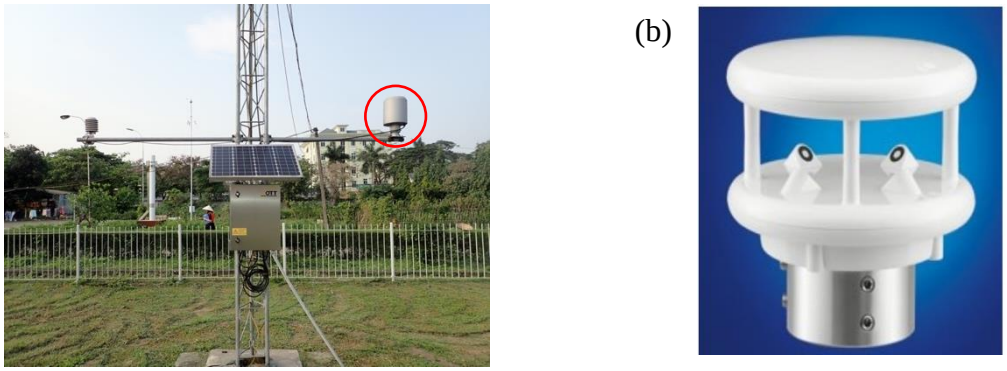

Figure 5. (a) An appearance of WB AWS system (Vinh Regional Hydro–Met Center). The rain gauge sensor is shown in red circle. And (b) wind speed and direction sensor settled at the top of the 10m tower.

As shown in Table 2, this AWS system measures surface pressure, temperature, humidity, wind direction, wind speed and precipitation. The wind sensor is an ultrasonic type sensor having maximum wind speed rang of up to 90 m/s and the accuracy is ±0.2 m/s or ±2% (Figure 5b). Compared to the 3–cup anemometer, the ultrasonic anemometer has less deterioration in measurement accuracy during long–term field use. The thermometer is a Pt resistance type sensor. The resolution, measuring range and accuracy are 0.01 °C, –40 to +80°C, and ±0.1 °C at 20 °C and/or ±0.5 °C at –40 °C, 80 °C, respectively. And the resolution, measuring rang and accuracy of the relative humidity sensor are 0.1%, 0 to 100% RH, and Max. ±2% RH (0 to 90% RH) and Max. ±3% RH (90 to 100% RH), respectively. Both temperature and relative humidity sensors are settled inside the weather and radiation protection shield that protects the sensor from solar radiation, precipitation and wind (Figures 6a and 6b). The barometer is a resistive type sensor (Figure 6c) and the resolution, measuring range and accuracy is 0.01 hPa, 500 to 1100 hPa, and 0.2 hPa at 20 °C, respectively.

The rain gauge is a tipping bucket type sensor with an opening diameter of 15.96 cm with orifice of 200 cm^2 and the resolution and maximum capacity are 0.2 mm and up to 16 mm/min of precipitation, respectively (Figure 6d). Similar to the Korean AWS, this rain gauge does not come with windshield. In addition, this sensor is fixed to a pillar that extends horizontally from the center pole, and the ground clearance of the opening is 1.8m in height (Figure 5a). For these reasons, it is considered that the capture rate of precipitation is considerably influenced by wind speed [3], and, similar to the AWS in North–East RMHS, it needs careful consideration when using precipitation data under strong wind. The data logger set inside the main body calculates the average values for 10 minutes and then sends the data to RHMC data center.

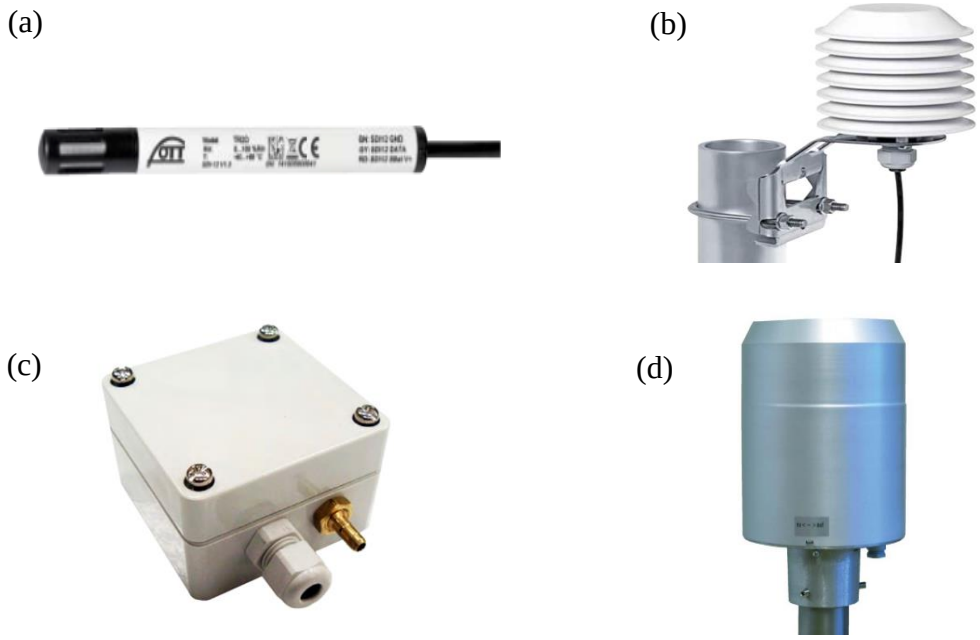

Figure 6. Sensors used in the World Bank AWS: (a) thermometer and hygrometer sensors; (b) radiation shield for thermometer and hygrometer; (c) digital barometer and (d) rain gauge.

2.2.3. Italian AWS

In Mid–Central Region, SMP20 system by CAE Technology Company, donated by Italy, has been operated since 2010. Totally 17 AWS sites are located in this region. An original system by CAE technology is used for data network transmission and application for data viewer. And the management/display system application is installed only on one PC in the monitor room of the observation section of the Mid–Central Regional Center in Da Nang, and it is contractually impossible to copy and use it to other PCs at the same time. For this reason, at the time of the BLS, real-time information of the AWSs cannot be monitored by forecasting operation room or weather stations in Mid–Central RHMC. Therefore, real-time AWS information was not fully available for the forecast operation at that time.

Table 3. Specifications of Italy AWS instruments.

Element	Type	Range	Accuracy	Comment
Atmospheric Pressure	BA20	600 – 1100 hPa	±0.3 hPa in range –10 to 50°C	Sensitivity: Higher than 0.1 hPa
Air Temperature	TU20	–30°C– +50°C	0.27°C over the whole range	Resolution: <0.02 °C
Humidity	TU20	0 – 100 %RH	at 25°C; ±2 % (0 – 100%)	Operating teperature: –20 to 50°C
Wind Direction	DV200	0 – 360°	±2 gradi	
Wind Speed	VV200	0 – 180 km/h	1 km/h (0.27 m/s) % read process	
Precipitation	PMB2	0 – 300 mm/h	< 3 % up to 300 mm/h	Orifice=1000 cm^2; Diameter 35.7cm

Figure 7. An appearance of Italian AWS system (Da Nang Regional Hydro–Met Center).

The specification of the observation elements and instruments of this AWS system are shown in Table 3. Figure 7 shows AWS system installed at Da Nang meteorological station in Mid–Central Region. The temperature sensor is a Pt 100Ω type sensor, whose resolution, range, and accuracy are 0.02 ℃, –30 to 50 ℃, and within ± 0.27 ℃, respectively. The hygrometer has an accuracy of ±3 % RH and the measurement range are 0 to 100%. Differ from other AWS system, both temperature and relative humidity sensors are settled inside a Stevenson screen box that can protect the sensor from solar radiation, precipitation and wind (Figures 8a–8b). The anemometer is a 3–cup type and has maximum range of 0 to 50 m/h and the wind direction sensor has an accuracy of ± 2º.

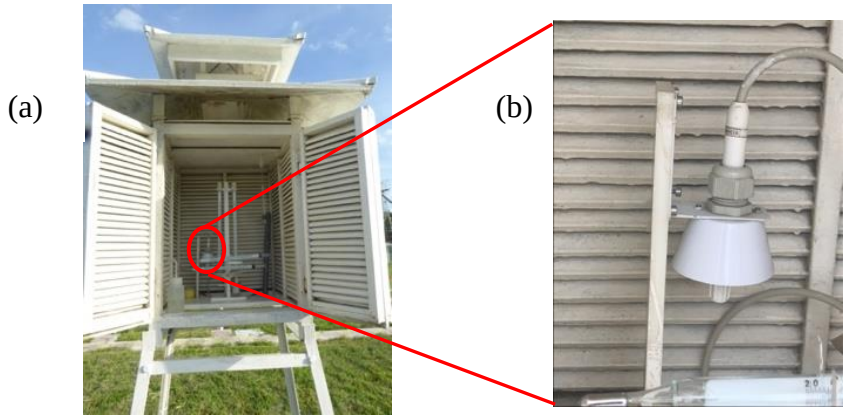

Figure 8. (a) Stevenson screen box for temperature and hygrometer, shown in red circle and (b) air temperature and hygrometer sensors of Italy AWS (Da Nang Regional Hydro–Met Center).

The barometer can measure 600 to 1100 hPa of pressure with an accuracy of ± 0.3 hPa (–10 to 50 °C). This is a digital type sensor that is mercury free (Figure 8b). The rain gauge is a tipping bucket type sensor with an opening diameter of 35.7 cm with orifice of 1000 cm^2 and the resolution and maximum capacity are 0.2 mm and up to 300 mm/h of precipitation, respectively.

Similar to other AWS system, this rain gauge also does not come with wind shield (Figures 9a and 9b). Data collected by the AWS stations will be transmitted in real–time to the 5 Provincial Centers and Mid–Central RHMC in Da Nang, and then converge at IDC in VNMHA.

Figure 9. (a) Appearance and (b) inside view of rain gauge (PMB2) of Italian AWS (Da Nang Regional Hydro–Met Center).

2.2.4. Current situation of traceability and calibration of AWS instruments

VNMHA has three Instrumentation Center for verification of SYNOP surface observation instruments in Hanoi, Da Nang, and Ho Chi Minh City. SYNOP instruments are regularly certificated by standard instruments with guaranteed traceability, and certification records are kept in every observatory. On the other hand, regarding the maintenance and traceability of the three AWS systems we have seen so far, initial certification was conducted at the VNMHA's instrument center before the installation of AWS at each site, and the traceability of each observation element is guaranteed at the time of installation. However, after installation, periodic maintenance and calibration of AWSs have not been properly done.

In order to test the current measurement accuracy of AWS observation equipment and to examine the possibility of implementing on–site traceability, comparison of the barometer used in AWS with the Vaisala PTB330 type barometer, whose accuracy was confirmed by the Japan Meteorological Agency (JMA), was conducted at Uong Bi Observatory and at North–Central RHMC in Vinh. Using the Vaisala digital barometer type PTB330 brought from Japan as a reference, comparative measurements with two AWS barometers were performed, and the results shown in Table 4 were obtained. The minimum display digit of the pressure value shown in the data logger of WB AWS is one digit in hPa. For use in periodic calibration, it is necessary to display at least one digit in 0.1hPa, which is recommended in [1].

Table 4. Results of comparative measurement of barometer.

Target barometer	Korea Barometer	WB Barometer
Location	Uong Bi	Vinh
Index error (hPa)	+0.6	+1

From this result, it was also found that the calibration of AWS instruments can be done by performing comparative measurement at the AWS site using traveling standard instruments as a reference, whose traceability is guaranteed by VNMHA, as in this case.

2.3. Issues found by the Base Line Survey

In June 2018, we have conducted the BLS for understanding the current situation of VNMHA's AWS system as a part of the activity of this project. For this purpose, we have inspected the SYNOP and AWS sites in North–East, North–Central, and Mid–Central RHMCs. It is found that in order to enhance the reliability and accuracy of AWS in VNMHA, the following issues were summarized as challenges for this project. (1) AWS of each donor has not been subjected to periodic verification by VNMHA and/or calibration by inter–comparison using the traveling standard after the pre–installation verification at the VNMHA headquarters. (2) Response at the occurrence of a technical trouble is guaranteed by the donor during the warranty period. Response after that is managed by each RHMC. However, periodic maintenance and calibration require more human resource. (3) No metadata record has been retrieved for each AWS site. In order to maintain the long–term reliability of AWS system, it is necessary to archive the periodic maintenance report as metadata historical

record. (4) No equipment is available at AWS sites to perform maintenance and calibration after AWS installation. In addition, at present, there is not enough opportunity for the staff of the meteorological observatory to take lecture and training on AWS system maintenance and calibration procedures for AWS sensors.

3. Introduction of a unified digital maintenance report and calibration tools for AWS

As mentioned in the introduction, AWS is expected to play an important role in monitoring severe weather event such as heavy rainfall and strong winds associated with mesoscale meteorological disturbances. And based on the consideration of current situation of AWS systems in VNMHA discussed in 2.3, it was proposed to practice actions in this project as counter measures of enhancing reliability and accuracy of AWS measurement in VNMHA. In the following sections, we will explain the measures proposed in this project in detail.

3.1. Introduction of unified digital maintenance report for AWS system

In VNMHA's SYNOP observations, metadata report, such as verification history of measuring instruments, changes in the observation environment, changes and updates of measuring instruments, staff changes, etc., has been regularly recorded at the observation site. However, AWS does not have a similar metadata record. Since AWS automatically operates and observes, it is difficult to detect a trouble in advance, unless regular inspection and maintenance are performed. With periodic AWS system maintenance and calibration for instruments, we may take timely countermeasures without missing a data.

In addition, VNMHA has introduced different AWS systems by multiple donors. However, for AWS maintenance, it is desirable to establish a unified maintenance system nationwide. That is, it is desirable to record the regular maintenance based on the unified maintenance form. It is also desirable that the inspection report is shared as a digitized report at VNMHA's AWS supervisory department, nine RHMCs and AWS observatories, which will have a great advantage in managing long–term stable operation of AWS. For these reasons, in this project, it was proposed to use a report form on MS–EXCEL format. Because, this report can save as a digital file. Then, it is easy to share this report among each VNMHA's office.

Since 1 November 1974, the JMA has installed approximately 1300 ARGs throughout Japan, of which 840 are AWSs that observe wind direction/speed, temperature, and sunshine duration hours in addition to precipitation. JMA named these systems as AMeDAS (Automated Meteorological Data Acquisition System) and regularly conducts on-site inspections, which enable to keep the missing rate quite low. Similar to this, regarding AWS maintenance in VNMHA, we proposed to establish a maintenance report form as shown in Figures 10a and 10b with reference to the JMA inspection items. This maintenance report is designed to be selectively input the results of each check items with the toggle button (normal, abnormal, etc.). Then, we can immediately send a maintenance report by e–mail to the regional center and VNMHA's AWS supervisory department and can share the problem as soon as possible. And we will be able to find a technical issue and its solution more quickly and accurately.

(a) (b)

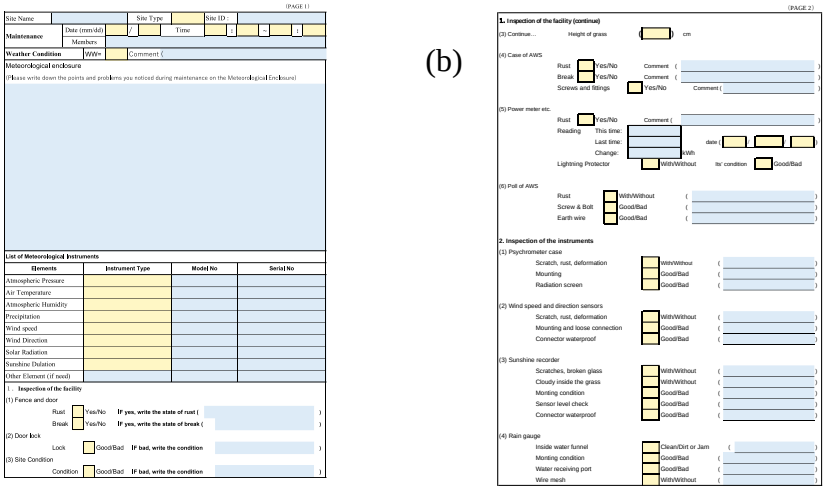

Figure 10. Examples of unified AWS maintenance report form (a) page 1 and (b) page 2.

3.2. Introduction of calibration tools for periodic calibration of AWS instruments

The major observation items of the AWS operated by VNMHA are precipitation, air temperature, humidity, wind direction and wind speed, and atmospheric pressure. These six meteorological elements are essential information for the surface weather condition and are important information for disaster prevention.

An important target of this project is introduced the radar QPE technology. For this purpose, it is necessary to adjust the parameters of the *Z–R* relation equation using the radar signal intensity, *Z*, and precipitation, *R*. For this reason, the stable and accurate operation of precipitation observation by AWS and ARG are important mission of Output 1 activities of this project.

In this project, we proposed to use four sets of highly accurate and portable sensors for calibration of precipitation, air temperature, humidity, and atmospheric pressure sensors. These tools will be used at periodic AWS maintenance. Before using these calibration tools, they are verified at the instrument center of VNMHA to ensure traceability. As a result, it is possible to ensure traceability by performing comparative measurement between the AWS sensors and the calibration tools. Below, we introduce calibration tools for atmospheric pressure, air temperature, humidity, and precipitation sensors.

3.2.1. Digital Barometer

For on–site calibration of AWS barometer, a portable type digital barometer, Vaisala PTB–330TS will be used. This instrument can accurately measure atmospheric pressure with accuracy of ±0.10 hPa at 20 ℃.

The verification of PTB–330TS will be done at the VNMHA instrument center before using this tool for calibration of the AWS barometer at each AWS site during periodic inspection. An overview of the device is shown in Figure 11 and a specification is shown in Table 5a.

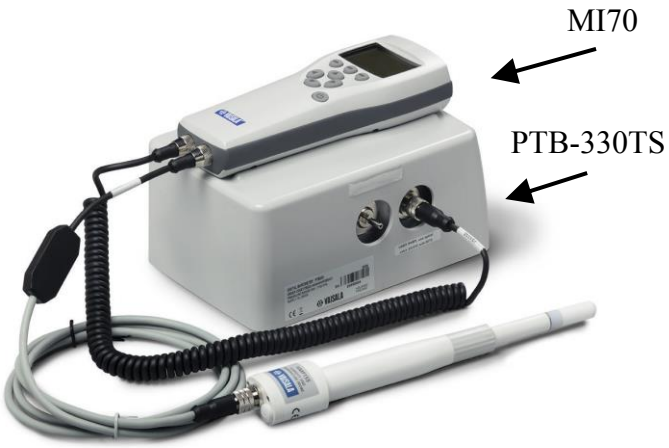

Figure 11. Portable digital barometer (Vaisala PTB–330TS) attached with controller MI70.

3.2.2. Digital Assmann Ventilating Psychrometer

Assmann ventilating psychrometers are widely used at surface meteorological observation site because of their high accuracy in measuring temperature and humidity. In general, Assmann ventilating psychrometer has a double radiation shield, which protect thermometer body from infrared radiation effect, and is forcedly ventilated in the space between the shield and the thermometer body, so heat effect due to solar radiation can be negligible. For this reason, we decided to use an Assmann ventilating psychrometer (JS–410) as a periodic calibration tool for AWS temperature and humidity sensors.

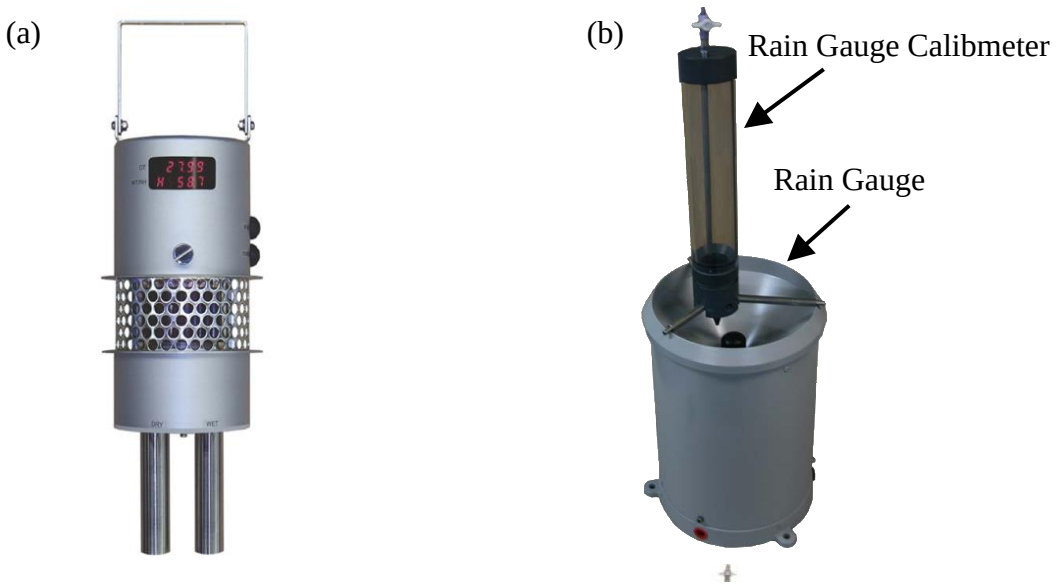

Figure 12. (a) Digital Assmann ventilating psychrometer (JS–410) and (b) rain gauge calibmeter (FCD–653).

In recent years, a digital Assmann ventilating psychrometer that uses a platinum resistance thermometer as a temperature sensor has been developed in place of the manual Assmann ventilation psychrometer that requires the observer to read the temperatures of dry and wet bulb temperature manually by eye. This is because there is no reading error by the

observer, and it has a monitor screen that displays the wet and dry bulb temperatures and relative humidity, and the data is recorded in the micro–SD memory inside the main body, so it is possible to minimize human error. For ensuring traceability of temperature sensors, periodic verification is recommended using Thermostat Water Chamber, which will be procured by this project. An overview of the digital type Assmann ventilating psychrometer adopted in this project is shown in Figure 12a and the specification is shown in Table 5b.

Table 5. Specifications of AWS calibration tools; (a) Digital barometer, (b) Digigal Assmann psychrometer, and (c) Rain gauge calibmeter.

(a)

Item	Specification
Range	800 – 1100 hPa
Accuracy	±0.1 hPa
Stability	±0.1 hPa/year
Display	LCD display
Operating range	–10 – +40°C
Output	0 – 1V

(b)

Item	Specification
Sensor	Pt 100Ω
Range	–30 – +50°C
Resolution	0.01°C(dry), 0.1% RH
Display	LCD display
Ventilation	Sirocco fan
Ventilation speed	4 – 6 m/s

(c)

Item	Specification
Body	Portable type
Volume	653 mL
Nozzle	100 mm/h, 300 mm/h
Size (mm)	400x290x100
Weight	2.0 kg

3.2.3. Rain Gauge Calibmeter

Unlike other meteorological factors, precipitation has low spatiotemporal uniformity, and precipitation phenomena do not always occur. Therefore, it is not realistic to carry out comparative observation of rain gauges for actual precipitation during inspection period. For this reason, calibration of rain gauges during inspection period will be carried out using a calibration device. In this project, we will introduce rain gauge calibmeter, HyQuest Solutions FCD–653 (Figure 12b).

This device consists of a transparent cylinder with a capacity of 653 ml and a nozzle that screwed into the bottom of the cylinder. A pre–set volume of water will discharge to the tipping bucket rain gauge. This process is to be repeated a second time for an accurate calibration check. In order to confirm that the results come within the acceptable range, the number of tips will be manually counted or stored on the data logger and then compared with the total volume of water dropped from FCD 653. Two types of nozzles are available: 100 mm/h and 300 mm/h rainfall intensity, respectively. This makes it possible to confirm the linearity of rain gauge data with respect to rainfall intensity. The specification of this device is shown in Table 5c.

3.3. Analysis of continuity of observation from SYNOP to AWS

Wind speed, temperature, and humidity in the surface boundary layer, from surface to 20 to 50 m in height, have a strong height dependency, and the catching rate of the rain gauge strongly depends on the wind speed, too. For these reasons, if the heights and/or site location of the rain gauge, anemometer, and thermo–hygrometer will change, precipitation, wind speed, temperature, and relative humidity data will be suffered non–negligible effect [4].

Changes of sensor type and/or in the location of sensor may also have a significant effect on the observation data.

In recent years, in VNMHA, the surface meteorological observation is shifting from manned SYNOP observation to AWS observation. In that case, even if AWS is installed in the same observation field, the sensor type, location, and sensor height are generally different. Surface meteorological observation has a mission not only to monitor nowcasting for meteorological disaster prevention but also to monitor long–term climate change. Therefore, when the surface meteorological observation is changed from SYNOP to AWS, in order to ensure the continuity of observation, it is necessary to check its continuity and, if needed, to correct the AWS observation data.

Double mass analysis is a simple analytical method to inspect the continuity of rain gauge observations and correct the data [5]. In this project, we have practiced training on double mass analysis to members of the working group of the surface meteorological observations.

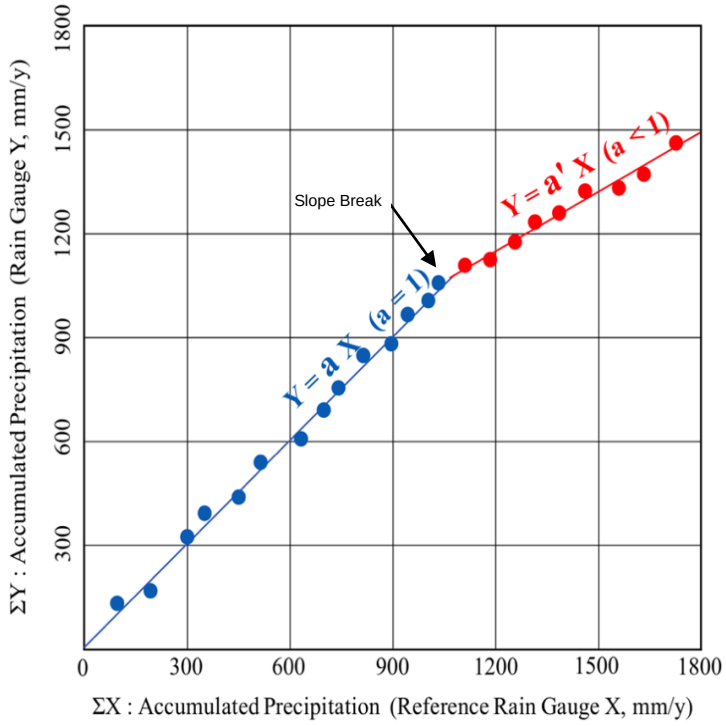

Figure 13. An example of double mass plot of rain gauges X and Y (mm/y).

The consistency of a rainfall record can be tested with double–mass analysis, which compares the cumulative annual (or alternatively, seasonal) value of station Y with those of a reference rain gauge X. In this case, the reference rain gauge is the SYNOP rain gauge adjacent to the AWS rain gauge. This method compares the cumulative annual (or alternatively, seasonal) value, ΣY, of rain gauge Y with those, ΣX, of a reference rain gauge X. The cumulative pairs (double-mass values) are plotted in an x–y arithmetic coordinate system (Figure 13). If the relation between X and Y is linear, the relation of $Y = aX$ is obtained. And if $a = 1$, it can be said that there is no difference in the measurement of both rain gauges. If a is not equal 1, the observation of rain gauge Y is underestimated ($a < 1$) or overestimated ($a > 1$) compared with reference rain gauge X. Also, if the plot shows a "slope break" (Figure

13), the observation at station Y has been inconsistent with the reference rain gauge since the slope changed and should be corrected.

3.4. Seminar and training on maintenance and calibration of AWS for observatory staff

In order to perform reliable and accurate AWS observation, it is necessary to keep AWS in good condition so that each sensor and each part of the AWS system can function properly. For that purpose, it is not enough to carry out a maintenance and comparative observation check according to a set procedure on the manual. For example, questions such as "has there been any change in the system status compared to the previous maintenance record?" and "what will be the cause?" are important attitude in advance to the inspection. Such consideration may lead to the early detection of instrument abnormality. In addition, "why a significant difference was observed in comparative observation?", such consideration may deepen the understanding of meteorological phenomenon and of the meaning of the observed data.

Therefore, this project has conducted training and seminars on the surface meteorological observation technology for VNMHA's WG members and staff. The contents are (1) the introduction of the WMO surface meteorological observation guideline, (2) an introduction of the atmospheric boundary layer near the surface, which has different characteristics from the free atmosphere, and (3) the introduction of principles and features of various meteorological observation instrument. Hereafter, we would like to share these training materials to the staff who could not attend the training and seminars.

In the training in Japan from June to July 2019, experts from JMA conducted a lecture on the meteorological agency's surface meteorological observation technology and practiced the training on the calibration of AWS instruments using periodic calibration tools proposed in this project. And we will plan to perform On the Job Training (OJT) for AWS periodic maintenance and calibration at the AWS sites in the North–East and North–Central RHMCs using these calibration tools.

4. Installation of ARG for radar data calibration

This section presents installation of ARGs for the calibration of two radars located at Phu Lien and Vinh towards upcoming QPE. The ARG installation is planned as one of the activities in this project, which is tightly linked to advanced activities such as accurate precipitation estimates based on QPE and development of Mobile Website in the JICA project. JICA expert team designed an implementation plan consists of five steps, i.e. survey, design, preparation, installation and evaluation based on their experiences in ARG installation in other countries. Based on this implementation plan, JICA experts promoted various practical works in cooperation with VNMHA staffs. The following sections give an outline of their remarkable works.

4.1. Survey

From the outcome of the BLS in June 2018, it was confirmed that all ARGs should be installed at VNMHA observation stations and that ARG data should be collected at real time by VNMHA headquarters in Hanoi.

To find candidate stations within coverages of Phu Lien and Vinh Radars, radar–beam shadow diagrams shown in Figures 14a and 14b were used.

Site survey of 20 candidate stations had been implemented for 15 days. The survey consists of 47 check items technically inclined and staff interview mainly about operation and natural disaster risks around the station. Survey results and recommendation of ARG installation sites (stations) were reported to VNMHA and then ARG installation at 18 ARG sites was approved in December 2018. 18 ARG installation sites are shown in Figure 15.

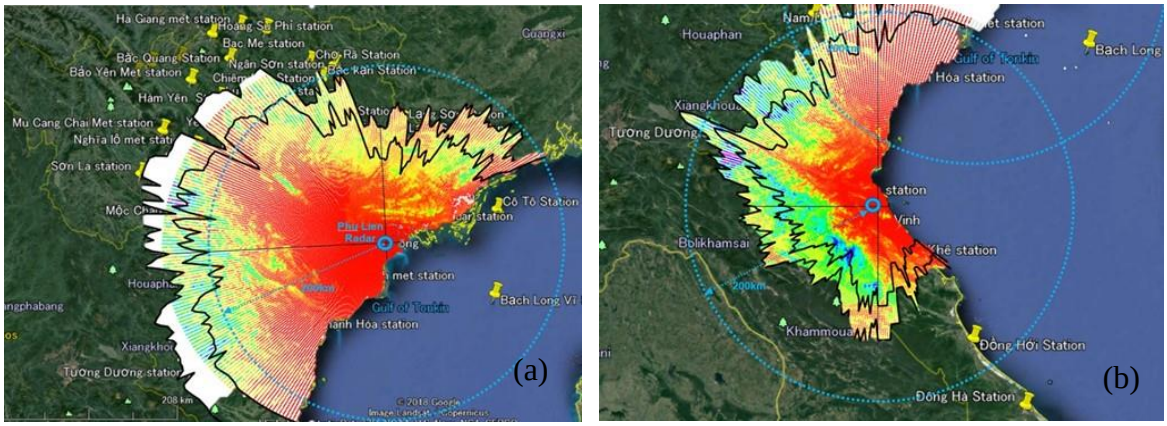

Figure 14. (a) Phu Lien; (b) Vinh radar–beam shadow diagrams.

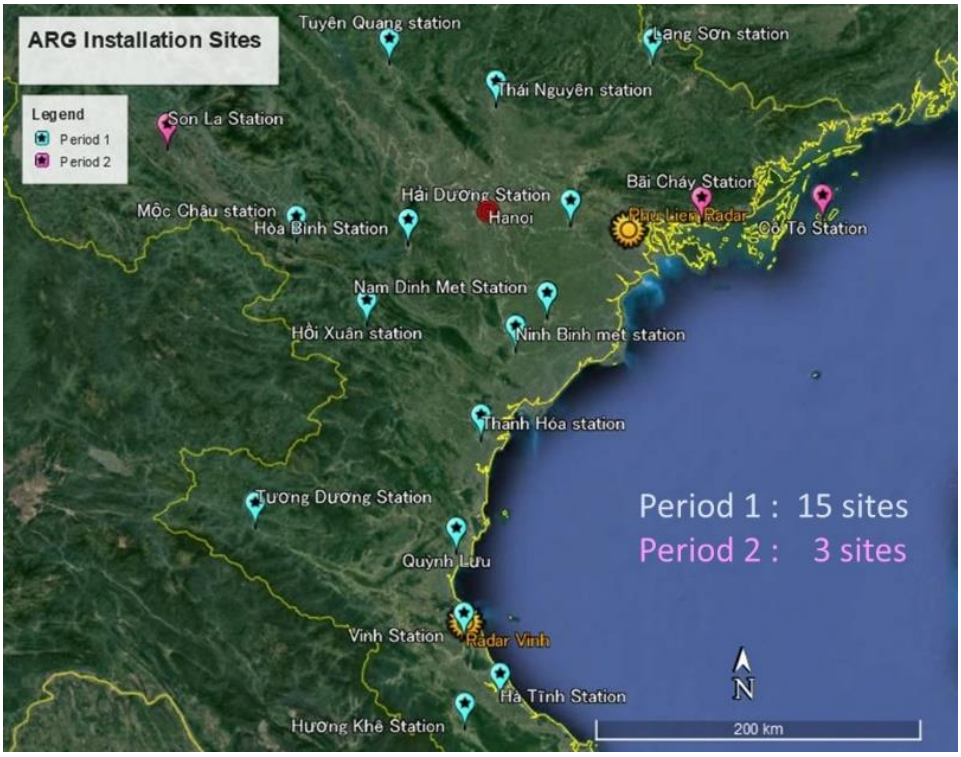

Figure 15. Map for ARG installation sites within Phu Lien and Vinh radar coverages.

4.2. Design

Most of design factors for ARG equipment were easily decided thanks to the site survey and experiences of ARG installation projects in other countries. On the other hand, telecom means from the equipment at local site to a data collection server in Hanoi and civil work

design required additional study and deep considerations. The final design to procure ARG equipment is illustrated in Figure 16.

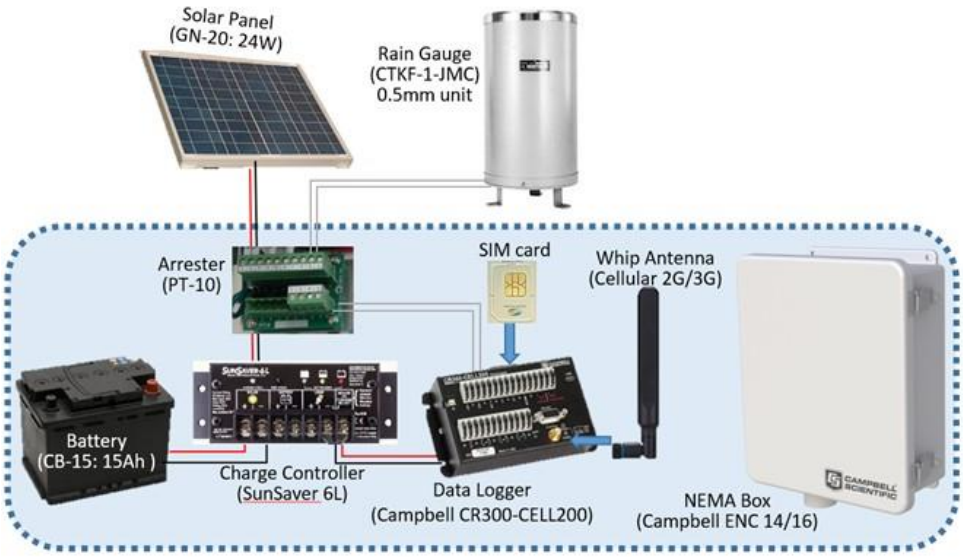

Figure 16. Design for ARG equipment.

To find most appropriate telecom means for ARG data collection, several options were studied such as Internet IP socket, email on the Internet via mobile networks, long distance Wi–Fi and Short Message Sending (SMS) on mobile telephone network. After the study, actual verification tests of a few options were implemented in November and December 2018. The Working Group with IDC experts discussed and finally decided a telecom means based on the test results as a real–time data collection network shown in Figure 17.

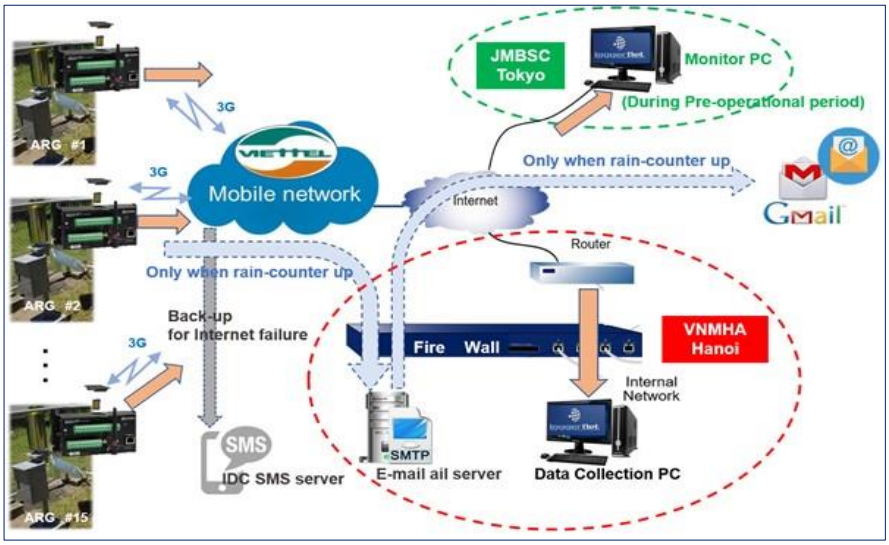

Figure 17. Design of ARG data collection network.

3G mobile network provided by Viettel is used for site access. Three telecom methods are configured to correct ARG data at every 10-minute interval. The main method is TCP Socket connection and the supplementary one is e–mail via the Internet. As the third one

Short Message Sending (SMS) is used for backup when the collection via the Internet failures. To finalize the civil work, design the issues of foundations and stanchions were studied and concluded in cooperation with a constructive material manufacturer. In the site survey at North Central RHMC (Vinh), a new foundation and a stanchion preliminary manufactured were strictly evaluated by JICA experts and counterparts under the manufacturer stands. Figure 18 illustrates a final design for a foundation and a stanchion.

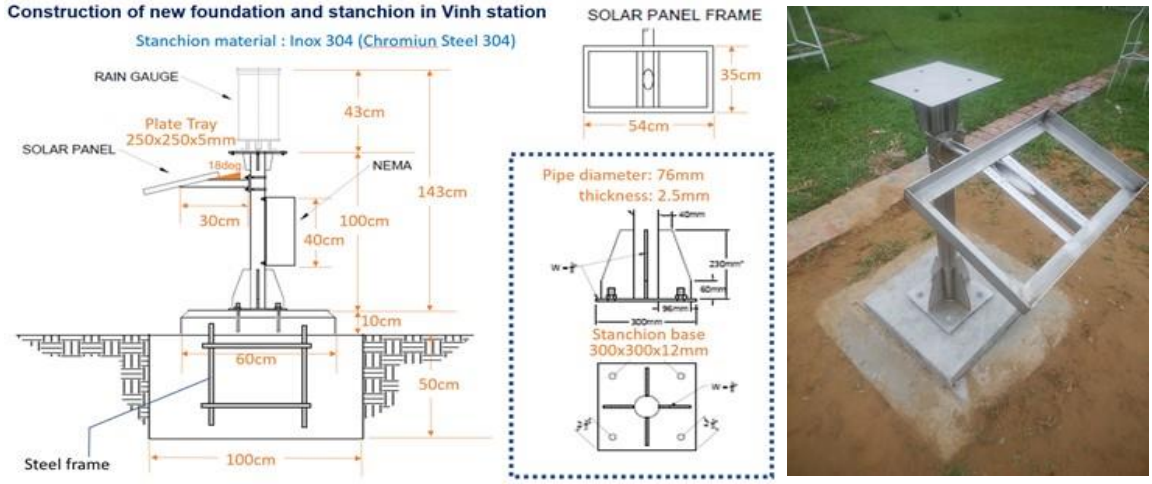

Figure 18. Foundation and stanchion for ARG (left: design drawing, right: real ones in Vinh).

4.3. Preparation

According to JICA guidelines, procurement of ARG equipment for installation in Period I of the project, development of data logger programs and functional inspection were implemented in Japan by the end of February 2019.

Although there was delay due to trouble of tax exemption procedures in shipping, 15 ARGs for Period I became available at VNMHA HQs in September 2019. Then VNMHA staff and JICA experts commenced practical preparation at VNMHA HQs such as acceptance test, procurement and establishment of data collection servers, development of installation guides and check list and schedule for the on–site installation. Figure 19 shows preparation examples.

Since 15 Rain Gauges of tipping bucket type at 0.5 mm unit were required accuracy and reliability, they were certificated by VNMHA as an item for the acceptance test in addition to the certification by JMA.

Figure 19. Preparation examples for ARG installation.

4.4. Installation

After reconfirmation of the civil work at 15 sites, two installation teams which consist of JICA experts and VNMHA staffs were formed and then conducted the installation parallelly in September and October 2019. Installation procedures were instructed in detail according to about 30 work items in the installation guide. At the same time technical transfer to VNMHA staffs including on-site observers was practically implemented through preliminary installation rehearsal and on–site OJT. Figure 20 shows installation works and pictures of on–site OJT.

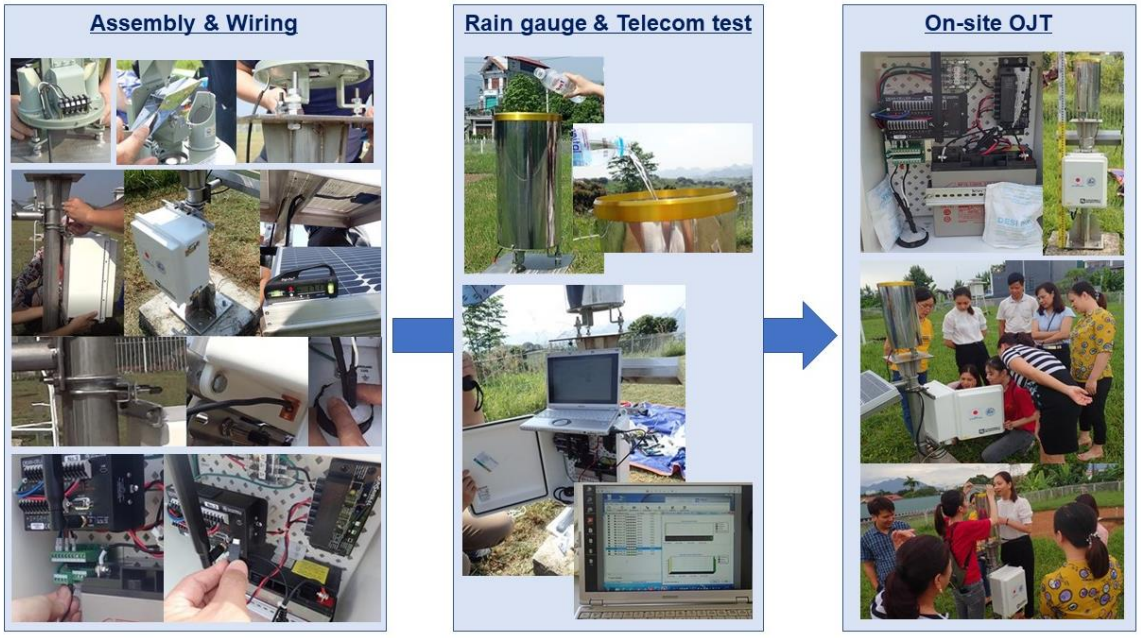

Figure 20. Installation works and on–site OJT.

4.5. Evaluation

After installation of 15 ARGs for Period I and ARG data collection servers, the ARG network system entered the pre–operational phase from 19 October 2019. Thereby pre–operating environment to use ARG data for radar calibration was established. JICA experts have been monitoring to evaluate the long–running status to adjust operational parameters towards official operation phase. The monitoring result is shown in Table 6.

Table 6. Monitoring results of the pre–operation.

Station Name	Transmission Success Rate [%]			3G Signal Intensity [dBm]			Battery Voltage [V]		
	TCP Socket	E-mail	SMS	max	min	ave	max	min	ave
Moc Chau	99.9	51.9	94.3	–51	–73	–52	14.6	12.7	13.3
Hoa Binh	100.0	68.8	96.1	–51	–81	–55	14.5	12.8	13.2
Lang Son	99.8	76.9	92.7	–57	–73	–62	14.7	12.7	13.3
Tuyen Quang	99.9	58.0	89.7	–51	–63	–53	14.6	12.7	13.2
Thai Nguyen	99.8	51.2	96.1	–51	–91	–53	14.5	12.7	13.3
Hai Duong	91.5	54.3	0.9	–51	–85	–73	14.5	12.8	13.3
Nam Dinh	100.0	79.8	76.2	–61	–69	–64	14.5	12.8	13.3
Ninh Binh	99.9	52.0	77.3	–51	–69	–59	14.5	12.8	13.3
Hoi Xuan	99.8	51.7	77.1	–51	–69	–59	14.6	12.8	13.3
Thanh Hoa	100.0	70.7	60.3	–51	–69	–55	14.5	12.6	13.3
Tuong Duong	99.8	54.0	71.2	–55	–69	–61	14.6	12.7	13.2
Quynh Luu	97.2	49.7	77.1	–57	–91	–75	14.5	12.8	13.3
Vinh	99.8	58.2	60.4	–53	–77	–65	14.5	12.8	13.2
Ha Tinh	100.0	85.0	72.2	–51	–69	–61	14.4	12.8	13.2
Huong Khe	99.9	66.6	65.7	–51	–87	–75	14.5	12.5	13.2

5. Summary and Discussion

On 17th of November 2017, VNMHA and JICA exchanged the Record of Discussion (R/D) for "the project for enhancement of capacity in weather forecasting and flood early warning system". In this project, a unified AWS maintenance report and calibration tools were proposed to enhance reliability of long–term operation of AWS and its observation accuracy.

By sharing the AWS unified maintenance report as a digital metadata file among the observation site, regional hydro–meteorological centers and VNMHA data center, it will be capable of maintaining and managing the AWS system and equipment for many years.

The proposed AWS calibration tools consist of digital barometer, digital Assmann ventilating psychrometer, and rain gauge calibmeter. Each instrument will be verified by the standard instruments of Instrumentation Center in Hanoi, Da Nang, and Ho Chi Minh to ensure traceability. Then, they are used for comparative observations with AWS instruments for the purpose of calibration of each sensor.

In addition to introducing measures at observation sites that we have seen so far, for the purpose of improving the reliability of AWS data, the following technical development can

be considered as the next target. That is, a feasibility study for introduction of the QC and AQC technologies at the data center of VNMHA for the purpose of improving the reliability of AWS data. Currently, center QC of observation data collected in VNNHA's IDC is not performed, and there is a risk of missed preliminary warnings and false announcements due to data whose quality is not guaranteed. Currently, the AWS data format of each donor and the measurement time interval are not uniform, for this, it is a challenge to introduce AQC immediately. But there are rooms to make a technical consideration for introducing AQC as pre–process after archiving AWS data to IDC.

As we have seen, in order to calibrate the radar signals of Phu Lien and Vinh for the development of QPE, we have planned to install the ARG network totally 18 locations in this project. As of June 2020, we have already completed the installation at 15 locations.

Author Contributions: Analysis and writing–original draft preparation, Dr. Mikami, Mr. Matsubara, Mr. Ichijo, L.X. Duc and N.H. Anh; writing–review and editing, Dr. Mikami and Mr Ichijo; All authors have read and agreed to the published version.

Acknowledgments: This JICA technical cooperation project was supported by the people of Japan as JICA projects and technical assistances by JMA as DRR technical cooperation of WMO international cooperation frame for southeast Asian countries. Specific thanks to JICA Tokyo experts who supports the project and Meteorological and Hydrological Administration (VNMHA) who have joined in the JICA Project for Strengthening Capacity in Weather Forecasting and Flood Early Warning System in the Social Republic of Vietnam.

Conflict of interest: The authors declare no conflict of interest.

References

1. World Meteorological Organization. Guide to the Global Observing System, **2014**, *WMO–No.488*; 1163p.
2. Harrison, R.G.; Wood, C.R. Ventilation effects on humidity measurements in thermometer screens. *Q. J. R. Meteorol. Soc*. **2012**, *138*, 1114–1120. DOI:10.1002/qj.985.
3. Nakai, S.; Yokoyama, K. The importance of the correction of wind–induced under catch of the gauges: The necessity for compilation of metadata on the gauges. *Tenkii.* **2009**, *56*, 11–16 (in Japanese).
4. Stull, R.B. An Introduction to Boundary Layer Meteorology. Kluwer Academic Publishers, Dordrecht, The Netherlands, 1988, pp. 376–389.
5. Searcy, J.K.; Hardison, C.H. Double–Mass Curves. *Geological Survey Water–Supply Paper,* **1960**, *1541–B*, 34–40.

VIETNAM JOURNAL OF HYDROMETEOROLOGY

Research Article

Quantitative Precipitation Estimation by Combining Rain gauge and Meteorological Radar Network in Viet Nam

Chiho Kimpara[1], Michihiko Tonouchi[2], Bui Thi Khanh Hoa[3], Nguyen Viet Hung[3], Nguyen Minh Cuong[3], Kenji Akaeda[4,*]

[1] Japan Weather Association, Tokyo170–6055, Japan; kimpara.chiho@jwa.or.jp
[2] Japan Meteorological Business Support Center, Tokyo101-0054, Japan; tono@jmbsc.or.jp
[3] Aero–Meteorological Observatory, Hanoi 10000, Vietnam; khanhhoa303@gmail.com; truongphi115@gmail.com; nguyenminhcuong_T59@hus.edu.vn
[4] Japan International Cooperation Agency, Tokyo102–0084, Japan; akaeda191@yahoo.co.jp
***** Correspondence: akaeda191@yahoo.co.jp; Tel.: +84–82–976–1096

Received: 17 July 2020; Accepted: 20 August 2020; Published: 25 August 2020

Abstract: Real–time monitoring of quantitative precipitation distribution is essential to prevent natural disasters caused by heavy rainfall. Precipitation distribution by rain gauge network or combined with radar/satellite data is operationally used in Viet Nam. Previously, meteorological radar data was simply converted to precipitation amount by using simple Z–R relationship. In order to get the accurate quantitative precipitation estimation (QPE) data, converted precipitation amount from radar should be corrected by rain gauge data. In the ongoing JICA technical cooperation project, preliminary development of the QPE product has been conducted by utilizing the data from the automatic rain gauge network and meteorological radar network in Viet Nam. The fundamental part of this QPE algorithm has been used and updated in Japan Meteorological Agency (JMA) for more than 25 years. This is the first attempt to get quantitative precipitation distribution with precise resolution by combining radar and rain gauge data in Viet Nam. This paper describes each process to introduce this QPE method to Viet Nam and indicates some preliminary results. Several issues to improve its accuracy is also proposed.

Keywords: Radar; Rain gauge; QPE; Quality Control; JICA.

1. Introduction

Natural disasters such as landslides, floods, and inundations caused by heavy rainfall occur in Viet Nam every year. These disasters cause not only human damage but also economical loss to the country. To mitigate these damages, it is necessary to statistically analyze hydrological and geological relationship between precipitation amount and the occurrence of disaster. Based on these relationships, accurate and prompt meteorological information and/or warning should be issued before a disaster occurs. As an indicator for precipitation monitoring, quantitative precipitation estimation (QPE) plays a central role and therefore should be calculated and monitored in real–time.

Since June 2018, a bilateral cooperative project between the Japan International Cooperation Agency (JICA) and the Viet Nam Meteorological and Hydrological Administration (VNMHA) named “Strengthening capacity in weather forecasting and flood early warning system in Viet Nam” has been conducted. This project is related to the quantitative utilization of S–band radars that were installed at Hai Phong (Phu Lien) and Vinh

in September 2017 by another grant aid project. Detailed reviews of this JICA project are given by Tonouchi et al. (2020) [1]. One of the main targets of the JICA project is the quantitative utilization of these radar data and precipitation estimation.

Three observation systems are used to estimate precipitation distributions in VNMHA; (1) meteorological radar, (2) meteorological satellite and (3) rain gauge. Each system has its strengths and weaknesses as follows. First, the major remote sensing tool for precipitation land is the meteorological radar. Key topographic uncertainties in radar observation are due to the curvature of the Earth and radar beam broadening with detection range; moreover, precipitation estimation is expected to be the most accurate where the radar beam is close to the ground. Therefore, scanning strategy is important to get observational data close to the ground while avoiding beam blockage by the mountain. Other sources of uncertainties in radar precipitation estimation include radar reflectivity–rain rate (Z–R) relations resulting from variable drop size distributions, lack of consistent radar hardware calibration, evaporation of raindrops as they fall through the air, and horizontal advection below the radar sampling volume due to wind shear. Improvements are also needed on quality control (QC) of radar data to remove ground/sea clutter, biological targets, and other non–precipitation echoes.

While generally acknowledged to have significantly greater uncertainty than radar, precipitation estimation from satellite data provides continuous spatial coverage and can be valuable where radar data are unavailable or known to be unreliable. Various techniques have been developed to estimate precipitation from infrared (IR) and microwave satellite observations [2]. IR data corresponds to cloud top feature which is not directly related to precipitation amount. Passive microwave sensors provide a stronger indicator of precipitation than IR sensors, although microwave instruments are presently available only on limited satellites with a typical sampling frequency of twice per day per satellite and a spatial resolution on the order of 15 km. Satellite estimates also need to be quality controlled to screen out non–precipitating clouds.

In situ rain gauges provide direct measurement of point precipitation as well as a surface reference for adjustment and evaluation of, and merging with, remotely sensed precipitation. Because of the various limitations of radar and satellite estimations as described earlier, rain gauge data secures the accuracy of QPE. Improved precipitation products must draw from each system's strength in an optimal way. In particular, meteorological radar can provide high–quality estimation in regions of appropriate observation conditions. Satellites are the secondary source of data followed by radars. Detailed description of the characteristics of these three observation systems are referred [3].

In Viet Nam, radar reflectivity data is previously converted to precipitation amount by simple Z–R relationship by assuming Marshal–Palmer size distribution. This relation is commonly used as an averaged raindrop size distribution and therefore estimation error becomes large when the drop size distribution is different from Marshal–Palmer's. In order to get the accurate precipitation amount, converted precipitation amount from radar should be corrected by rain gauge data. In this paper, new method of combining radar and rain gauge is applied [4–5] and shows some preliminary results.

2. Observation network in Viet Nam

In VNMHA, two types of rain gauge stations are under operation. One is manual rain gauge stations which are located at 370 locations as shown in Figure 1a. The staff on duty at the station measures the accumulated rain amount every six hours. The other is automatic rain gauge (ARG) stations located around 1400 points as shown in Figure 1b. In these ARG stations, 10–minutes rainfall amount is recorded and transferred to the data center at the VNMHA headquarter every hour. However, different ARG systems have been installed depending on the organization that installed them, such as VNMHA, the World Bank, Italy

and South Korea. Their data formats and data monitoring/controlling systems differ, depending on their manufacturers.

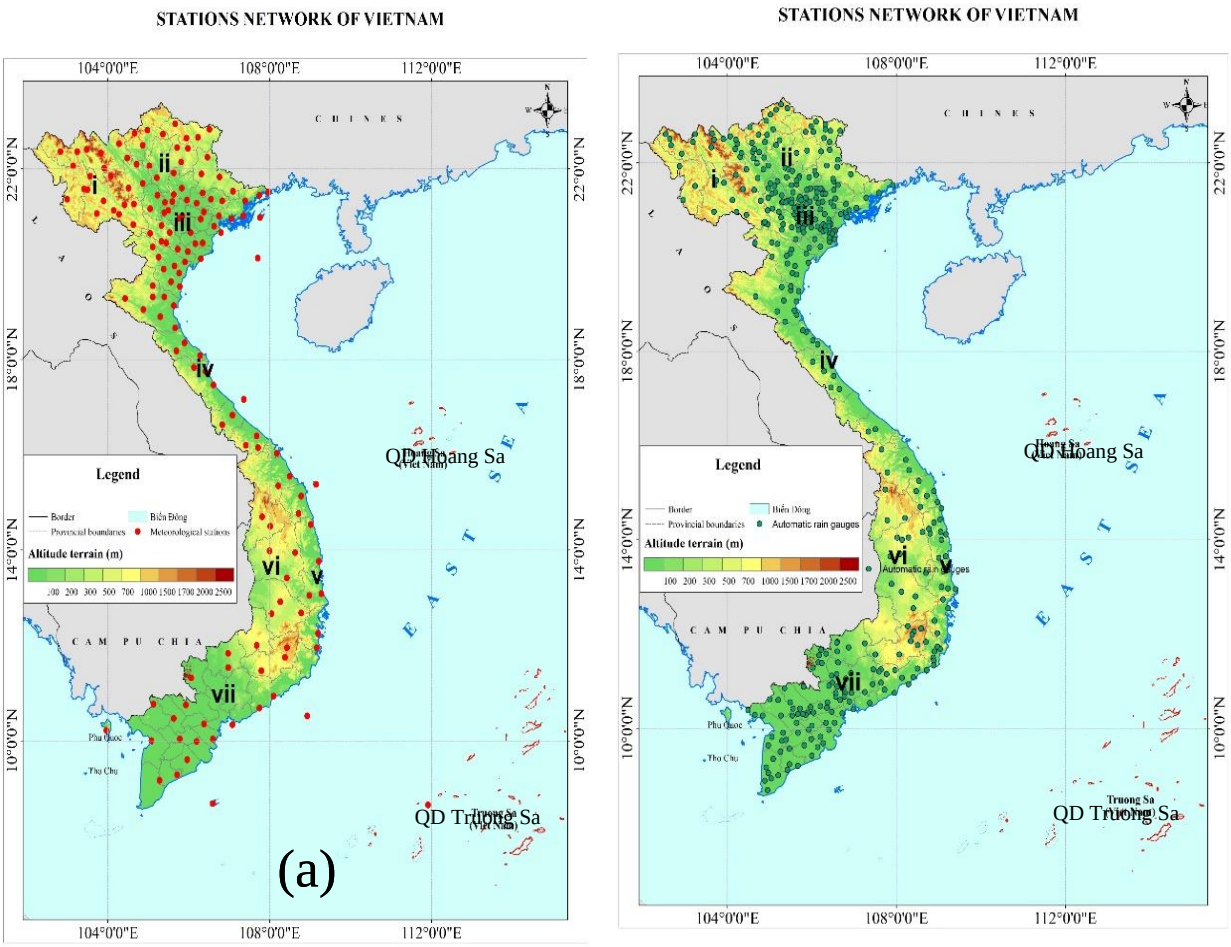

Figure 1. Surface rainfall observation network in Viet Nam: (**a**) Meteorological stations; (**b**) Automatic rain gauge (ARG) stations.

Currently, ten meteorological radars of VNMHA are operated by the Aero–Meteorological Observatory (AMO). Their locations and maximum detection range are shown in Figure 2 and their characteristics are shown in Table 1. Several different generations and types of radars are operated. The radar network consists of two S–band radars and eight C–band radars, and consists of one conventional radar, six Doppler radars, and three dual–polarized Doppler radars. Eight radars are newly replaced ones (including a minor upgrade of signal/data processing unit) in the past few years and the remaining two radars are scheduled to be replaced shortly. These radars almost cover the whole country and surrounding sea except some undetectable areas in the northwestern mountainous region.

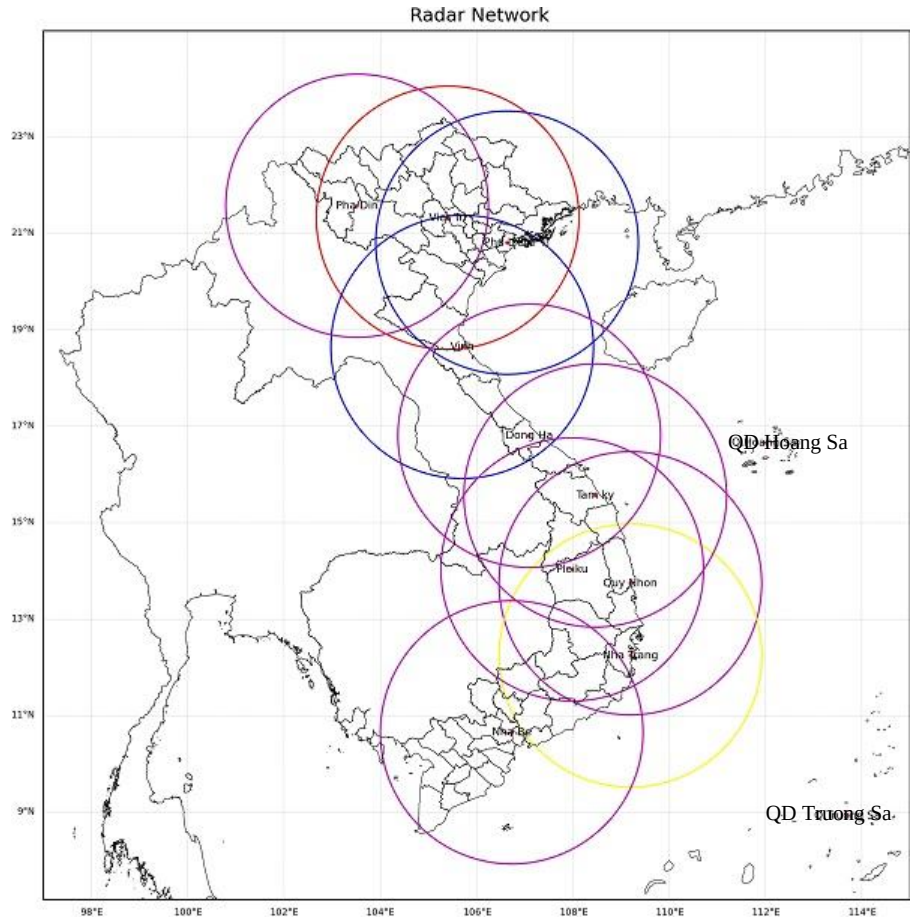

Figure 2. Meteorological radar network in March 2020. Purple circles represent Vaisala radars, blue circles as Japan Radio Company (JRC) radars, red circle as Thompson radar and yellow circle as Enterprise Electronic Corporation (EEC) radar.

Table 1. Characteristics of radars. D and S in the third column indicate dual–polarized radar and single–polarized radar, correspondingly. First and second values in the detection range column show maximum detection range in intensity mode and Doppler mode respectively.

Radar Site	Height (m)	Type	Band	Detection Range (km)	Beam Width (deg)	Manufacturer
Pha Din	1470	D	C	300/120	1.0	Vaisala
Viettri	40	S	C		1.1	Thompson
Phu Lien	146	S	S	450/200	1.7	JRC
Vinh	92	S	S	450/200	1.7	JRC
Dong Ha	40	S	C	300/120	1.2	Vaisala
Tam Ky	52	S	C	300/120	1.2	Vaisala
Pleiku	842	D	C	300/120	1.0	Vaisala
Quy Nhon	582	D	C	300/120	1.0	Vaisala
Nha Trang	57	S	C	240/120	1.0	EEC
Nha Be	35	S	C	300/120	1.0	Vaisala

3. Method of quantitative precipitation estimation

As mentioned in the introduction, rain gauge and radar have both strengths and weaknesses to estimate precipitation distribution. Rain gauges can measure accurate precipitation amounts, but they provide only point measurements. In case of convective rain, precipitation intensity changes within the scale of several kilometers. Therefore, numbers of rain gauges are necessary to estimate the distribution of precipitation. On the contrary, radar can estimate qualitative precipitation distribution with the resolution of 1 km. Radar measures the intensity of return echoes from targets (hydrometeors) but therefore it does not have direct relationship with the amount of precipitation. The physical unit of precipitation amount is related to the third power of raindrop diameter, but echo intensity is proportional to the sixth power of raindrop diameter. To link these two parameters to derive precipitation amount, Z–R relationships are used but various drop size distributions of the precipitation are assumed as one. In this project, one from Marshall–Palmer's observation is used. When radar–derived precipitation is calibrated with rain gauges, more accurate QPE is available while compensating weakness of radar and rain gauges.

In this project, one–hour accumulated rain gauge data and one-hour accumulated radar intensity are combined based on the method developed by JMA [4]. Rain gauge data and radar intensity data have different characteristics such as the difference between point data and spatial data or surface data and low–level not surface data. In order to calculate QPE stably, data accumulation is necessary. By using this method, the QPE product with 1 km resolution is calculated every 1 hour for 1 hour accumulated rainfall amount.

The algorithm of QPE is summarized in Figure 3. This algorithm consists of five major processes, 1) quality control and one hour accumulation of rain gauge data, 2) convert from radar volume scan intensity data to lowest level distribution and one–hour accumulation, 3) 1st calibration by rain gauge data, 4) 2nd calibration by rain gauge data, 5) produce a national composite map.

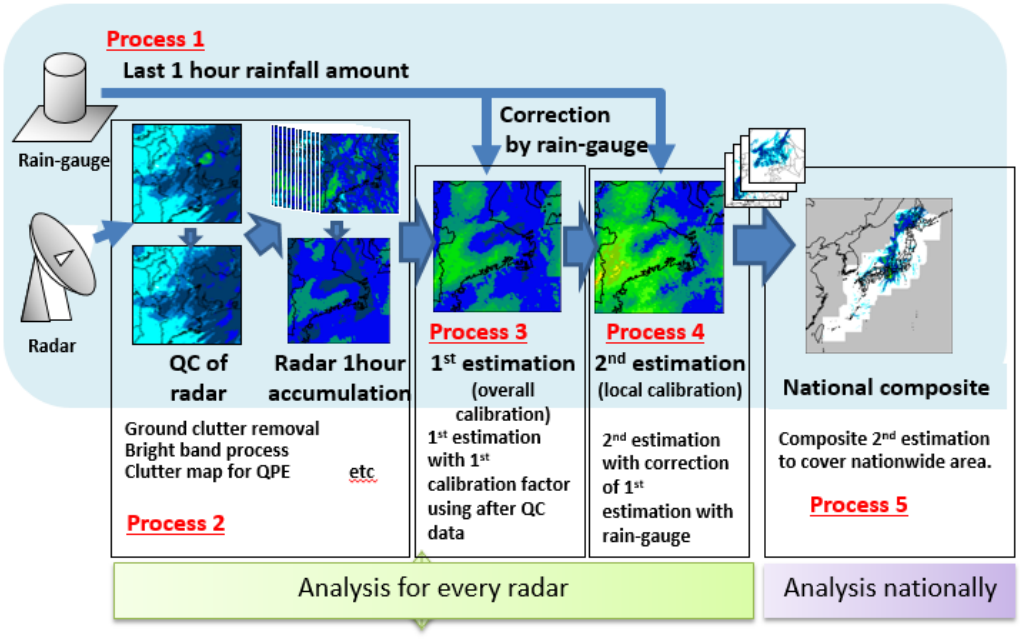

Figure 3. Schematic algorithm for QPE.

Even if several radars observe the same grid mesh, the values of one–hour accumulated precipitation may not be the same. Also, the values of one–hour accumulated precipitation right above a rain gauge may not be the same as the one–hour precipitation amount of the rain gauge. This is because of the following reasons;

- Error due to the assumption in Z–R relationship.
- The mechanical characteristics of the receiving sensitivity in each radar.
- Radio wave attenuation due to precipitation in the transmission path and wet radome.
- Error due to the different rain distribution between the upper air and the ground. The higher the radar beam passes through, the larger the error will be.

Therefore, one–hour accumulated precipitation E_0 from the radar must be calibrated to fit the value of the rain gauge. The calibrated one–hour accumulated precipitation value is called the 1st calibrated value E_1, and the correction quantity is called the 1st (precipitation) calibration factor. Several conditions to determine the 1st calibration factor σ are as follows,

- The factors for the errors differ in each radar and time, therefore the 1st calibration factors σ are determined in each radar and in each hour.
- The 1st calibrated precipitation E_1 should take the same value at the area where two neighboring radar overlap.
- The 1_{st} calibrated precipitation E_1 should be corresponding to the amount of the one–hour precipitation from rain gauge.

For estimating the 1st calibration factor σ, first we determine 1st calibrated precipitation E_1 as in below.

$$E_1=\sigma E_0 \tag{1}$$

From Condition 1, σ is the function of time t, which can be written as $\sigma(t)$. From Condition 2, assume that there is common observation area A and B, and at the certain point, the calibrated precipitation from both radars should be the same value. But in actual cases, it will not be the same. Therefore, we need to consider the residue δ_1 as;

$$\delta_1=(\sigma_a\,(E_{ab}\,)-\sigma_b\,(E_{ba}\,))^2 \tag{2}$$

where E_{ab} is the reflectivity from Radar A and E_{ba} is from Radar B at the certain point.

From Condition 3, where $\langle R_{ab}\,\rangle$ is defined as the mean value of 1–hour precipitation among rain gauges in area A∩B, and mean values from the radar are defined as the figure, it can be written as;

$$\sigma_a\,\langle E_{ab}\,\rangle=\langle R_{ab}\,\rangle,\ \sigma_b\,\langle E_{ba}\,\rangle=\langle R_{ab}\,\rangle, \tag{3}$$

But in actual cases, they will not be as the equation. Therefore, we need to consider the residue δ_2 as below.

$$\delta_2=(\sigma_a\,\langle E_{ab}\,\rangle-\langle R_{ab}\,\rangle)^2+(\sigma_b\,\langle E_{ba}\,\rangle-\langle R_{ba}\,\rangle)^2 \tag{4}$$

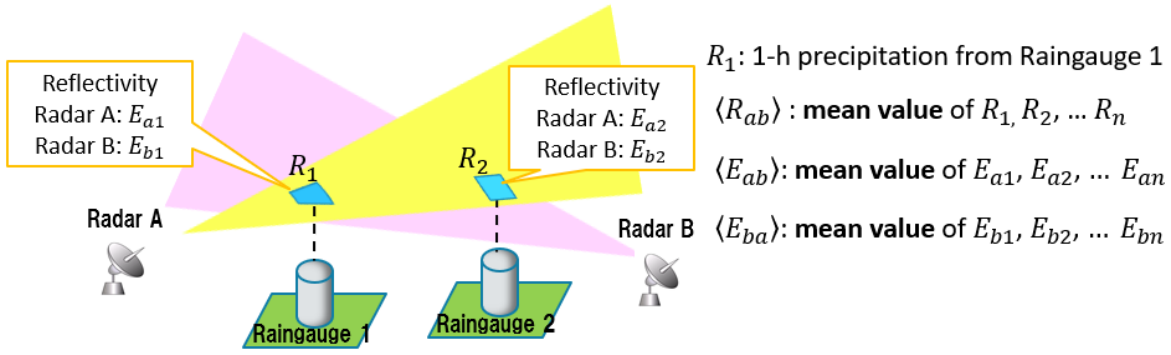

Figure 4. Schematic view of parameters for estimating 1st calibration factor σ.

Residue δ_1 and δ_2 are summed up in Equation 5 as residue Δ, where α is a parameter.

$$\Delta \equiv \delta_1 + \alpha \delta_2 \tag{5}$$

When δ_1 and δ_2 take the optimum value, residue Δ takes the minimum value. First calibrated factor may be determined by solving the simultaneous partial differential equation for σ_a and σ_b on this residue Δ.

Second calibration is a process to calibrate locally to each rain gauge sites. The 2nd calibration factor is determined at each rain gauge mesh by comparing 1st calibrated precipitation and rain gauge one–hour precipitation. At the grid of raingauge, the ratio of 1st calibrated precipitation and 1–hour rainfall of the rain gauge is set as the temporal 2nd calibration factor.

When $R(\vec{r})$ is 1–hour rainfall of the rain gauge at point $\vec{r}$ and E_1 $(\vec{r})$ is 1st calibrated precipitation at that grid, temporal 2nd calibration factor at point $\vec{r}$ is described as below.

$$\varphi(\vec{r}) = \frac{R(\vec{r})}{E_1(\vec{r})} \tag{6}$$

When the temporal 2nd calibration factor is set at the grid of rain gauge, 2nd calibration factor at the other grid is calculated by interpolating the temporal 2nd calibration factor $\varphi(\vec{r})$. The 2nd calibration factor $\chi(\vec{r_0})$ at the grid $\vec{r_0}$ can be described when using $\varphi(\vec{r_i})$ as the temporal 2nd calibration factor at rain-gauge i grid $\vec{r_i}$, parameter ϖ and weight w_i

$$\chi(\vec{r_0}) = \exp\left\{\frac{\sum_i(\varpi w_i + 1)\ln\varphi\,(\vec{r_i})}{\sum_i(\varpi w_i + 1)}\right\} \tag{7}$$

where

$$w_i = w_D \times w_R \tag{8}$$

This calculation will be repeated three times to make well–fit and smooth interpolation. Finally, these 2nd calibration factors at each rain gauge mesh are interpolated to make a distribution of 2nd calibration factor. The weighting factor for interpolation is a function of distance between the target mesh and rain gauge and precipitation type. By using the 2nd calibration factor, 1st calibrated precipitation E_1 is converted to 2nd calibrated precipitation E_2, which is the result of the QPE. Detailed explanations on this QPE algorithm are given in [4–7].

4. Characteristics of rain gauge data and quality control

The total number of ARG stations is around 1400 from the station list. In order to keep a qualified QPE product, quality control of rain gauge data is vitally important. There are three types of errors affecting rain gauge data such as trouble of rain gauge system, transmission error, and environmental change surrounding rain gauge. Before the test operation of QPE started in July 2019, all ARG data with the present format were temporarily checked. Since ARG did not have enough data for the rainy season, the main targets were to detect the transmission error and abnormal values to remove suspicious ARG stations. We used the following simple conditions to check the quality of each ARG.

The ratio of missing data is less than 5% or not

Comparing rain amount with an adjacent station located around 5 to 10 km and both observational values are not so different

By using the observation data between December 2018 and June 2019 at about 950 ARG stations, we checked the missing rate. Figure 5 shows the distribution of the missing rate. 745 stations have less than 5% of the missing rate. Figure 6 shows the locations of high missing stations. They distribute extensively in the country and need to know the cause of these missing stations to improve the quality of rain gauge data.

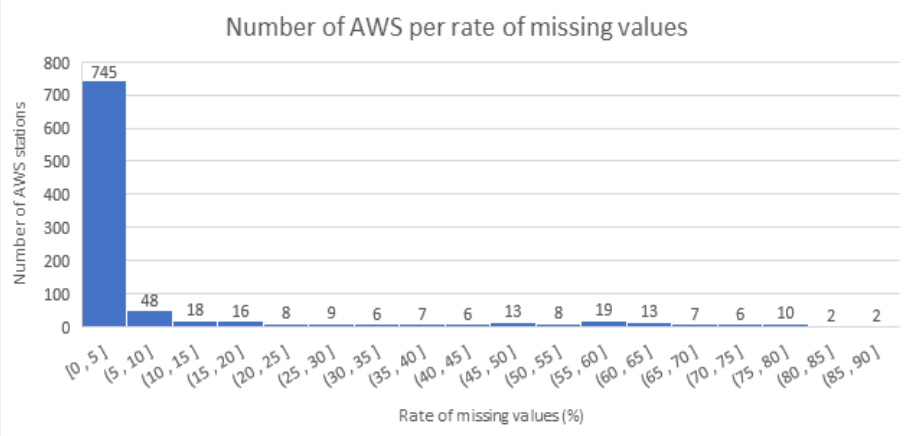

Figure 5. Number of ARG per rate of missing values.

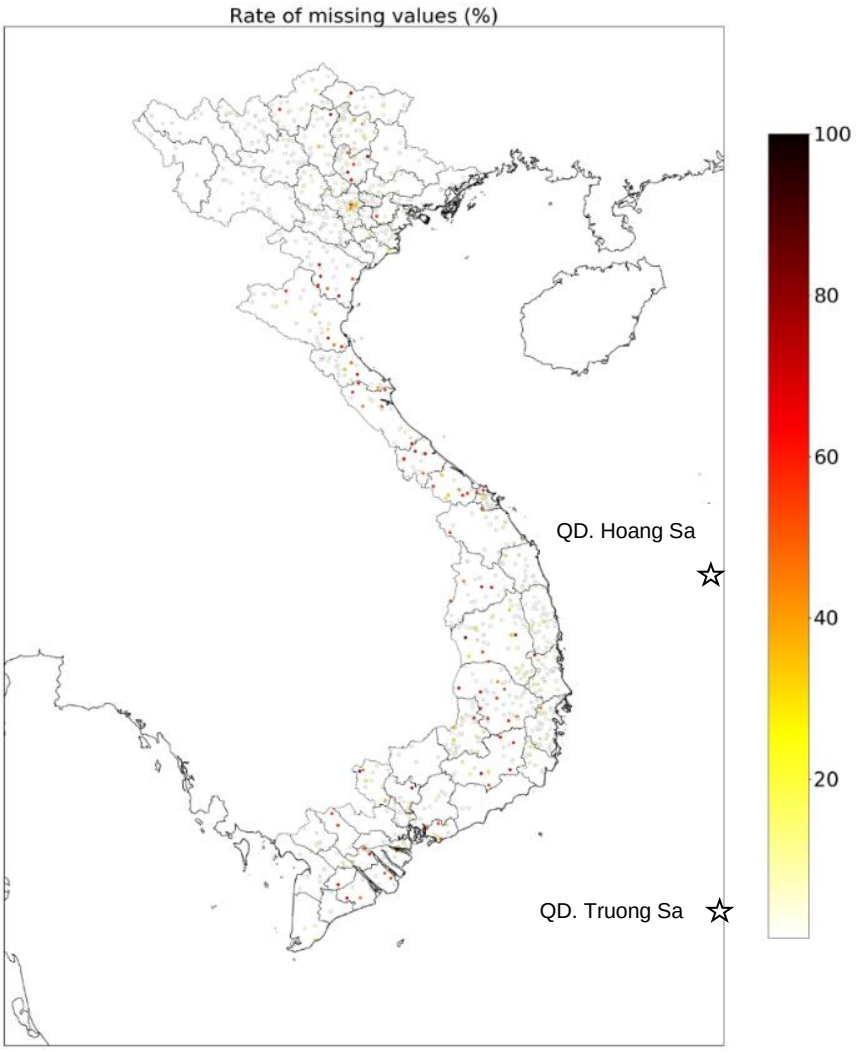

Figure 6. Distribution of ARG missing rate.

Some stations have unnatural low value compared with nearby ARG. Figure 7 shows an example of comparing the time change of precipitation amount at three nearby stations. Their distances are 5–10 km. In this case, precipitation amount at station No.23584 is much less than station No.731750 and station No.92510. Therefore, the data from station No.23584 is not used for QPE calculation. Similarly, several other stations are not used according to the manual check.

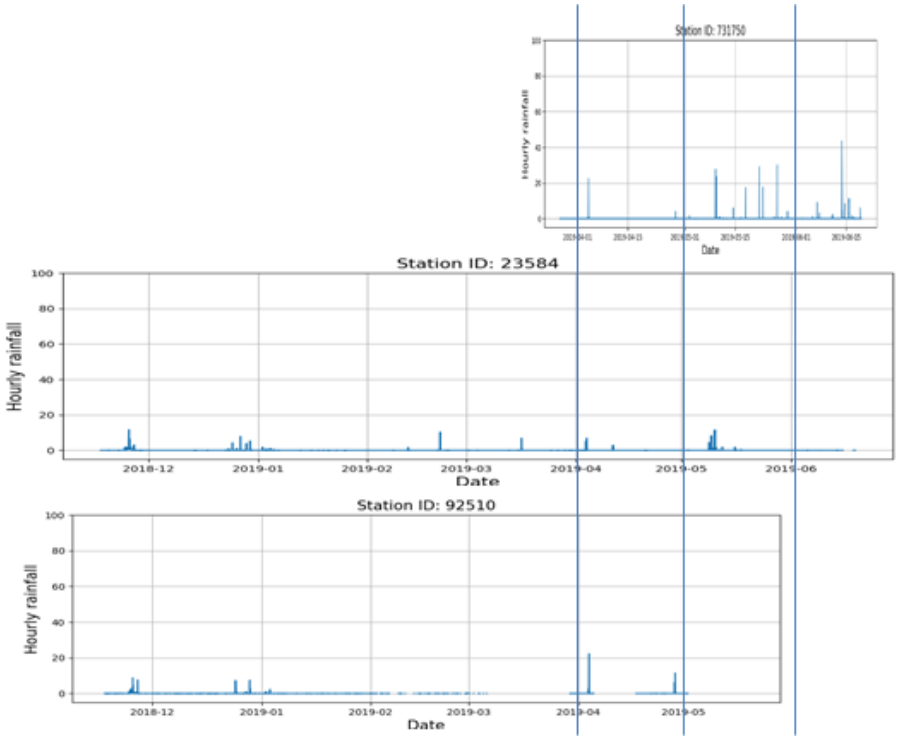

Figure 7. Time changes of three ARG stations located nearby within the distance of 5–10 km.

Based on these two conditions, we finally selected 750 ARG stations for QPE calculation. (The final number of stations increased more than 745 by adding other type of ARG data.) About half of the ARG data are not used for QPE calculation. In order to improve the accuracy of QPE, the cause of errors should be checked and the number of qualified ARGs should be increased.

5. Characteristics of radar and QPE product

Each radar scans in Intensity mode or Doppler mode. Intensity mode is a type of observation with low Pulse Repetition Frequency (PRF) and can detect with a longer range than Doppler mode. Vaisala radar has a maximum detection range of 300 km and JRC radar of 450 km in Intensity mode. Several specifications of these observation modes are summarized in Table 1. In this QPE calculation, Intensity mode data is used.

Radar scans with a sequence of multiple elevations in six to ten minutes. In order to get precise precipitation distribution, echo intensity data at the lowest altitude is necessary. Low elevation scans are often affected with ground clutter, sea clutter, or non–precipitation echoes. A combination of different elevations depending on the surrounding situations around the radar, is determined as a composite table. This method is called “Pseud Constant Altitude Plan Position Indicator (PCAPPI)” in this QPE algorithm.

Figure 8 shows the PCAPPI elevation table of three radars. In order to avoid the effect of ground clutter, some radars located close to the mountainous region have a complicated table. Statistical quality control of PCAPPI data is useful to check the effect of beam cut by mountain or interference. For quality control of PCAPPI data, accumulation of PCAPPI data for appearance frequency and intensity are two important indicators to determine whether the

echo is from precipitation or not. Figure 9 shows examples of these accumulations. Table 2 indicates the meanings of each category. Precipitation echo shows high frequency and high intensity. Area of beam cut shows low frequency and low intensity and partial beam cut shows high frequency and low intensity. Interference shows high frequency and extremely high intensity and extremely high frequency area becomes a linear shape.

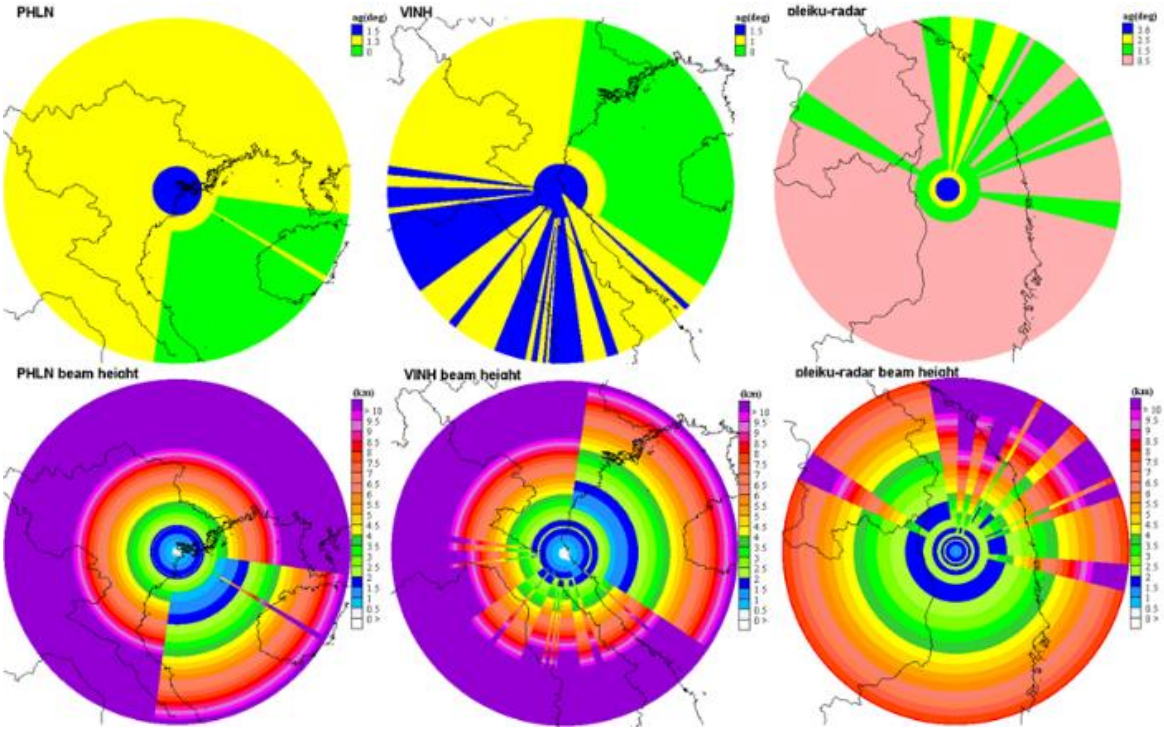

Figure 8. PCAPPI elevation settings for Phu Lien, Vinh and Pleiku radars (from left to right).

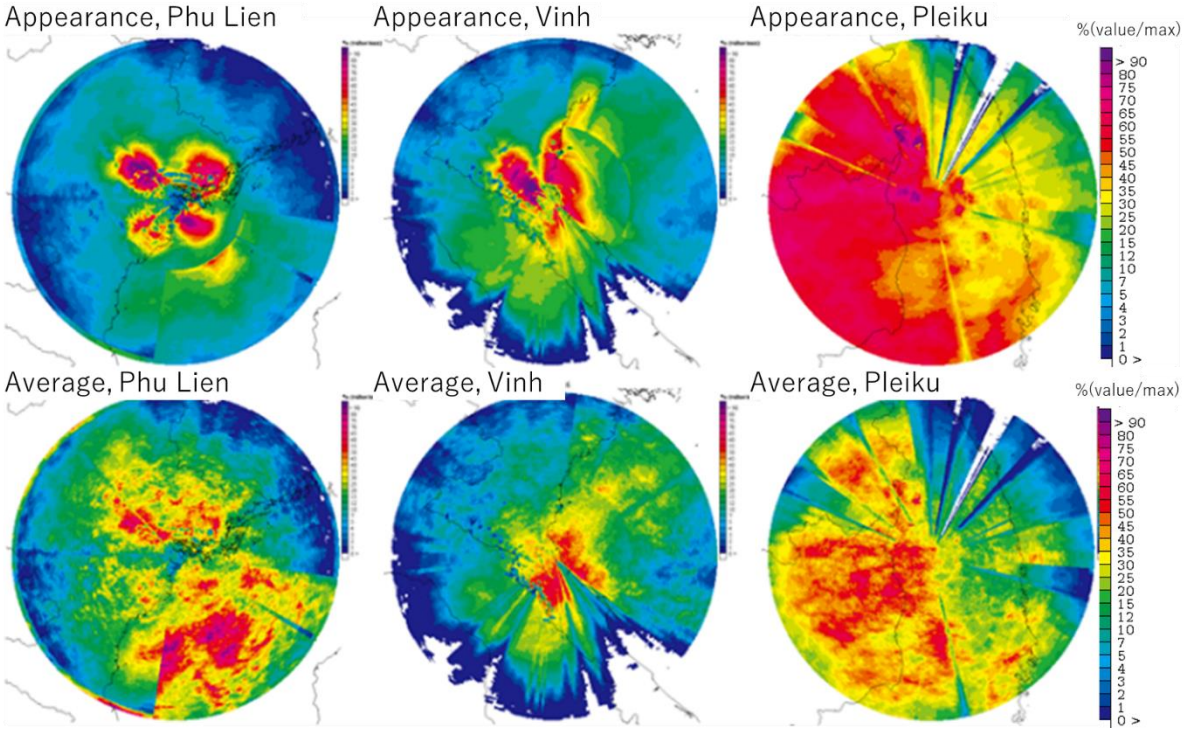

Figure 9. Appearance frequency (upper row) and average reflectivity (lower row) of one–month accumulated PCAPPI data from September 1st to 30th, 2019.

Table 2. Characteristics of several noisy situation

	Appearance frequency	Average reflectivity	Echo pattern
Beam blockage	Low	Low	Wedge
Low–frequency interference	Low	High	Wedge
High–frequency interference	High	Low	-
Strong interference or clutter	High	High	-

Based on this statistical check, elevation settings for the PCAPPI products are optimized in each radar to make them less influenced by clutters or beam blockage. By combining PCAPPI and rain gauge data, a preliminary QPE product is created. Time sequence of QPE calculation is shown in Figure 10.

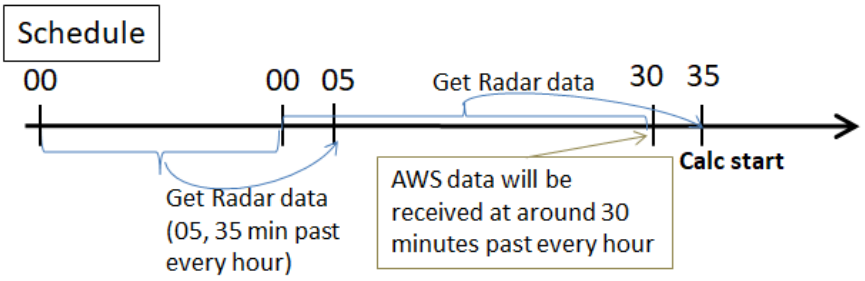

Figure 10. Calculation schedule of QPE.

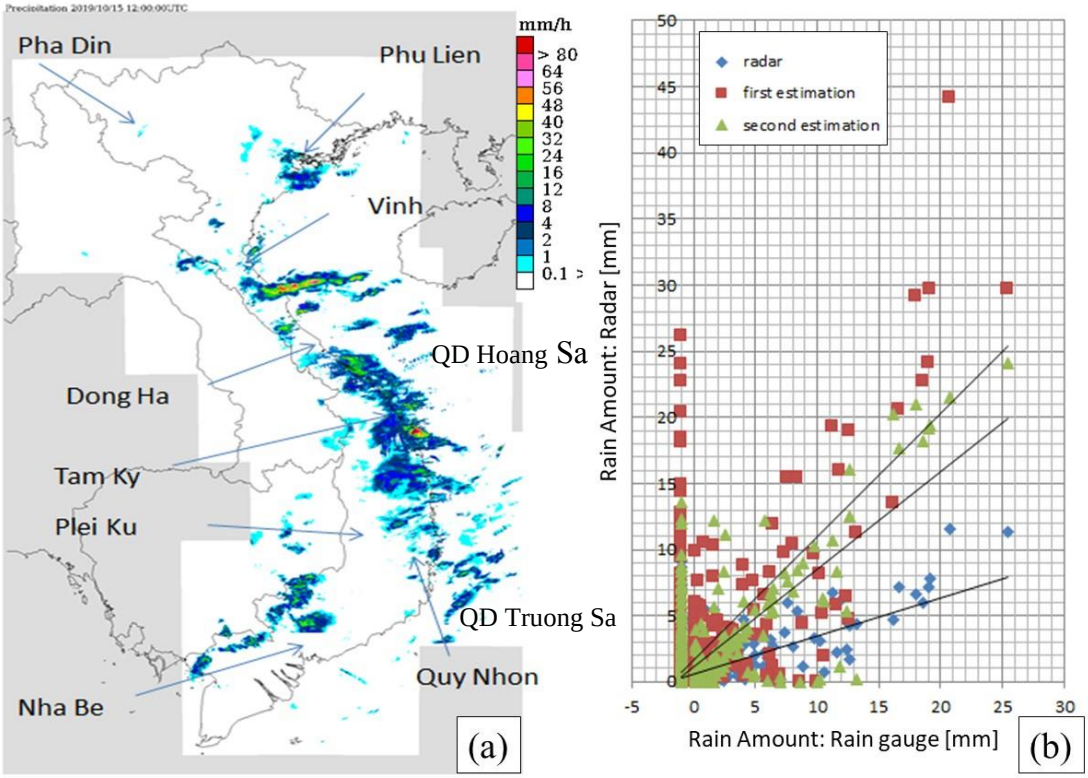

Figure 11. (a) Sample result of QPE; (b) Evaluation of three types of estimated precipitation. (1) Estimation only by radar, (2) 1st calibrated precipitation, (3) 2nd calibrated precipitation.

The first version of QPE calculation started its operation from July 2019. At this stage, two JRC radars and four Vaisala radars were used for QPE calculation. After the number of Vaisala radars increased to six, the algorithm has been improved for several issues. Finally, the current version of the calculation was started from March 2020. The detailed installation process is referred to [8].

Figure 11a shows an example of a QPE product. QPE results can be overlaid on satellite data by using the Satellite Animation and Interactive Diagnosis (SATAID) system. Figure 11b shows the result of the preliminary evaluation of QPE products. Accuracy of the precipitation improves from estimation only by radar to 1st calibrated precipitation and further to 2nd calibrated precipitation. In this case, rain gauge data used in the calculation are employed for evaluation.

6. Improvement of scan strategy of JRC radars

As mentioned in introduction, scan strategy is one of the important issues to improve the quality of QPE. JRC radar's scan sequence has three elevation angles for Intensity mode and 10 elevation angles for Doppler mode. QPE calculation uses only intensity mode data and the quality of this mode is important to keep the accuracy of QPE. There are enough volume scans for Doppler mode, but only three elevations for Intensity mode. Furthermore, two scan angles in Phu Lien radar are so similar such as 1.3 degree and 1.5 degree, which means not enough scan angles for Phu Lien radar as intensity mode. In order to make optimal PCAPPI products avoiding the effect of ground clutter, sea clutter and non–precipitating echo, it is essential to have the choice of elevations in Intensity mode. Vaisala radar changed its scan strategy from August 2019 and increased the number of elevations for Intensity mode to four or five angles.

Table 3 and Figure12 show the current scan sequence and proposed new ones. In the new scan sequence, four elevations for intensity mode and 10 elevations for Doppler mode with different angle settings from the current scan sequence. The merits of the new scan sequence are as follows:

- The number of elevation angles for intensity mode increases and have a better choice of elevation for PCAPPI product
- Qualified of low elevation angle data with combining Intensity mode and Doppler mode data
- Higher vertical resolution in the range between 200 to 300 km
- Smoother change of vertical resolution in the range between 0 to 200 km
- Improvement of detectability of high-altitude echo close to the radar site

Table 3. Elevation angle table of current scan sequence (upper 2 lows) and newly proposed scan sequence (lower 2 lows) for JRC radars (unit is degree). Phu Lien radar currently uses 1.3 degree in the second elevation in Intensity mode and Vinh radar uses 1.0 degree.

Int	0.0	1.3 1.0	1.5							
Dop	0.0	0.5	1.0	1.5	2.0	3.0	4.0	6.0	9.0	12.0
Int	0.0	0.5	1.0	1.5						
Dop	0.5	1.0	1.5	2.5	3.6	5.0	7.2	10.4	15.0	21.5

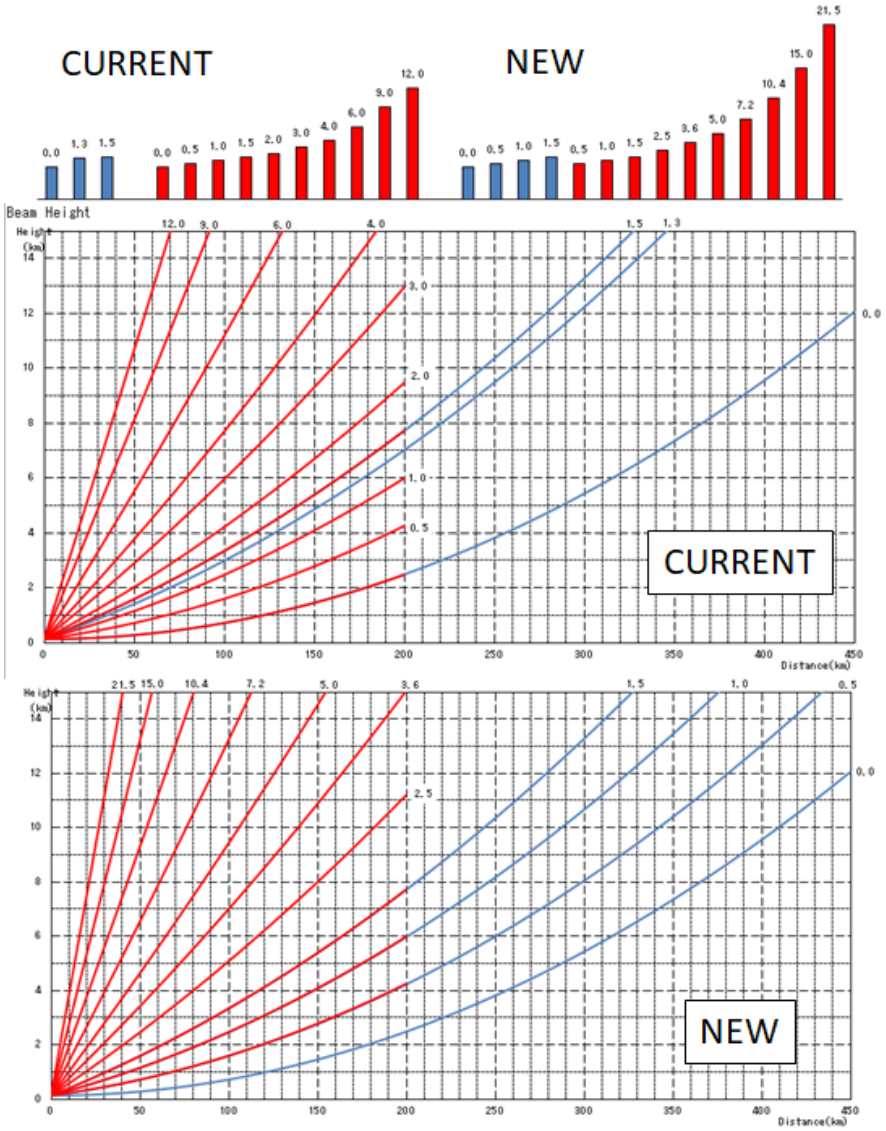

Figure 12. Current scan sequence and newly proposed scan sequence on Phu Lien radar.

7. Summary and future issues

Currently eight meteorological radars and about 750 ARG data are combined to make hourly QPE product. In the early stage, sometimes there were sudden increases in QPE value. Several improvements were made such as correction of locations of radar and ARG, quality control of radar and ARG data, optimal parameter settings of the QPE algorithm and suppression of these abnormal values. Even if these improvements increased the stability of calculation, there still are several issues regarding the optimal setting of radar and QPE software, quality control of ARG and radar data to further improve the accuracy of QPE. Detailed issues are listed as follows:

- Increase reliability and availability of ARG data
- Optimal elevation setting in PCAPPI
- Improvement of scan strategy of JRC radars
- Proper setting of clutter maps
- Evaluation of QPE product with independent ARG
- Optimal parameter setting of QPE algorithm

Radar estimated precipitation amount without rain gauge correction has sometimes large errors. This is due to the Z–R relation based on Marshal–Palmer distribution tend to correspond to stratiform precipitation. In case of convective precipitation, drop size distribution is different from Marshall–Paler and varies with different convective cases. Radar estimated precipitation for convective cases underestimate the amount. By using QPE method with rain gauge correction as proposed in this paper, heavy rain events are expected to estimate accurately. Evaluation of QPE product is necessary for various types of precipitation.

Accurate QPE data is a base of various information for disaster prevention and there are two major ways to further utilize QPE data. One is an application to various indexes of disaster risk prediction. Usually precipitation amount is used to predict the occurrence of disaster, but in order to improve the prediction indexes including other factors such as soil water for land slide and runoff for flood are necessary. Archive data set of QPE with the occurrence of disaster is useful to formulate the relationship between these indexes and the occurrence of disaster. The other is an application to quantitative precipitation forecast (QPF). There are several techniques for QPF and the merging of extrapolation of QPE with forecast by numerical weather prediction (NWP) model is one of the useful methods.

Author Contributions: Conceptualization, C. Kimpara and M. Tonouchi; methodology, C. Kimpara, N.V. Hung and N.M. Cuong; software, C.Kimpara and B.T.K. Hoa; validation, C.Kimpara, M.Tonouchi and B.T.K. Hoa; formal analysis, K. Akaeda; writing–original draft preparation, C.Kimpara and B.T.K. Hoa; writing–review and editing, All authors have read and agreed to the published version of the manuscript.

Funding: This study is supported by the JICA project for strengthening capacity in weather forecasting and flood early warning systems in Viet Nam.

Acknowledgments: The authors thank the Japan Meteorological Agency for providing the package for calculating QPE products and their support for the installation. Also, authors thank Nguyen Vinh Thu, Director of the Aero Meteorological Observatory for his support and suggestions to this project. Thanks are extended to Nguyen Quang Vinh of the Aero Meteorological Observatory for his technical support to various radar analysis.

Conflicts of Interest: The authors declare no conflict of interest.

References

1. Tonouchi, M.; Kasuya, Y.; Tanaka, Y.; Akatsu, K.; Akaeda, K.; Nguyen, V.T. Activities of JICA on disaster prevention and achievement of JICA project in Period 1. *VN J. Hydrometeorol*., **2020**, *5*, 1–12.
2. Vicente, G.; Scofield, R. A.; Mensel, W.P. The operational GOES infrared rainfall estimation technique. *Bull. Amer. Meteor. Soc.* **1998**, *79*, 1881–1898. doi: 10.1175/1520-0477(1998)079<1883:TOGIRE>2.0.CO;2
3. Vasiloff, S.V.; Seo, D.J.; Howard, K.W.; Zhang, J.; Kitzmiller, D.H.; Mullusky, M.G.; Krajewski, W.; Brandes, E.A.; Rabin, R.M.; Berkowitz, D.S.; Brooks, H.E.; Mcginley, J.; Kuligowski, R.J.; Brown, B.G. Improving QPE and very short term QPF. *Bull. Amer. Meteor. Soc.*, **2007**, *88*, 1899–1911. doi: 10.1175/BAMS–88–12–1899

4. Makihara, Y. A method for improving radar estimates of precipitation by comparing data from radars and rain gauges, *J. Meteor. Soc. Japan*, **1996**, *74*, 459–480. doi: 10.2151/jmsj1965.74.4_459
5. Makihara, Y. Algorithms for precipitation nowcasting focused on detailed analysis using radar and rain gauge data, *Technical Reports of the MRI*, **2000**, *39*, 63–111. doi:10.11483/mritechrepo.39
6. Observation Department. Radar/rain gauge-analyzed precipitation, *Weather Radar Application Technology at the Japan Meteorological Agency*, 2017, pp. 62–70.
7. Makihara, Y. Quantitative Precipitation Estimation, Training for QPE derived from the combination of radar and rain gauge data, Hanoi, *Training Material*, 2020, ##5.
8. JICA and JMBSC. The Project for Strengthening Capacity in Weather Forecasting and Flood Early Warning System in Vietnam, *Final report (First period)*, 2020, pp. 147.

VIETNAM JOURNAL OF HYDROMETEOROLOGY

Research Article

Development of maximum and minimum temperature guidance with Kalman filter for 63 cities in Vietnam up to 10 days ahead

Kiichi Sasaki[1*], Vu Tuan Anh[2], Nguyen Thu Hang[2], Do Thuy Trang[2]

[1] Japan Meteorological Business Support Center, Tokyo101–0054 Japan; k–sasaki@jmbsc.or.jp
[2] National Center for Hydro–Meteorological Forecasting, Hanoi 10000, Vietnam; lamhoaanh@gmail.com; nthang0676@gmai.com; dotrang111@gmail.com
[*] Correspondence: k–sasaki@jmbsc.or.jp; Tel.:(+81–3–5281–0440)

Received: 10 July 2020; Accepted: 12 August 2020; Published: 25 August 2020

Abstract: Development of forecast guidance is one of the main activities of Output 3 of the JICA project to improve forecasting services of VNMHA. We applied the Kalman filter (KF) technique by using a calculation package which was provided in the JICA group training course in meteorology by the Japan Meteorological Agency (JMA) to Vietnam for the development of temperature guidance. Maximum and minimum temperature guidance was developed for 63 cities up to 3 days ahead using JMA Global Spectral Model (GSM) Grid Point Value (GPV) data and up to 10 days ahead using ECMWF Integrated Forecasting System (IFS) GPV data. Verification results show that Root Mean Square Errors (RMSEs) of GSM and IFS KF guidance are relatively large in the northern region in both maximum and minimum temperatures, but KF guidance greatly reduces RMSEs of direct model outputs in all regions throughout the year. RMSEs of IFS guidance become smaller than those of GSM guidance with increasing forecast time. Averaged RMSEs of KF guidance for 63 cities are smaller than those of city forecasts issued by forecasters in Nov–Dec 2019 and Jan–Feb 2020. These verification results suggest that accuracy of maximum and minimum temperature city forecasts will be improved by using KF guidance in daily forecasting.

Keywords: Temperature guidance; Kalman filter; Grid Point Value (GPV); City forecast.

1. Introduction

The JICA Project for Strengthening Capacity in Weather Forecasting and Flood Early warning System started in April 2018 [1]. The Project has four components: Output 1 (surface observation), Output 2 (radar products), Output 3 (weather forecasting) and Output 4 (local weather dissemination). This article describes development of maximum and minimum temperature guidance for 63 major cities in Vietnam as a main activity of Output 3 to improve forecasting services of VNMHA. A forecast working group (WG3) of 5 members from VNHMA and 2 members from the Japan Meteorological Business support Center (JMBSC) was organized to achieve the purpose of Output 3. In addition, a development team of 5 members from National Center for Hydro–Meteorological Forecasting (NCHMF) for operational use of forecast guidance was set up under the WG3.

JMBSC once implemented the technical cooperation project for enhancing capacity on weather observation, forecasting and warning in the Republic of the Philippines from 2014

to 2017 [2]. Maximum temperature (T_{max}) and minimum temperature (T_{min}) KF guidance was successfully introduced to forecasting services in the Philippines through the technical cooperation project. Based on the experience of JMBSC in the Philippines, we applied the Kalman filter technique used in the projects to Vietnam. In Vietnam, the KF technique has been applied to improve surface variable forecasts from the global model (GSM) and the High Resolution regional Model (HRM, developed by German Weather Service) for period 2000–2010 [3–4].

This paper will show the application of JMA's KF guidance scheme to improve temperature forecast guidance in Vietnam. The JMA's KF guidance scheme is based on the basis of earlier works [5–6], and started KF temperature guidance in 1996. Daily maximum temperature (T_{max}) and minimum temperature (T_{min}) KF guidance was developed for 63 cities in Vietnam up to 3–days ahead using JMA GSM GPV data and up to 10 days ahead using ECMWF IFS GPV data.

2. Materials and Methods

2.1. MOS and Kalman filter

NWP model products are fundamental materials for weather forecasting, but have systematic errors caused by difference between actual and NWP model topography and caused by approximation in physical process of NWP. The guidance produced from NWP and observation data with statistical interpretation is a useful prediction to reduce errors of NWP model output. Model Output Statistics (MOS) and Kalman filter (KF) are widely used for temperature guidance in many countries.

2.1.1. MOS

MOS is a popular guidance and is really simple and easy to use. MOS is used in US, Canada etc., and JMA used MOS until 1996 for temperature guidance. Its forecast equation is the Multiple Linear Regression (MLR) given below:

$$y = a_0 + a_1x_1 + a_2x_2 + \dots , \quad (1)$$

where y is the predictand (guidance); x_i the predictors and a_i the coefficients.

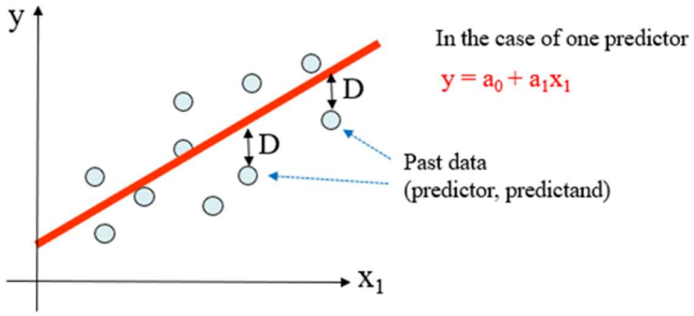

Figure 1. Image of simple Linear Regression (MOS).

Coefficients a_i are decided to minimize total errors by the least–squares method (Figure 1). Effective predictors x_i are objectively selected from potential predictors with stepwise method etc. MOS is easy to make and operate, but a large amount of data (about 2 years data)

are necessary. In this JICA activity, as a preliminary survey, we calculated MLR guidance using every 2–month observation and NWP data of the latest 2–year period to evaluate performance of the MOS technique compared to the KF technique. As the result, KF guidance was better than MOS guidance in many cases. So, we decided to investigate the performance of KF guidance only in the following experiments.

2.1.2. Kalman filter

The Kalman filter is used for the same purpose as MOS to reduce systematic errors of NWP output. MOS's forecast equation uses fixed coefficients calculated with past NWP and observation data, while the KF forecast equation uses coefficients updated successively depending on deference between guidance and observation. The KF forecast equation is given below:

$$f(x)^{(t)} = a_0^{(t)} + a_1^{(t)}x_1 + a_2^{(t)}x_2 + \dots , \quad (2)$$

where *f(x)* is predictand (guidance), x_i the predictors, a_i the coefficients, and *t* means the time. Forecast equations of MOS and KF are similar, but the particular difference is that the coefficients of KF are updated successively to reduce the error:

$$\text{error} = \text{observation } (y^{(t)}) - \text{guidance } (f(x)^{(t)}) \quad (3)$$

The coefficients are updated to reduce the error:

$$a_i^{(t+1)} = a_i^{(t)} + K_i^{(t)} * \text{error} \quad (4)$$

where $K_i^{(t)}$ is called "Kalman gain" which is estimated based on Bayes' theorem. This study used the calculation package developed by JMA to calculate the Kalman gain ($K_i^{(t)}$) and update coefficients ($a_i^{(t)}$) of the KF equation. In the calculation, constant measurement error variance (4: about RMSE*RMSE of guidance) and constant covariance matrix of process noise (diagonal components: 0.01 for constant, 0.0001 for each predictor component, others: 0) are used. JMA's KF guidance is described in Outline of the Operational Numerical Weather Prediction at JMA [7]. At first, one predictor of model surface temperature (2 m temperature) was chosen to develop KF guidance for maximum and minimum temperatures.

2.2. NWP GPV and T_{max}/T_{min} observation data set

For executing successive KF updating cycle, the latest NWP GPV data and T_{max}/T_{min} observation data are necessary. As a first step of the guidance development, we decided to use JMA High–Resolution GSM Data Service for NMSs and started downloading GSM surface GPV data of 00 UTC initial (https://www.wis–jma.go.jp/cms/gsm/download.html). They are 0.25x0.25–degree grid point data of 3–hourly up to 84 hours, and available at around 11 a.m. in local time in Vietnam.

As for observation data, National Center for Hydro–Meteorological Forecasting (NCHMF) prepares Excel data set of 186 stations (186smMMyYY.xls) every day including T_{max}, T_{min}, precipitation and wind observations. These NWP GPV and observation data are used for KF updating cycle. A sample of GSM GPV and observation data set for Hanoi Day1 in May–Jun 2018 is shown in Figure 2.

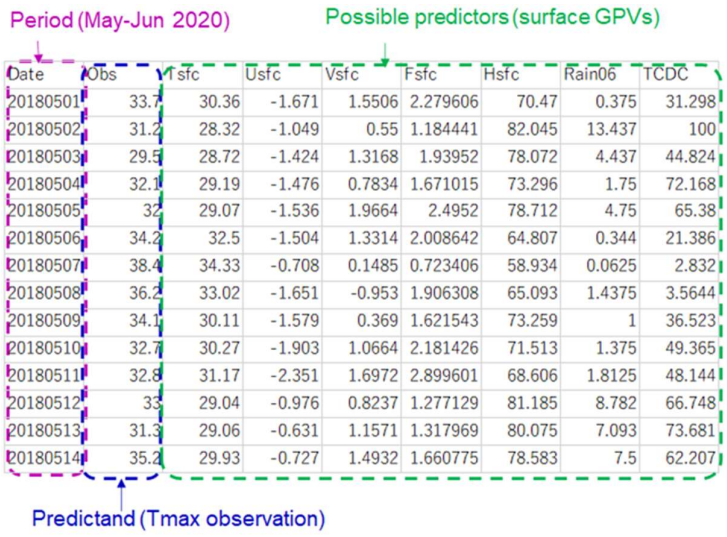

Date	Obs	Tsfc	Usfc	Vsfc	Fsfc	Hsfc	Rain06	TCDC
20180501	33.7	30.36	-1.671	1.5506	2.279606	70.47	0.375	31.298
20180502	31.2	28.32	-1.049	0.55	1.184441	82.045	13.437	100
20180503	29.5	28.72	-1.424	1.3168	1.93952	78.072	4.437	44.824
20180504	32.1	29.19	-1.476	0.7834	1.671015	73.296	1.75	72.168
20180505	32	29.07	-1.536	1.9664	2.4952	78.712	4.75	65.38
20180506	34.2	32.5	-1.504	1.3314	2.008642	64.807	0.344	21.386
20180507	38.4	34.33	-0.708	0.1485	0.723406	58.934	0.0625	2.832
20180508	36.2	33.02	-1.651	-0.953	1.906308	65.093	1.4375	3.5644
20180509	34.1	30.11	-1.579	0.369	1.621543	73.259	1	36.523
20180510	32.7	30.27	-1.903	1.0664	2.181426	71.513	1.375	49.365
20180511	32.8	31.17	-2.351	1.6972	2.899601	68.606	1.8125	48.144
20180512	33	29.04	-0.976	0.8237	1.277129	81.185	8.782	66.748
20180513	31.3	29.06	-0.631	1.1571	1.317969	80.075	7.093	73.681
20180514	35.2	29.93	-0.727	1.4932	1.660775	78.583	7.5	62.207

Figure 2. GSM GPV and T_{max} observation data set for Hanoi Day1 T_{max} May–Jun 2018. Surface GPVs (Tsfc: temperature, Usfc: wind u–component, Vsfc wind v–component, Fsfc: wind speed, Hsfc: humidity, Rain06: 6–hour rainfall, TCDC: total cloud amount).

Two–monthly Obs–GPV data set like Figure 2 was prepared for 63 cities, for Day1, Day2 and Day3 from Jan–Feb to Nov–Dec in 2018. Statistical interpretation was made with past 2–month Obs–GPV data set and we applied the obtained forecast equation to the next 2–month period with KF cycle (Figure 3). In this process, only surface model temperature (Tsfc) was used as a predictor for easy understanding of the interpretation and verification results.

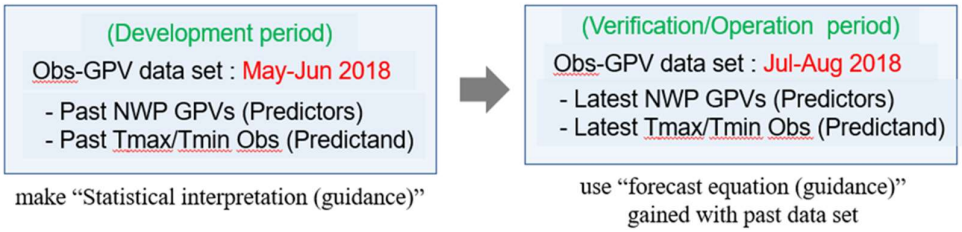

Figure 3. Calculation procedure with past–2month and the next 2–month Obs–GPV data set.

3. Result

3.1. Preliminary investigation

WG3 agreed to set a goal to improve T_{max} and T_{min} city forecasts which NCHMF started issuing in 2018, and decided to develop guidance to improve accuracy of T_{max} and T_{min} forecasts for 63 cities up to 3 days ahead as a first step. After the baseline survey in July 2018, collection of necessary observation data and GSM GPV data, and preliminary investigation on the development of T_{max} and T_{min} guidance were conducted. In the investigation, MOS and KF temperature guidance was developed for 13 stations of major cities with T_{max} and T_{min} observation and GSM GPV data from January 2017 to April 2018. Through the comparison of RMSEs of GSM surface temperature GPVs and KF guidance, we

confirmed that KF guidance greatly reduced RMSEs of GSM model surface temperature throughout the year (Figures 4a, 4b).

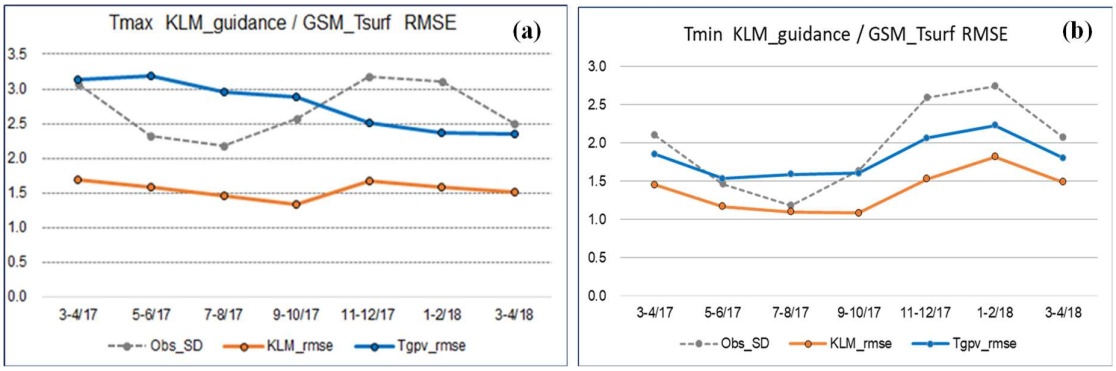

Figure 4. (a) Average RMSEs of Tmax_Day1 KF guidance for 13 cities every 2–month period from Mar 2017 to Apr 2018. Standard Deviation of T_{max} and T_{min} observations (Obs–SD) is shown to see the seasonal change of variability of temperature fluctuation, RMSE of KF guidance (KLM_rmse) and RMSE of GSM surface temperature (Tgpv_rmse); (b) Average RMSEs of Tmin KF guidance; others are the same as (a).

3.2. T_{max} and T_{min} KF guidance with GSM up to 3 days ahead

Using the prepared Obs–GPV data set, T_{max} and T_{min} KF guidance for 63 cities up to 3 days ahead was developed with JMA GSM GPV data of 00 UTC initial. This study followed the method used in the JICA Group training course in meteorology implemented by JMA for the development of the KF guidance.

In order to understand the performance of developed KF guidance, we carried out accuracy verification of T_{max} and T_{min} city forecasts for 63 cities issued by forecasters and KF guidance with JMA GSM GPV data. Figure 5 shows averaged RMSEs of persistence forecasts, city forecasts and KF guidance for T_{max} and T_{min} in Nov–Dec 2018. RMSEs of KF guidance were smaller than those of persistence forecasts and city forecasts, and we confirmed that accuracy of city forecasts would be improved by introducing KF guidance.

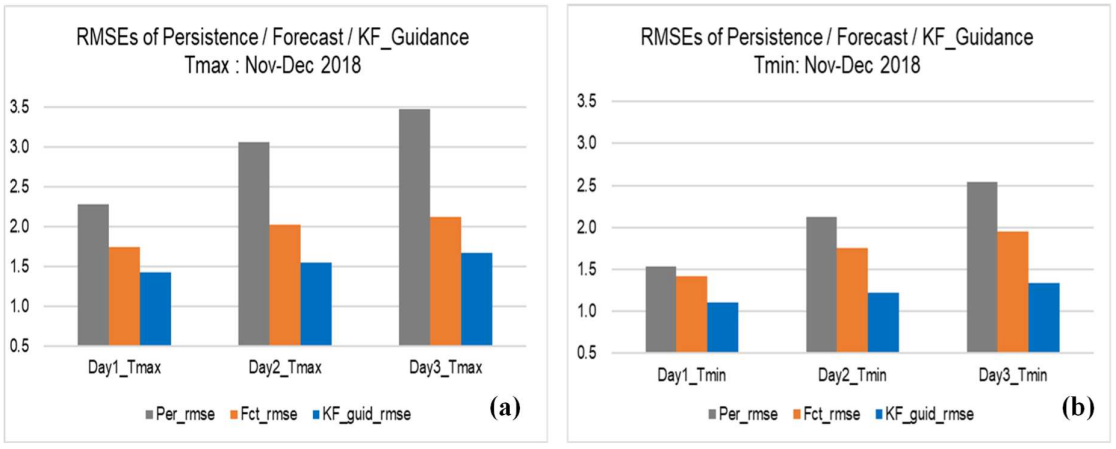

Figure 5. Averaged RMSEs of persistence forecast, city forecast and KF guidance for 63 cities: (a) T_{max} and (b) T_{min} in Nov–Dec 2018. Persistence forecast assumes conditions of the day are unchanged up to 3days ahead.

In 2019, we undertook development of T_{max} and T_{min} guidance for 63 cities up to 3 days ahead for operational use to improve accuracy of T_{max} and T_{min} city forecasts. First, a R–script for preparing necessary dataset for daily calculation of KF guidance with JMA GSM GPV data of 00 UTC initial and SYNOP observation data of 63 stations in the cities was developed in July 2019.

3.3. T_{max} and T_{min} KF guidance with IFS up to 10 days ahead

3.3.1. Development of T_{max} and T_{min} KF guidance with IFS GPV data

In addition to the development of KF guidance with JMA GSM GPV data, this study developed T_{max} and T_{min} KF guidance with ECMWF IFS GPV data in response to the request by NCHMF. Figure 6 shows RMSEs of IFS–KF guidance and GSM–KF guidance for T_{max} at every city forecast points in May and June 2019. RMSEs of IFS–KF guidance are slightly smaller than GSM–KF guidance in the northern region, where daily change of the maximum temperature is rather large in May and June. RMSEs of them for minimum temperature are almost the same.

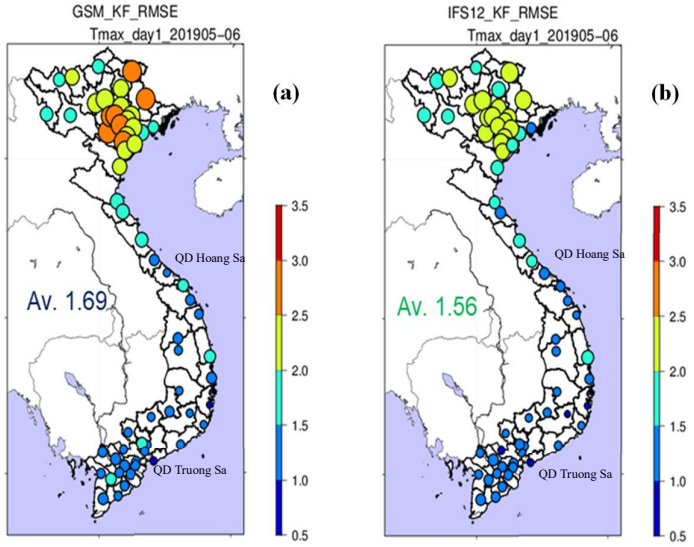

Figure 6. Distribution of RMSEs: (a) GSM–KF guidance; (b) IFS–KF guidance in May–June 2019 for T_{max}, Day1 (tomorrow).

3.3.2. Trial operation of KF guidance, monitoring and improvement

We set a PC for guidance development at the forecasting room of NCHMF for auto download of JMA GSM GPV data, auto copy of SYNOP Excel data and collecting IFS GPV data through the internal network. Then we started trial operation of GSM–KF guidance and IFS–KF guidance for 63 cities up to 3 days ahead.

KF guidance needs the daily update process of observation data to update coefficients of KF equation according to errors between KF guidance outputs and observations. As observation data missing was found sometimes during the trial operation, we checked daily observation update process and improved the process.

3.3.3. Development of T_{max} and T_{min} guidance with IFS up to 10 days ahead

VNMHA issues T_{max} and T_{min} city forecasts up to 10 days ahead, and we need to develop KF T_{max} and T_{min} guidance up to 10 days ahead. As previous verification results showed RMSEs of IFS KF guidance were smaller than GSM KF guidance with increasing forecast time, we developed IFS–KF T_{max} and T_{min} guidance up to 10 days ahead with 00 UTC and 12 UTC initials and started its trial operation.

IFS GPV data of 12 UTC initial are available at around 3 to 4 am in local time of Vietnam, and IFS GPV data of 00 UTC initial are available at around 3 pm and GSM GPV data of 00 UTC initial are available at around 11 am. Considering these data availability, IFS KF guidance with 12 UTC initial (IFS12) up to 10 days ahead is prepared at around 10:30 am, GSM KF guidance with 00 UTC initial (GSM00) up to 3 days ahead at around 11:30 am and IFS KF guidance with 00 UTC initial (IFS00) up to 10 days ahead at around 3:30 pm Examples of IFS KF Guidance up to 10 days ahead and monitoring sheets of GSM KF guidance for every station are shown in Table 1 and Figure 7, respectively.

Table 1. Example of IFS–KF T_{max} and T_{min} guidance up to 10 days ahead (IFS12UTC on 30th Nov 2019 initial).

Station	IFS Day0	Day1 min	Day1 max	Day2 min	Day2 max	Day3 min	Day3 max	Day4 min	Day4 max
LaiChau	20191201	14.3	17.4	10.9	18.2	10.6	19.8	10.1	19.2
DienBien	20191201	16.4	25.3	13.4	25.8	13.9	26.0	11.6	26.0
SonLa	20191201	12.2	19.5	9.2	20.9	9.3	21.0	8.3	21.6
HoaBinh	20191201	14.1	21.2	11.9	22.2	12.8	21.6	11.4	21.7
LaoCai	20191201	15.4	19.3	14.3	20.0	14.5	22.7	15.8	24.8
YenBai	20191201	16.2	17.7	14.6	18.6	13.6	20.4	15.7	21.3
HaGiang	20191201	16.0	20.7	14.5	22.5	12.8	23.8	12.4	24.3
TuyenQua	20191201	15.7	20.2	15.3	22.3	12.2	22.8	13.5	22.6

Day5 min	Day5 max	Day6 min	Day6 max	Day7 min	Day7 max	Day8 min	Day8 max	Day9 min	Day9 max
7.2	19.3	7.0	21.0	6.9	21.0	8.5	21.5	7.4	20.9
10.2	25.5	9.1	26.6	9.0	24.8	8.4	26.9	9.3	28.5
6.6	22.0	5.5	23.7	6.0	24.4	6.8	24.3	8.3	25.6
10.4	21.7	12.0	23.7	10.4	24.4	10.5	22.5	10.0	23.6
13.3	24.6	10.5	25.7	10.5	25.2	12.5	25.0	12.5	25.6
14.7	21.3	12.3	23.5	12.3	23.6	10.4	22.6	11.9	23.2
9.6	24.7	7.8	24.9	7.9	25.8	8.3	25.4	8.3	25.5
12.7	22.9	10.7	25.0	10.9	24.1	10.2	24.1	10.1	23.8

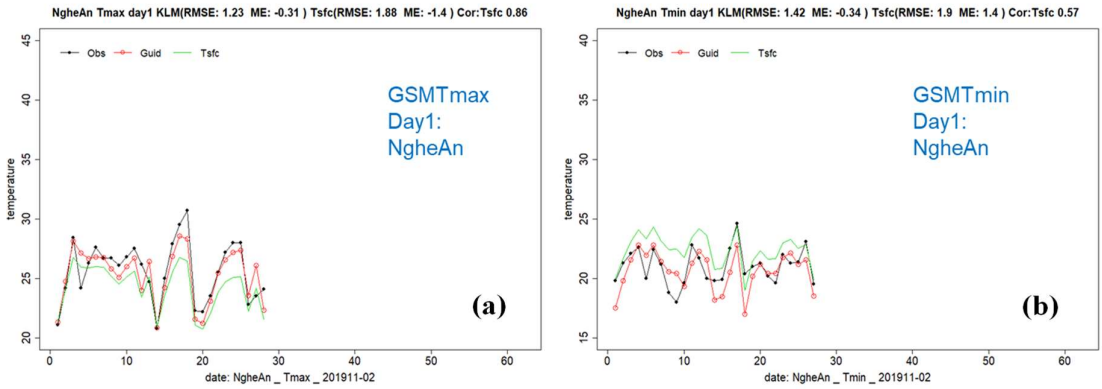

Figure 7. Example of Monitoring sheets of GSM–KF: (a) T_{max} and (b) T_{min} guidance for NgheAn (Black: Observation, Green: GPV Tsfc, Red: GSM–KF guidance).

3.4. Verification results of IFS KF and GSM KF guidance

3.4.1. Verification results of IFS KF guidance up to 10 days ahead

Figure 8 shows verification results of IFS12, IFS00 up to 10 days ahead in Nov–Dec 2019 and in Jan–Feb 2020. RMSEs of IFS Tsfc of 00 UTC initial, IFS00_KF and IFS12_KF increase gradually from Day1 to Day9. Both IFS00_KF and IFS12_KF RMSEs are significantly smaller than RMSEs of direct model output (Tsfc), and RMSEs of IFS00 KF guidance are slightly smaller than those of IFS12 KF guidance.

IFS00 KF guidance, however, is a bit late for issuing the city forecast from Day1 to Day 10 because forecasters have to issue city forecasts by 4 pm at the latest. So, IFS12 KF guidance are to be used mainly to issue city forecasts and IFS00 KF guidance are to be used as a reference for checking. RMSEs of IFS12 KF guidance are slightly larger than IFS00 KF guidance, and IFS12 KF guidance will work for issuing T_{max} and T_{min} city forecasts.

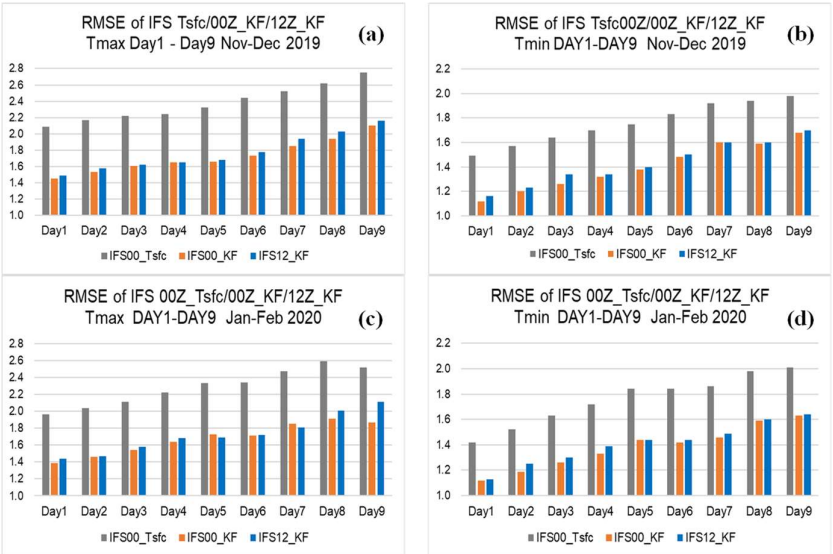

Figure 8. Averaged RMSEs of IFS surface temperature (Tsfc) of 00 UTC initial, IFS00 KF guidance and IFS12 KF guidance for Day1 to Day9: **(a)** T_{max}, Nov–Dec; **(b)** T_{min}, Nov–Dec; **(c)** T_{max}, Jan–Feb 2020, **(d)** T_{min}, Jan–Feb 2020.

3.4.2. Verification results of GSM and IFS KF guidance for Day1, Day2 and Day3

Figure 9 shows verification results of city forecasts issued by forecasters, GSM00 KF guidance, IFS00 KF guidance and IFS12 KF guidance for Day1, Day2 and Day3 in Nov–Dec 2019 and in Jan–Feb 2020. Verification results are summarized as follows:

· RMSE of IFS00 for T_{max} Day 1 is the smallest among these forecasts in Nov–Dec 2019. RMSEs of these forecasts increase gradually from Day1 to Day3: 1.45 (IFS00 Day1) to 1.61 (IFS00 Day3), 1.49 (IFS12 Day1) to 1.62 (IFS12 Day3), 1.52 (GSM00 Day1) to 1.76 (GSM00 Day3).

· Features of RMSEs for T_{max} in Nov–Dec 2019 are similar to those of T_{min} in Nov–Dec 2019, and those of T_{max} and T_{min} in Jan–Feb 2020. RMSEs of IFS12 KF guidance are smaller than those of GSM00 KF guidance and slightly larger than those of IFS00 KF guidance.

· RMSEs of KF guidance are smaller than those of city forecasts of T_{max} and T_{min} for Day1, Day2 and Day3 in Nov–Dec 2019 and Jan–Feb 2020.

The results show that IFS00 KF guidance could be used to improve accuracy of T_{max} and T_{min} city forecasts. However, as previously mentioned, IFS00 KF guidance is available at around 3:00 to 3:30pm, and it is a bit late to use operationally. So IFS12 KF guidance and GSM00 KF guidance are to be used mainly for daily forecasting.

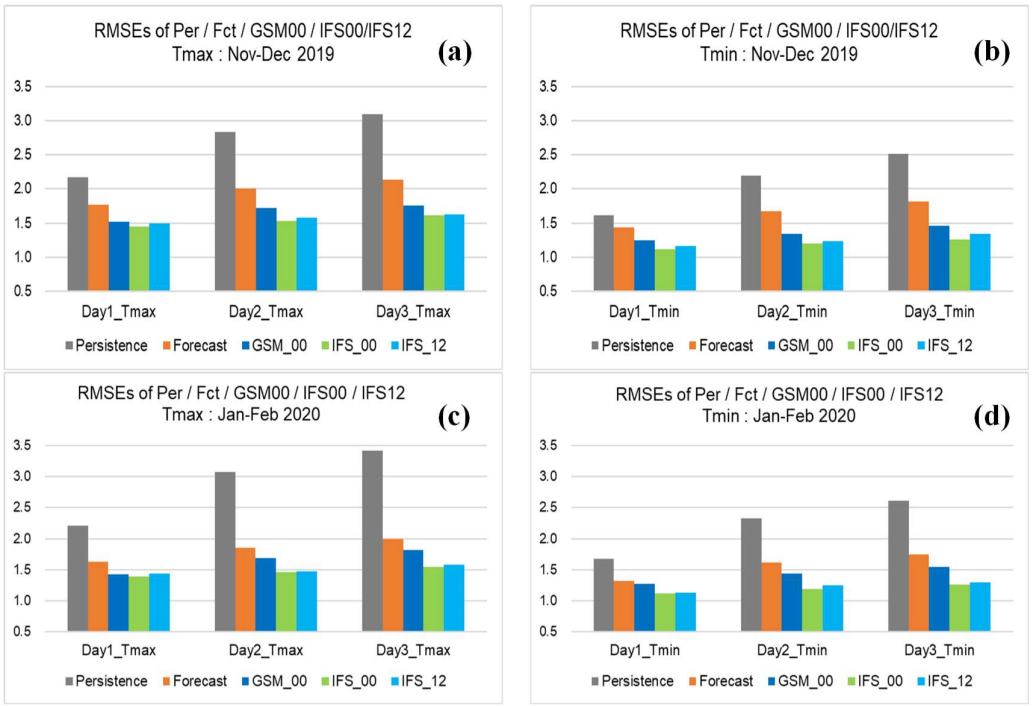

Figure 9. Averaged RMSEs of Persistence forecasts, City forecasts issued by forecasters, GSM00 KF guidance, IFS00 KF guidance and IFS12 KF guidance for Day1, Day2 and Day3 in Nov–Dec 2019 and in Jan–Feb 2020: **(a)** T_{max}, Nov–Dec 2019; **(b)** T_{min}, Nov–Dec 2019; **(c)** T_{max}, Jan–Feb 2020; **(d)** T_{min}, Jan–Feb 2020.

3.4.3. Verification results of GSM and IFS KF guidance at each station

RMSEs of previous verification results are averaged RMSEs of 63 stations for 2–month periods. Error features are likely different depending on the station and the season.

At first, we checked variability amplitude of observed T_{max} and T_{min} temperatures at each station. Figure 10 shows Standard Deviation (SD) of T_{max} and T_{min} observations at each station in Nov–Dec 2019 and Jan–Feb 2020. From these distribution charts of SDs, we get the following features:

· SDs are relatively large in the north region and they are small in the central and southern regions in Vietnam. Looking at those four distribution charts, SDs of T_{max} in Jan–Feb 2020 in the northern region are larger than others and over 4 degrees in many stations.

· Daily change of T_{max} and T_{min} are large in the northern region around Hanoi, particularly in the winter season.

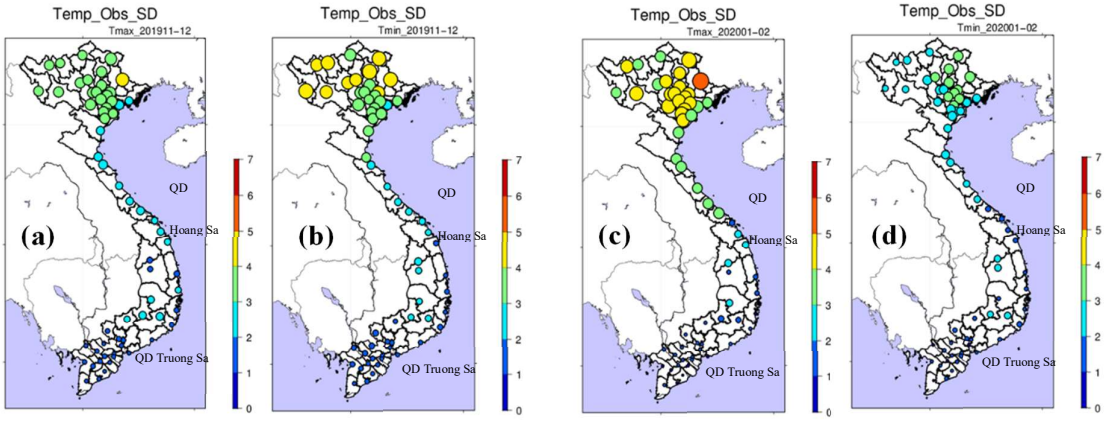

Figure 10. Standard Deviation (SD) of T_{max} and T_{min} observations at each station: **(a)** T_{max}, Nov–Dec 2019; **(b)** T_{min}, Nov–Dec 2019; **(c)** T_{max}, Jan–Feb 2020; **(d)** T_{min}, Jan–Feb 2020.

Figure 11 shows RMSEs of Tmin city forecasts, GSM00 KF guidance and IFS12 KF guidance for Day 1 at each station in Nov–Dec 2019. RMSEs are relatively large in the northern region compared to in the central and southern regions, because daily temperature changes are large and forecasts for cities in the northern region are relatively difficult. RMSEs of GSM00 KF guidance and IFS12 KF guidance are smaller than city forecasts in many stations around Hanoi in particular.

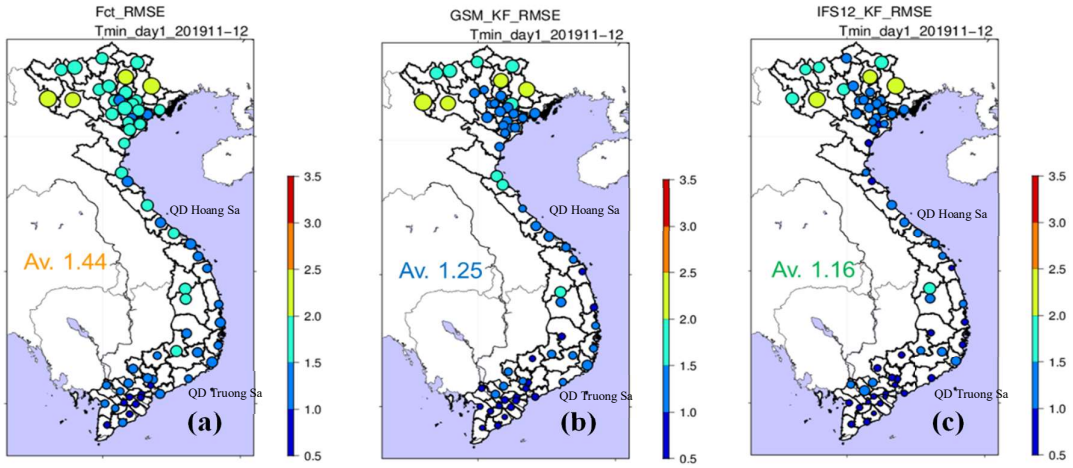

Figure 11. (a) RMSEs of city forecasts; (b) GSM00 KF guidance; (c) IFS12 KF guidance; for T_{min} Day 1 at each station in Nov–Dec 2019.

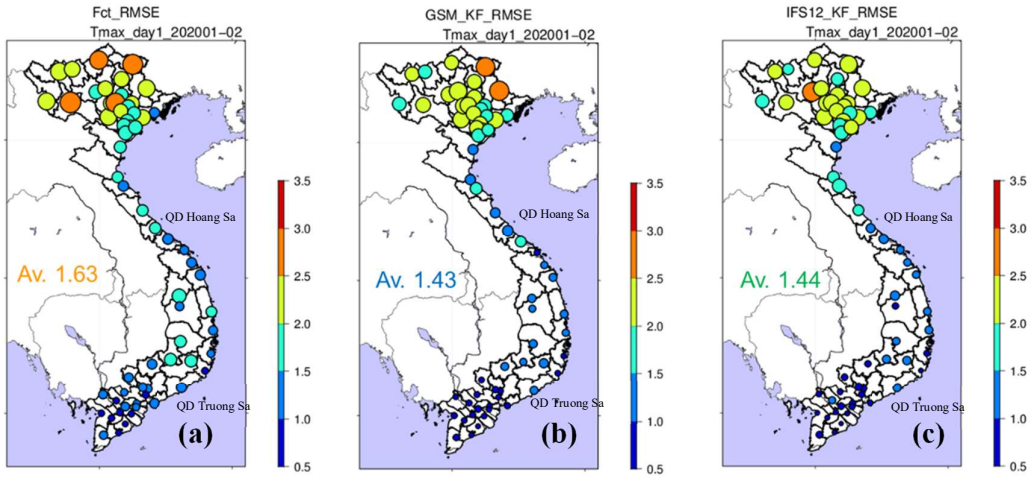

Figure 12. (a) RMSEs of city forecasts; (b) GSM00 KF guidance; (c) IFS12 KF guidance for T_{max} Day1 at each station in Jan–Feb 2020.

Figure 12 shows RMSEs of T_{max} city forecasts, GSM00 KF guidance and IFS12 KF guidance for Day1 at each station in Jan–Feb 2020. Features of RMSE distribution are similar to T_{min} RMSE distribution in Nov–Dec 2019. RMSEs are larger in the northern region than those of in the central and southern regions. RMSEs of KF guidance are smaller than city forecasts in many stations.

3.4.4. Consideration of predictors

Trial operation and verification of T_{max} and T_{min} KF guidance were made with one predictor; Tsfc (model surface temperature) of JMA GSM and ECMWF IFS surface GPV data. Some consideration to predictors was made by adding one or two predictors to Tsfc for further improvement of the KF guidance. Figure 13 shows RMSEs of GSM KF guidance of possible combination of predictors: "Tsfc", "Tsfc+Hsfc(humidity)", "Tsfc+U(wind_U–component)", "Tsfc+V(wind_V–component)", "Tsfc+TCDC(total cloud amount)", "Tsfc+Rain (rainfall)", "Tsfc+Hsfc+U" and "Tsfc+Hsfc+TCDC". Considerable reduction of RMSE was not found among these combinations of predictors, but small improvement was found in the combination of "Tsfc+Hsfc" for both T_{max} and T_{min} throughout the period from Nov 2019 to Feb 2020. We expected some improvement by adding wind component to Tsfc, but no substantial improvements were obtained.

By checking RMSEs of "Tsfc+Hsfc" at each station, 0.15 degrees to 0.3 degrees reduction of RMSE was found at several stations in the northern area including Hanoi and Haiphong. Figure 14 shows daily monitoring sheets of "Tsfc" KF guidance and "Tsfc+Hsfc" KF guidance of Hanoi and Haiphong for T_{max}–Day1 in Jan–Feb 2020. "Tsfc+Hsfc" predictors reduced RMSE of "Tsfc" predictor by 0.21 degrees in Hanoi and by 0.38 degrees in Haiphong. Errors of "Tsfc+Hsfc" predictors KF guidance are obviously smaller than "Tsfc" predictor KF guidance in a few days of H1 and H2 periods. We may have some improvement in the northern area, where daily changes of T_{max} and T_{min} are large and temperature forecasts are most difficult in the country, by using "Tsfc+Hsfc" predictors.

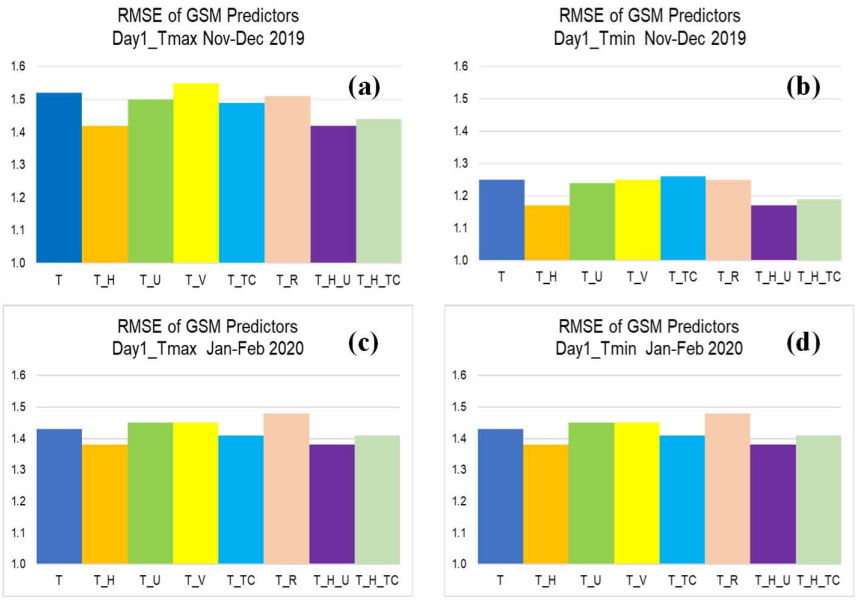

Figure 13. RMSEs of GSM00 KF guidance of City forecasts, GSM00 KF guidance of each combination of possible predictors: "Tsfc(T)", "Tsfc+Hsfc(T_H)", "Tsfc+U(T_U)", "Tsfc+V(T_V)", "Tsfc+TCDC(T_TC)", "Tsfc+Rain(T_R)", "Tsfc+Hsfc+U" and "Tsfc+Hsfc+TCDC" for Day1; (a) T_{max} Nov–Dec 2019; (b) T_{min} Nov–Dec 2019; (c) T_{max} Jan–Feb 2020; (d) T_{min} Jan–Feb 2020.

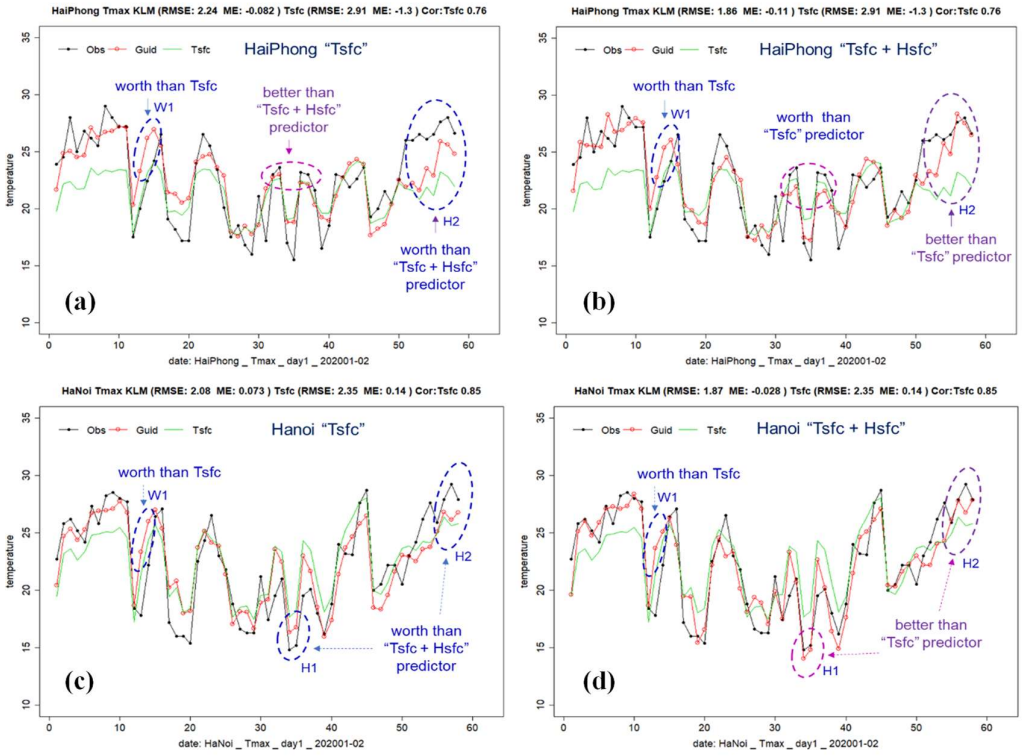

Figure 14. (a) monitoring sheets of "Tsfc" GSM00 KF guidance of Hanoi for T_{max}–Day1in Jan–Feb 2020; (b) "Tsfc+Hsfc" guidance of Hanoi; (c) "Tsfc" guidance of Haiphong; (d) "Tsfc+Hsfc" guidance of Haiphong.

We must note that the Kalman filter can catch up with a gradual weather change (seasonal weather change) but cannot catch up with the rapid weather change. A KF forecast may yield a large error when the weather changes suddenly, because the KF successive cycle is a "catch up with the previous relationship" system. For example, in Figure 14, T_{max} observations were higher than Tsfc at the beginning, then T_{max} observations became nearly equal to Tsfc (W1 period). As KF guidance caught up the relationship at the beginning, KF guidance were worth than Tsfc in the W1 period.

4. Conclusion and discussion

Maximum and minimum temperature guidance was developed with Kalman filter for 63 cities up to 3 days ahead using JMA GSM GPV data and up to 10 days ahead using ECMWF IFS GPV data as an activity of the JICA Project for Strengthening Capacity in Weather Forecasting and Flood Early warning System. Verification results show that RMSEs of GSM and IFS KF guidance are relatively large in the northern region, but KF guidance substantially reduces RMSEs of direct model outputs in all regions throughout the year. RMSEs of IFS guidance become smaller than those of GSM guidance with increasing forecast time. Averaged RMSEs of KF guidance for 63 cities are smaller than those of city forecasts issued by forecasters in Nov–Dec 2019 and Jan–Feb 2020. These verification results suggest that we will be able to improve accuracy of T_{max} and T_{min} city forecasts by using T_{max} and T_{min} KF guidance operationally in daily weather forecasting. We will continue to conduct verification and case studies for rapid weather change events in the next activities for operational use of KF guidance in daily weather forecasting.

Next our target is to develop rain guidance such as possibility of precipitation (PoP), mean precipitation amount or maximum precipitation amount. In preparation for development of rain guidance, we started collecting necessary observation data for rain guidance. As prediction accuracy of precipitation amount by NWP models is not so reliable compared to temperature predictions, we will start to grasp prediction accuracy and features in 3–regions; North–east region (PhuLien regional forecasting center), North–Central region (Vinh regional forecasting center) and Central–delta region (Hanoi central forecasting center). According to a first preliminary investigation, it seems rather difficult to prepare reliable rain guidance, but we will tackle to this challenging but important issue in the next activities.

Author Contributions: Conceptualization, K. Sasaki; methodology, K. Sasaki; software, K. Sasaki; observation and forecast data curation, V.T. Anh; IFS data curation, N.T. Hang and T. Trang; Verification, K. Sasaki; writing–original draft preparation, K. Sasaki; writing–review and editing, V.T. Anh, N.T. Hang and T. Trang.

Acknowledgments: Method of this work is based on training materials on guidance in the JICA group training course in meteorology being implemented by the Japan Meteorological Agency (JMA). We would like to thank JMA for their support. Mr. Ryusuke Taira of the Japan Meteorological Business Support Center helped us many times by sharing his knowledge and experiences on the Kalman filter technique obtained in the JICA Project for Enhancing Capacity on Weather Observation, Forecasting and Warning in the Philippines

from 2014 to 2017. We would like to thank the Working Groupe 3 members, NCHMF staff members and JICA experts of this Project for their cooperation to our activities.

Conflicts of Interest: The authors declare no conflict of interest.

References

1. Tonouchi, M.; Kasuya, Y.; Tanaka, Y.; Akatsu, K.; Akaeda, K., Nguyen, V.T. Activities of JICA on disaster prevention and achievement of JICA project in Period 1. *VN J. Hydrometeorol.* **2020**, *5*, 1–12.
2. Japan International Cooperation Agency; Japan Meteorological Business Support Center. OUTPUT 2–b (Weather Guidance), Project Completion Report, Technical Cooperation Project for Enhancing Capacity on Weather Observation, Forecasting and Warning in the Republic of the Philippines. 2017; 73–88. Available online: https://openjicareport.jica.go.jp/pdf/12289070.pdf
3. Hoa, V.V.; Hang, N.T.; Mai, N.C. Application of Kalman Filter method to correct surface variable forecast from HRM. *VN J. Hydrometeorol.* **2007**, *557*, 49–57.
4. Hoa, V.V.; Duc, L.; Thuy, D.L.; Tien, D.D. Application of the Updateable Model Output Statistics (UMOS) and Kalman Filter methods. Part II: results. *VN J. Hydrometeorol.* **2010**, *594*, 17–28.
5. Persson, A. Kalman filtering –A New Approach to Adaptive Statistical Interpretation of Numerical Forecasts. *WMO Tech. Doc.* 1991; No.421, XX–27–XX–32.
6. Simonsen, C. Self adaptive model output statistics based on Kalman filtering. *WMO Tech. Doc.* 1991; No.421, XX–33–XX–37.
7. Japan Meteorological Agency. Outline of the Operational Numerical Weather Prediction at the Japan Meteorological Agency March 2019. 2019; Chapter 4, pp. 139–168. Available online: http://www.jma.go.jp/jma/jma–eng/jma–center/nwp/outline2019–nwp/index.htm
8. Wilks, D.S. *Statistical Methods in the Atmospheric Sciences*, 3rd ed., Academic Press, 2011; Chapter 7, pp. 214–300.

VIETNAM JOURNAL OF HYDROMETEOROLOGY

Research Article

Heavy rainfall in central Viet Nam in December 2018 and modification of precipitation analysis at VNMHA

Kazuo Saito[1,2,3*], Mai Khanh Hung[4], Nguyen Viet Hung[5], Nguyen Quang Vinh[5], Du Duc Tien[4]

[1] Japan Meteorological Business Support Center, Tokyo101–0054, Japan; k–saito@jmbsc.or.jp
[2] Atmosphere and Ocean Research Institute, University of Tokyo, Kashiwa 277–8564, Japan; k_saito@aori.u.tokyo.ac.jp
[3] Meteorological Research Institute, Japan Meteorological Agency, Tsukuba 305–0052, Japan; ksaito@mri–jam.go.jp
[4] National Center for Hydro–Meteorological Forecasting, Hanoi 10000, Vietnam; maikhanhhung18988@gmail.com; duductien@gmail.com
[5] Aero Meteorological Observatory, Hanoi 10000, Vietnam; truongphi115@gmail.com; vinhnq83@gmail.com
***** Correspondence: k–saito@jmbsc.or.jp; Tel.: (+81–3–5577–2178)

Received: 11 June 2020; Accepted: 20 August 2020; Published: 25 August 2020

Abstract: On 9 December 2018, a heavy rainfall event occurred in central Viet Nam, and at Da Nang, a record–breaking rainfall of 972 mm was observed in 24 hours. The operational precipitation analysis at the Viet Nam Meteorological and Hydrological Administration (VNMHA) on the day considerably underestimated the intense rains. We checked causes of underestimation and modified the precipitation analysis by revising the use of observation data from Automated Weather Stations (AWS) and meteorological radar data. Since the cloud top height of the precipitation system was not high, satellite precipitation estimates using Himawari–8 data drastically underestimated intense rains around central Viet Nam. GSMaP on the day detected the intense rains to a certain extent, and their rainfall estimates (GSMaP_MVK and GSMaP_NOW) were applied to precipitation analysis as alternative satellite estimates. The revised precipitation analysis showed much better representation of the precipitation system. Verification of three precipitation estimates (Himarari–8, GSMaP_MVK, and GSMaP_NOW) against AWS observation was conducted. GSMaP products clearly outperformed precipitation estimates by Himawari-8, though their standard product (GSMaP_MVK) was better than the real time version (GSMaP_NOW).

Keywords: Heavy rainfall; JICA; GSMaP; Nowcast; Precipitation analysis; Himawari–8.

1. Introduction

In Viet Nam, meteorological disasters occur every year. In particular, disasters by heavy rains often cause the greatest damage, and improvement of nowcasting and forecasting of intense precipitation is a key issue for disaster prevention and mitigation. Since June 2018, a bilateral cooperative project between the Japan International Cooperation Agency (JICA) and the Viet Nam Meteorological and Hydrological Administration (VNMHA) for "Strengthening capacity in Weather Forecasting and Flood Early Warning System in the Social Republic of Vietnam" has been conducted. This project is related to S–band radars that were installed at Hai Phong (Phu Lien) and Vinh in September 2017 by another JICA

grant aid project. The Japan Meteorological Business Support Center (JMBSC) has been participating in the project as a main contributing organization of Japan. The project scopes are divided into four output targets: 1) surface meteorological observation; 2) radar maintenance and products; 3) weather forecasting; and 4) regional weather dissemination. More detailed reviews of the JICA project are given by [1].

One of the main targets of the JICA project is the quantitative precipitation estimation (QPE). Good QPE is attained by qualified networks of rain gauges and radars, and satellite data are used for supplementary information for filling data sparse areas as on the sea. QPE is important for disaster prevention/mitigation through detection of heavy rainfall areas. The application includes the very short–range forecast of precipitation, input of hydrological models, and verification of numerical weather prediction.

On 9 December 2018, a heavy rainfall event occurred in central Viet Nam, and at Da Nang, a record–breaking rainfall of 972 mm was observed in 24 hours. The operational precipitation analysis at VNMHA on the day considerably underestimated the intense rains. As the output 3 activity in the JICA project, we modified the precipitation analysis by revising the use of observation data from Automated Weather Stations (AWS) and meteorological radars. Since the cloud top height of the precipitation system was not high, satellite precipitation estimates using Himawari–8 data drastically underestimated intense rains around central Viet Nam. We applied GSMaP rainfall estimates to the precipitation analysis as alternative data for satellite estimates.

The organization of this paper is as follows. In Section 2, a heavy rainfall event in central Viet Nam on 9 December 2018 is introduced. In Section 3, operational precipitation analysis at VNMHA is introduced and modification of the analysis using AWS and radar data is described. In Section 4, application of GSMaP is shown. Verification of GSMaP and Himawari–8 satellite estimates of precipitation against AWS observation. Summary and concluding remarks are given in Section 5.

2. Heavy rainfall event in central Viet Nam on 9 December 2018

On 9th December 2018, a heavy rainfall event occurred in central Viet Nam, and at Da Nang, a record–breaking rainfall 972 mm was observed in 24 hours from 01 local standard time (LST) of December 9th (18 UTC of December 8th). Figure 1a shows three–hour rainfalls at Da Nang from 12 UTC December 8th to 18 UTC December 10th. The highest period of the heavy rainfall was from 18 UTC December 8th to 15 UTC December 9th. Observed 6–hour precipitation by SYNOP stations for 00 to 06 UTC of December 9th is indicated by Figure 1b.

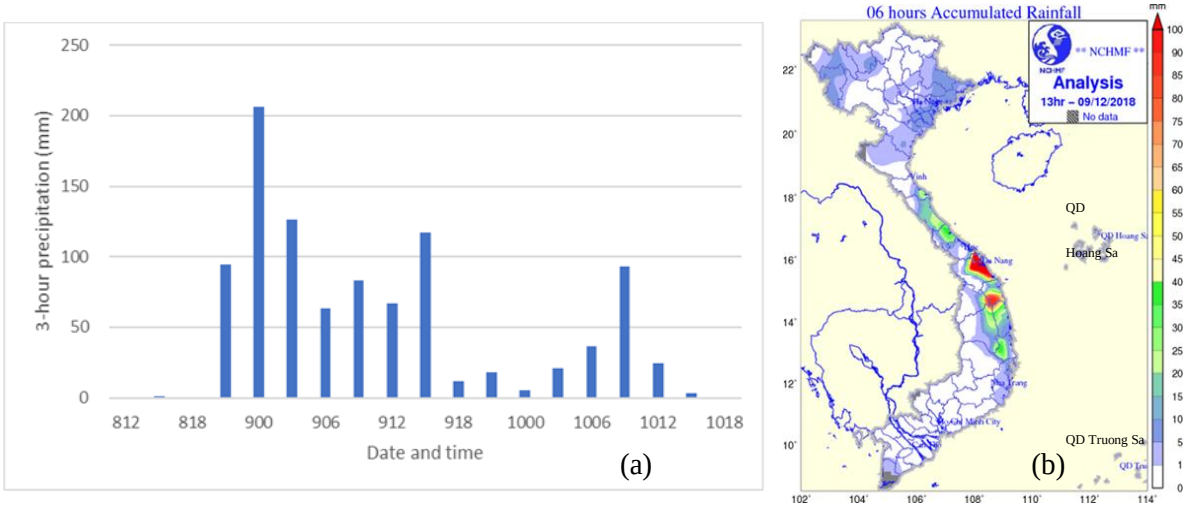

Figure 1. (a) Observed 3–hour rainfalls at Da Nang from 12 UTC 8th to 18 UTC 10th, December 2018; **(b)** Observed 6–hour precipitation at SYNOP stations for 00 to 06 UTC of December 9th.

This heavy rainfall occurred in a typical heavy rainfall situation in Viet Nam, relating to the northeasterly cold surge at the surface (Figure 2a). At 700 hPa level (Figure 2b), southeasterly moist air was lifted over the cold surge, suggesting abundant water vapor convergence in the lower troposphere.

Geostationary satellite (Himawari–8) images on the day suggested that this event was not brought by deep convection but mainly by the warm rain process, because the cloud top height of the rainfall system was not high (Figure 2c).

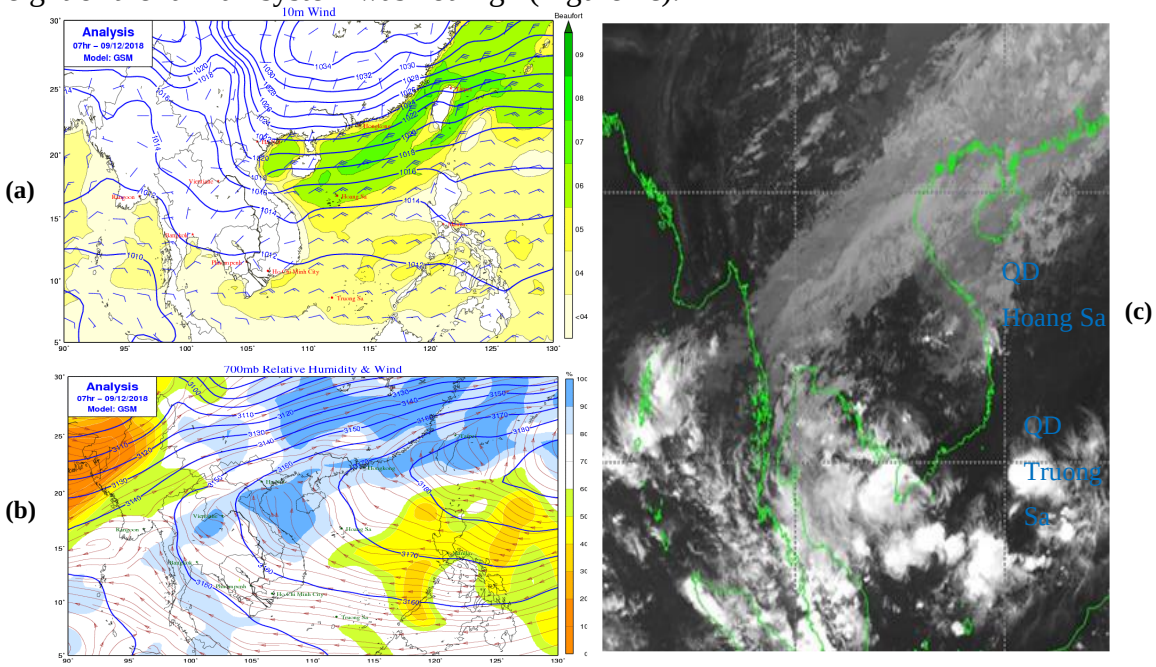

Figure 2. (**a)** Global analysis at 00 UTC 9 December 2018 by JMA. Mean sea level pressure and surface wind; (**b)** Relative humidity and wind at 700 hPa; **(c)** Infrared image by geostationary satellite (Himawari–8) at 00 UTC 9 December 2018.

3. Precipitation analysis at VNMHA

In VNMHA, 176 manned observatories (SYNOP) observe 6–hour accumulated rain at four times (00, 06, 12, 18 UTC) a day, and the rains are interpolated to 5 km grids to produce a rainfall map (Figure 1c). Since August 2018, a 3–hour accumulated rainfall map has been produced at the National Center for Hydro–Meteorological Forecasting (NCHMF) as a real time precipitation analysis, using observations from rain gauge data at about 1,100 AWS stations (Figure 3a) and precipitation estimates by meteorological radars (Figure 3b) and satellite. For details of meteorological radar observations at VNMHA [2].

Two kinds of precipitation analysis (“Mean” and “Max”) are produced at NCHMF. In “Mean”, a priority order of data, AWS, radar and satellite, is prescribed, and precipitation amount at each analysis grid (5 km resolution) is determined by higher priority data source in order among the available data (e.g., a mean value of AWS precipitation is taken first if AWS rain gauge data are available). In “Max”, the maximum value of the available data is selected.

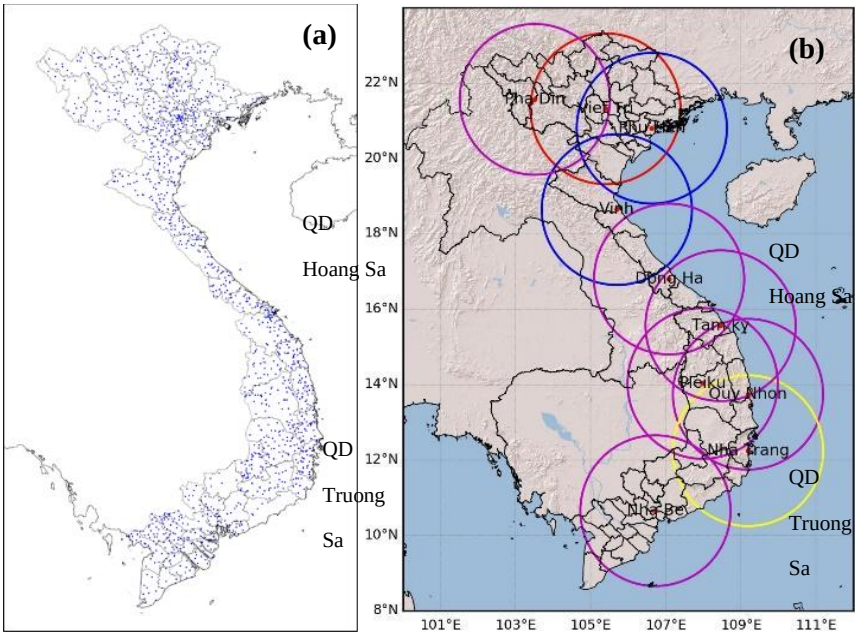

Figure 3. (**a**) AWS stations of VNMHA; (**b**) Meteorological radars of VNMHA (as of 2019). Purple circles represent Vaisala radars, blue circles as Japan Radio Company (JRC) radars, red circle as Thompson radar and yellow circle as Enterprise Electronic Corporation (EEC) radar.

4. Modification of precipitation analysis

Figure 4 is the precipitation analysis of 9 December 2018 that produced by NCHMF in operation on that day. Despite the intense rain observed by SYNOP (Figure 1b), no intense precipitation was analyzed over central Viet Nam. We checked three components of the precipitation analysis (AWS, radar, and satellite).

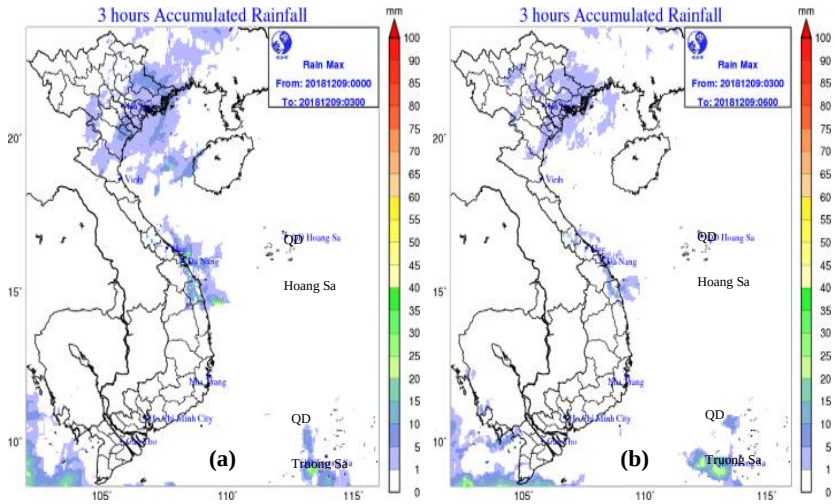

Figure 4. Precipitation analysis at VNMHA on 9th December 2018: **(a)** For 00 to 03 UTC; **(b)** For 03 to 06 UTC.

4.1. AWS observation

Figure 5 shows three–hour precipitation observed by AWS on 9th December 2018. For 00–03 UTC, seven AWS stations (Cau Lau, Cam Le, Hoi An, Da Nang, Thanh Binh, Trang Bom, Tay Thuan), and for 03–06 UTC, six stations (Cau Lau, Hoi An, Tam Ky, Thanh Binh, Ho Nui Mot, Duy Son) detected intense rains above 80 mm. Errors were found in the treatment of AWS observation data in real time operation of precipitation analysis at NCHMF

on the day. The errors were in data transfer and storing methods for AWS stations coming from different projects, and were fixed after the event.

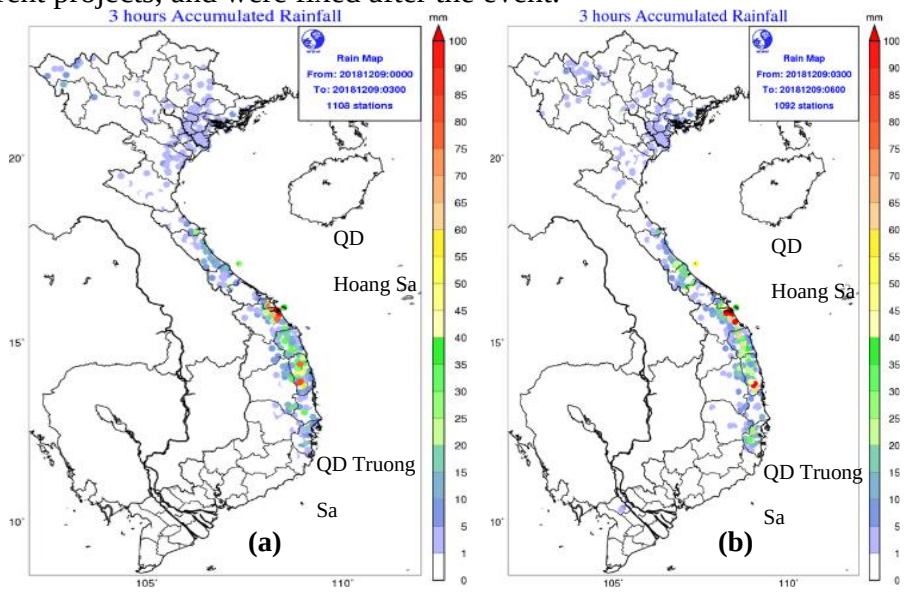

Figure 5. Three–hour precipitation observed by AWS on 9 December 2018: **(a)** for 00 to 03 UTC; **(b)** for 03 to 06 UTC.

4.2. Radar estimation

Figure 6 shows three–hour precipitation estimated from weather radars of VNMHA on 9th December 2018. The estimation is produced by Aero–Meteorological Observatory (AMO) of VNMHA from the radar reflectivity composite map using the Z–R relationship of

$$Z=200*R^{1.6} \quad (1)$$

Here, Z is the radar reflectivity factor in $mm^6\ m^{-3}$ and R the rain rate in mm. This relationship is based on the observation of raindrop size distribution [3].

In the radar composite map used for the operation on the day, data from Vinh radar were not used (Figure 7a). Actually, the Vinh radar was operated on the day, and its data were archived by the JICA team member. We added the data to the composited map (Figure 7b). Figure 8 is three-hour precipitation estimated from radars including Vinh. Precipitation areas near Vinh appeared, however, precipitation around central Viet Nam is not necessarily very strong.

Two C–band weather radars of VNMHA at Dong Ha and Tam Ky are located at east coastal areas of central Viet Nam and there are mountain areas in the west. Since their antennas' altitudes are low (about 40 m above the mean sea level), terrain shielding occurs for low elevation angle (0.5 degree) in the west side semicircle as shown in Figures 9–10. As for other factors, adjustment for attenuation by precipitation in C–band radars may be insufficient. There is room for reconsidering in the Z–R relationship, because when the warm rain process is dominant small size raindrop particles relatively increase compared with the intense rain case with the ice phase.

Figure 10 shows modified three–hour precipitation analysis using AWS data, radar data including Vinh radar and satellite estimated rainfall on 9 December 2018. Compared with the original analysis (Figure 4), improvement is distinct in the representation of rainfall areas in central Viet Nam, however, precipitations over the sea are likely still insufficient as suggested by the satellite image (Figure 2c).

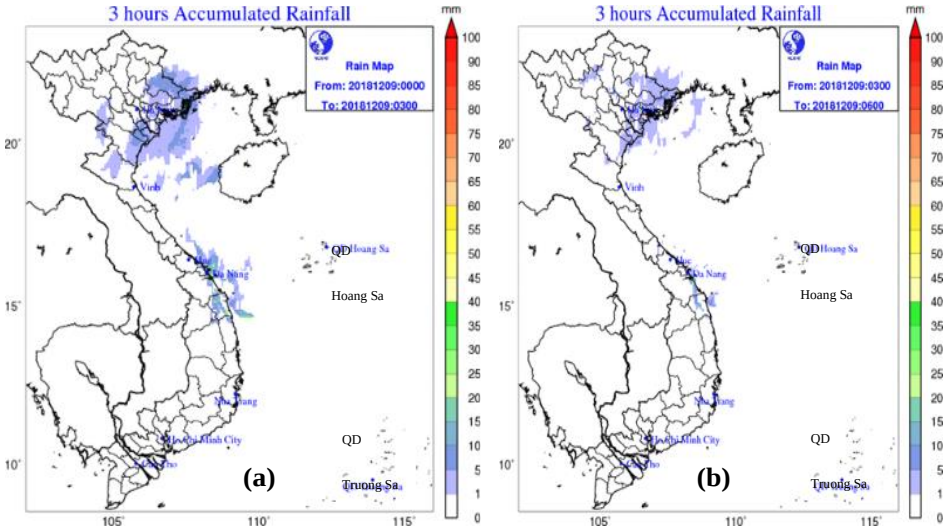

Figure 6. Radar estimated rainfall from reflectivity composite map on 9 December 2018; (a) For 00 to 03 UTC; (b) For 03 to 06 UTC.

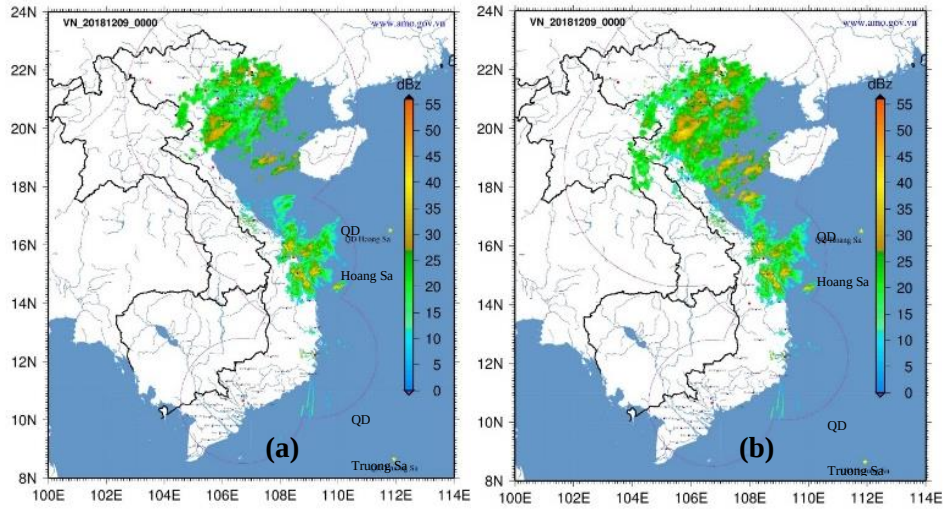

Figure 7. (a) Radar reflectivity composite map at 00 UTC, 9 December 2018; **(b)** Same as a) but with Vinh radar data.

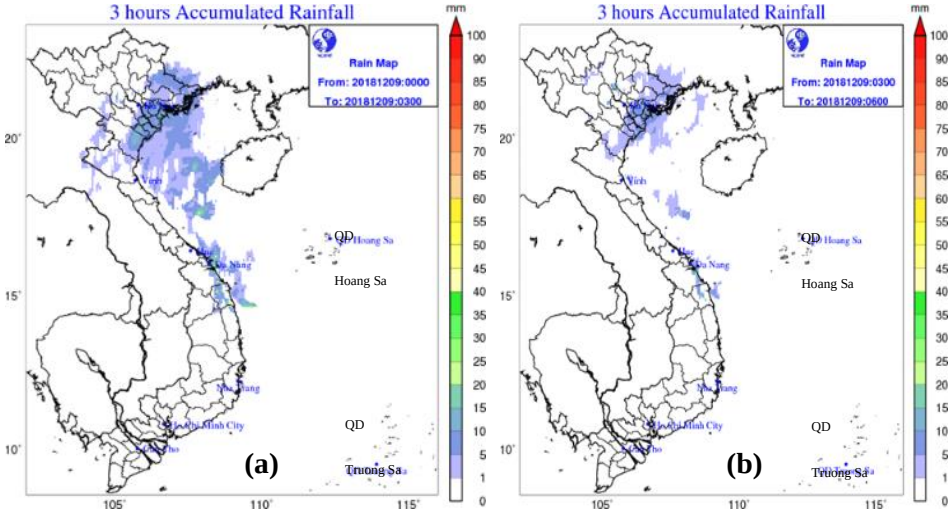

Figure 8. Radar estimated rainfall from reflectivity composite map on 9 December 2018 with Vinh radar data: **(a)** For 00 to 03 UTC; **(b)** For 03 to 06 UTC.

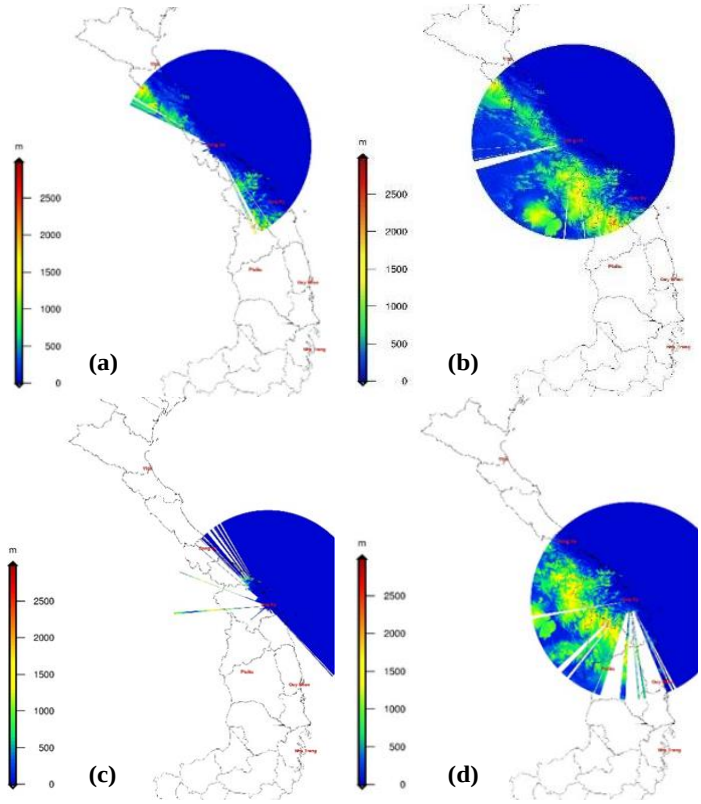

Figure 9. Terrain shielding at Dong Ha radar: **(a)** Elevation angle 0.5 degree; **(b)** Elevation angle 1.0 degree; **(c)** Same as Figures 9a but for Tam Ky radar; **(d)** Elevation angle 1.0 degree.

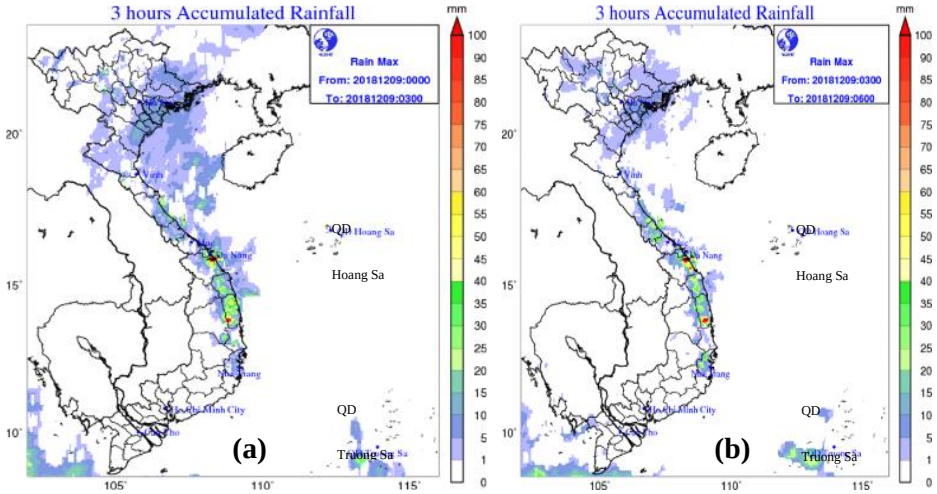

Figure 10. Modified three–hour precipitation analysis with AWS data and Vinh radar data on 9 December 2018: **(a)** For 00 to 03 UTC; **(b)** For 03 to 06 UTC.

4.2. Satellite rainfall estimation

Figure 11 shows three–hour precipitation estimates from the Himawari–8 satellite processed by AMO on 9 December 2018. Estimated rainfall intensity around central Viet Nam is very weak.

AMO uses relationship between cloud top brightness temperature (TBB) and rainfall intensity R (Figure 12a):

$$R = 1.1183*10^{11} exp(-3.6382*10^{-2} T_{BB}^{1.2}) \quad (2)$$

This relationship is based on statistics between TBB observed by the GOES satellite and radar–estimated rainfall over north America [4]. As shown in Figure 2c, cloud top height of the precipitation system near central Viet Nam on the day was not high. Indeed, its TBB by infrared image was around –4 ^{o}C (Figure 12b), which corresponds to only 1.2 mm/h in the rain rate by Eq. (2). Rainfall estimates based on brightness temperatures by a geostationary satellite have a limit in accuracy, because it does not observe the rain directly but is a statistical relationship.

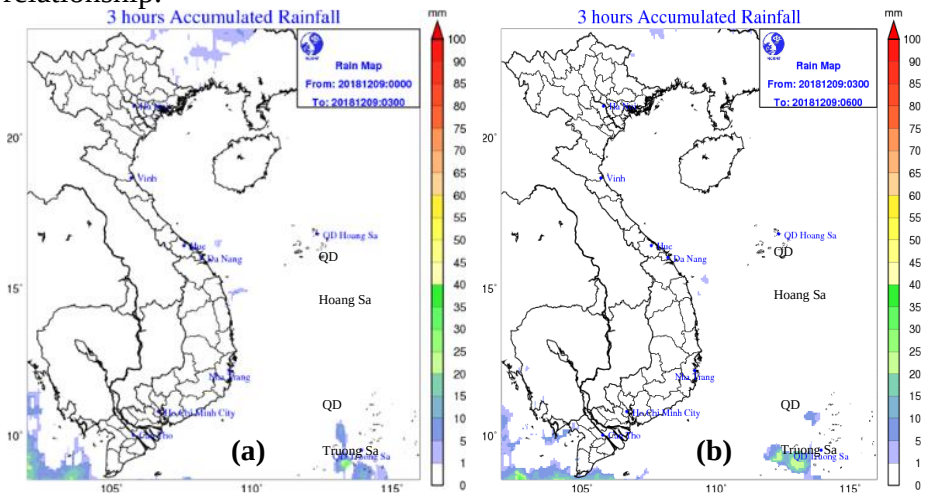

Figure 11. Estimated rainfall from satellite (Himawari–8) on 9 December 2018: **(a)** for 00 to 03 UTC; **(b)** for 03 to 06 UTC.

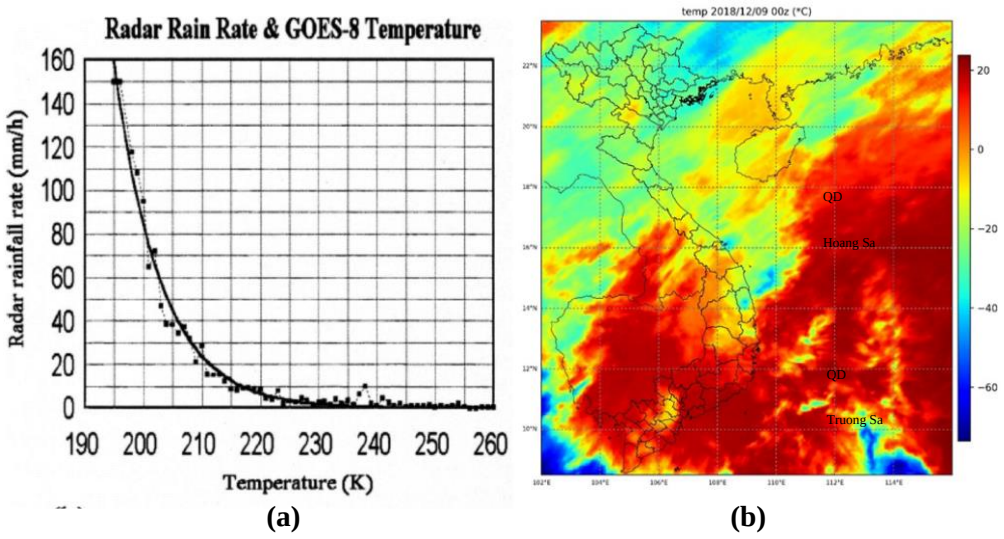

Figure 12. (a) Relationship between TBB and rainfall rate by Vicente et al. (1998); **(b)** T_{BB} observed by Himawari–8 at 00 UTC 9 December 2018, corresponding to Figure 2c.

5. Application of GSMaP estimated rain

5.1. GSMaP

GSMaP is the rainfall estimate operated by the Earth Observation Research Center (EORC) of the Japan Aerospace Exploration Agency (JAXA) based on satellite observations. Main source to observe rainfall is microwave radiometer data from Global Precipitation Measurement (GPM) satellites [5–7]. As shown in Figure 13a, operational GSMaP products are classified to several kinds according to their latencies. Standard product is GSMaP_MVK, whose latency is about 3 days. Since observation frequency of satellite

microwave data is about three hourly at each targeted point, in GSMaP_MVK, precipitation rates at no observation times are estimated by combining forward and backward extrapolations with observation data immediately before and after the analysis times. Extrapolations are conducted using horizontal winds based on cloud motion vectors (AMVs) by the geostationary satellite (Figure 13b).

GSMaP_NRT and GSMaP_NOW are products more focused on promptness. In GSMaP_NRT, the rain rate is estimated by forward extrapolation only using observation data immediately before for the near real time operation. In GSMaP_NOW, to provide the results at real time, the rain rate is estimated every 30 min based on extrapolation of GSMaP_NRT at immediately before and available satellite data at the analysis time.

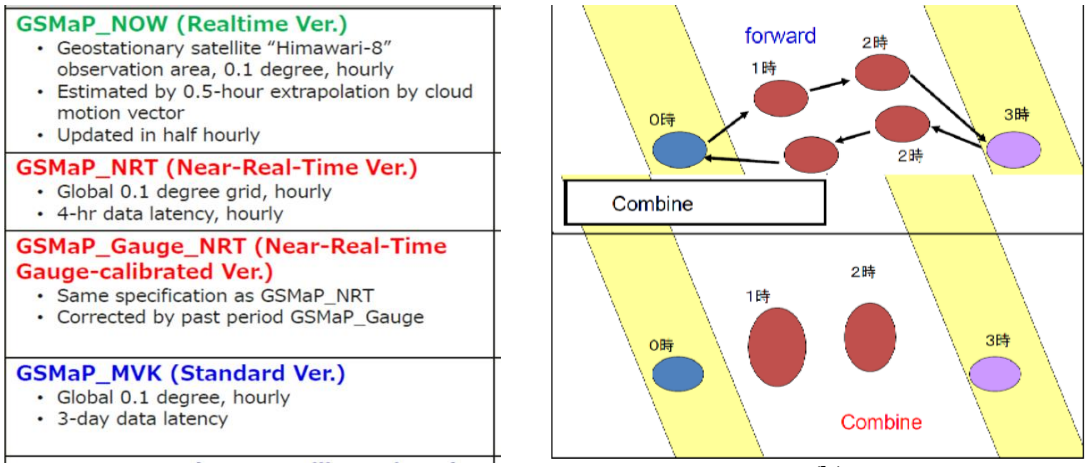

(a) (b)

Figure 13. (a) Classification of operational GSMaP data [6]; **(b)** Conceptual diagram of rain estimation by GSMaP_MVK [7].

5.2. GSMaP on the Da Nang heavy rainfall event

GSMaP detected the intense rains over central Viet Nam on 9th December 2018 up to a point. Figure 14 shows hourly rainfall estimates by GSMaP_MVK for 01 to 06 UTC of 9th December 2018. Rainfall intensity is strong at 02 and 05 UTC, when microwave data are available. At other times, rainfall rates are relatively weak due to interpolation (combination of forward and backward extrapolations).

Figure 15 is hourly rainfall intensity and accumulated rainfall amount at a grid point near Da Nang (16.04N, 108.21E) for 8th to 10th December by GSMaP_MVK. The accumulated rain amount is still underestimated, however, in maximum, 200 mm/h hourly rainfall intensity and 600 mm accumulated precipitation were estimated at another point (14.53N, 108.8E) in central Viet Nam (figure not shown).

In the viewpoint of real time disaster prevention, accuracy of GSMaP_NOW is more important. Figure 16 is hourly rainfall estimation by GSMaP_NOW corresponding to Figure 14. Here, the hourly rainfall amount was calculated by a sum of two 30 min rainfall intensities. Compared with GSMaP_MVK, there is a time lag in GSMaP_NOW in the timing of intense rains, which is attributable to the forward extrapolation used in GSMaP_NOW.

As shown in Figures 14 and 16, the hourly rainfall intensities by GSMaP fluctuate depending on available microwave data, however, the three–hour accumulated rainfall amount is likely usable to precipitation analysis because the GPM satellite microwave

observation is generally available three hourly. Figure 17 shows three–hour rainfall estimates for 9th December 2018 by GSMaP_MVK and GSMaP_NOW corresponding to Figure 11. The rainfall system around central Viet Nam is much well represented compared with the Himawari–8 satellite estimates.

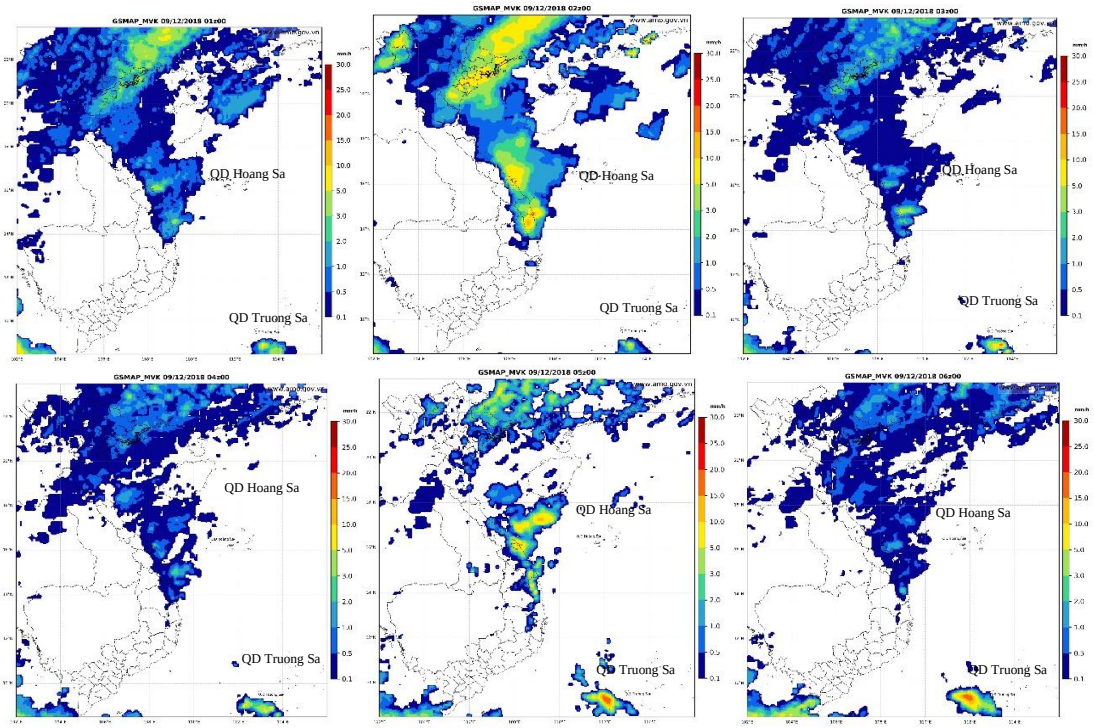

Figure 14. Hourly rainfall estimation by GSMaP_MVK for 01 to 06 UTC 9 December 2018.

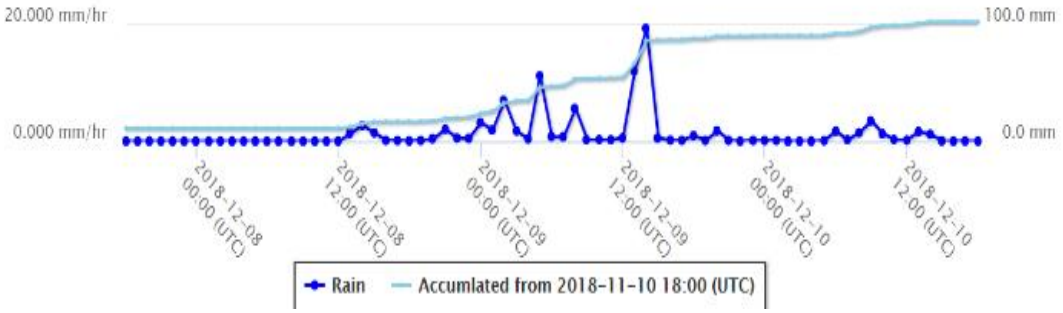

Figure 15. Hourly rainfall intensity (blue) and accumulated rainfall amount (light blue) at a point near Da Nang (16.04N, 108.21E) for 8th to10th Dec 2018 by GSMaP_MVK.

Figure 18 shows the modified 3–hour precipitation analysis using GSMaP data on 9 December 2018 corresponding to Figure 10. Here, satellite estimation by Himawari-8 was replaced by GSMaP data, and both AWS data and Vinh radar data are used in addition. Both figures with GSMaP_MVK and GSMaP NOW are seemingly much better than the original analysis (Figure 4) and improved from that using the Himawari–8 estimated rain (Figure 10).

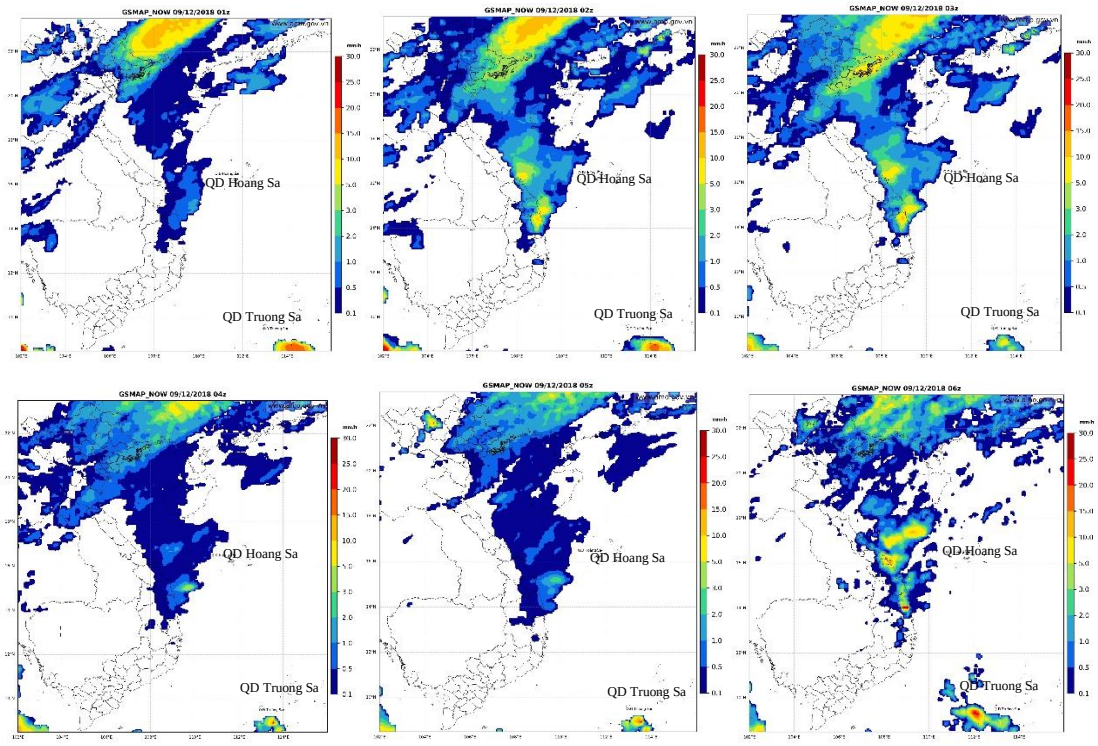

Figure 16. Hourly rainfall estimation by GSMaP_NOW for 01 to 06 UTC 9 December 2018.

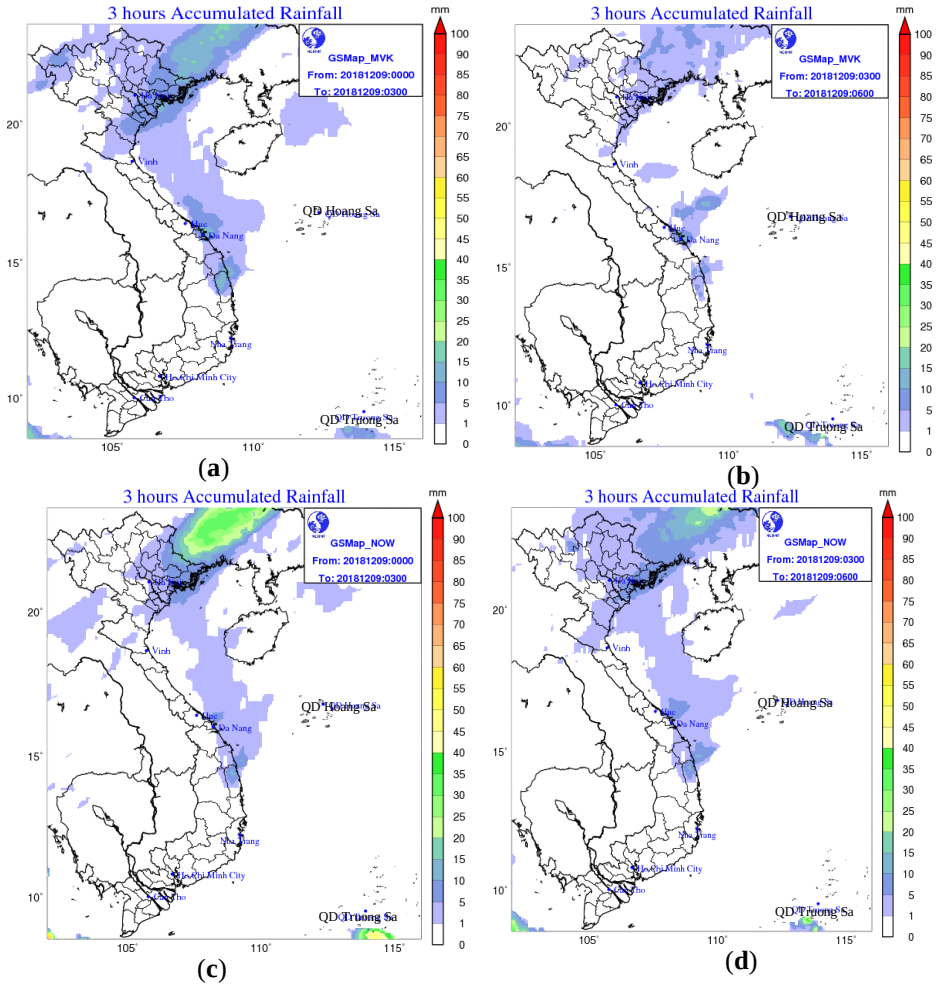

Figure 17. Three–hour rainfall estimation for 9 December 2018: **(a)** 00–03 UTC by GSMaP_MVK; **(b)** 03–06 UTC; **(c)** 00–03 UTC by GSMaP_NOW; **(d)** 03–06 UTC.

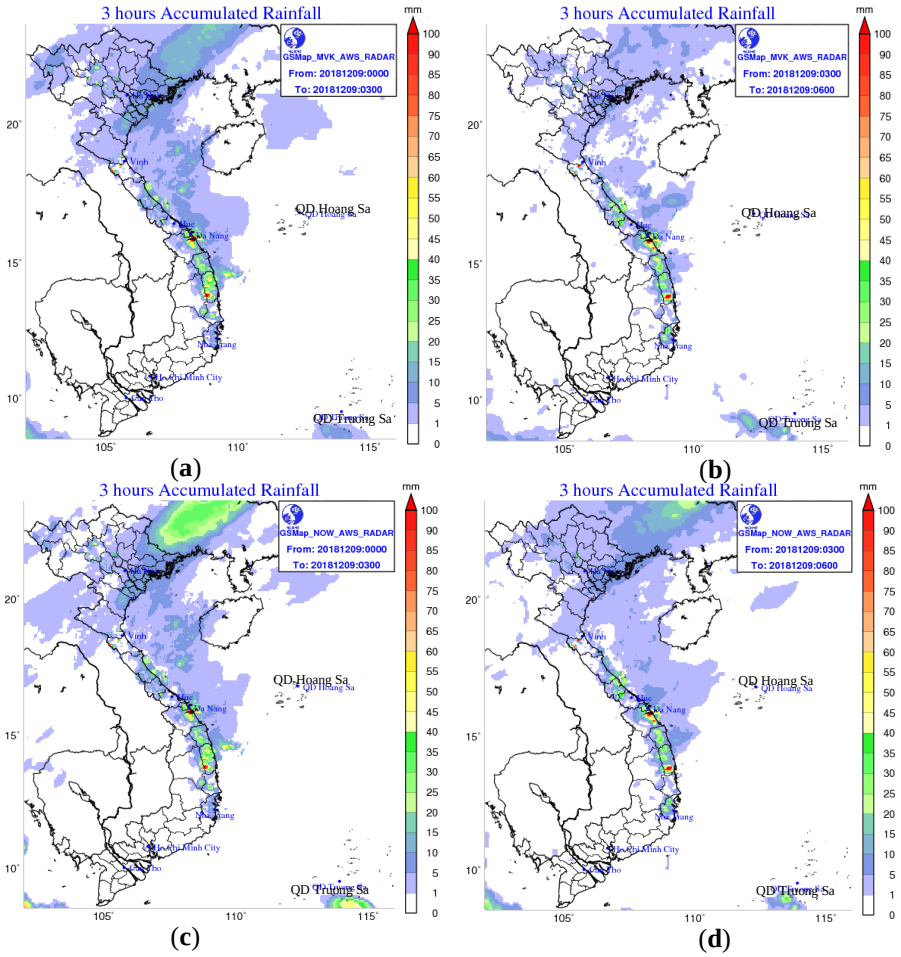

Figure 18. Modified precipitation analysis for 9 December 2018 using AWS and Vinh radar data with GSMaP data: **(a)** 00 to 03 UTC with GSMaP_MVK; **(b)** 03–06 UTC; **(c)** 00–03 UTC by GSMaP_NOW; **(d)** 03–06 UTC.

5.3. Verification

We verified the rainfall estimates by GSMaP_MVK, GSMaP_NOW and Himawari–8 on 9th December 2018 against AWS observations. Figure 19 shows scatter diagrams of the three estimates against AWS rains for 3–hour accumulated precipitation for 00 to 03 UTC. Here, verification was done with 5 km grids of precipitation analysis over the land. As suggested by Figures 11–12, Himawari–8 (Figure 19c) drastically underestimates intense rains, while both GSMaP_MVK and GSMaP_NOW express intense rains up to a point. Figure 21a shows threat scores of the three estimates. Threat scores of Himawari–8 are almost zero for thresholds over 3 mm per 3 hours. GSMaP_MVK is better than GSMaP_NOW, but both GSMaP estimates notably outperform the Himawari–8 for this period.

Figures 20 and 21b indicate results of the same verification of 3–hour rains for the whole day (00 to 24 UTC) of 9th December. In scatter diagrams, GSMaP sometimes overestimated rains, while no intense rains are seen in Himawari–8. The tendency of threat scores is almost the same as for 00–03 UTC. Himawari–8 drastically underestimates intense rains, and though GSMaP_MVK is better than GSMaP_NOW, both GSMaP estimates clearly outperform Himawari–8.

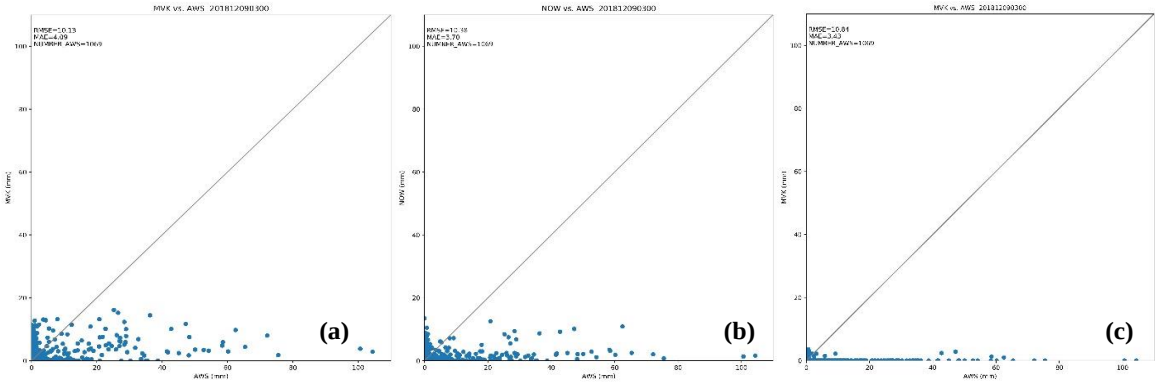

Figure 19. (a) Scatter diagram between GSMaP_MVK (vertical axis) and AWS (horizontal axis) for 3–hour precipitations on 9th December 2018 (00–03 UTC); **(b)** Same as in a) except for GSMaP_NOW; **(c)** Same as in a) except for Himawari–8.

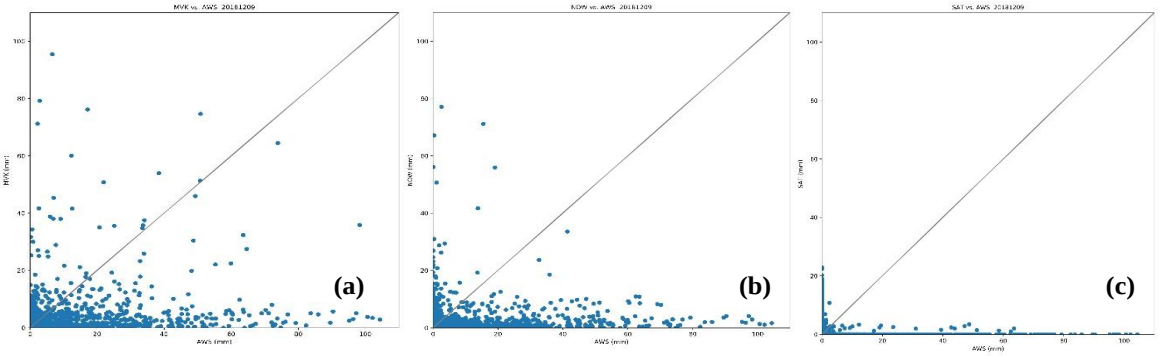

Figure 20. (a) Scatter diagram between GSMaP_MVK (vertical axis) and AWS (horizontal axis) for 3–hour precipitations on 9th December 2018 (00–24 UTC; eight 3–hour precipitations); **(b)** Same as in a) except for GSMaP_NOW; **(c)** Same as in a) except for Himawari–8.

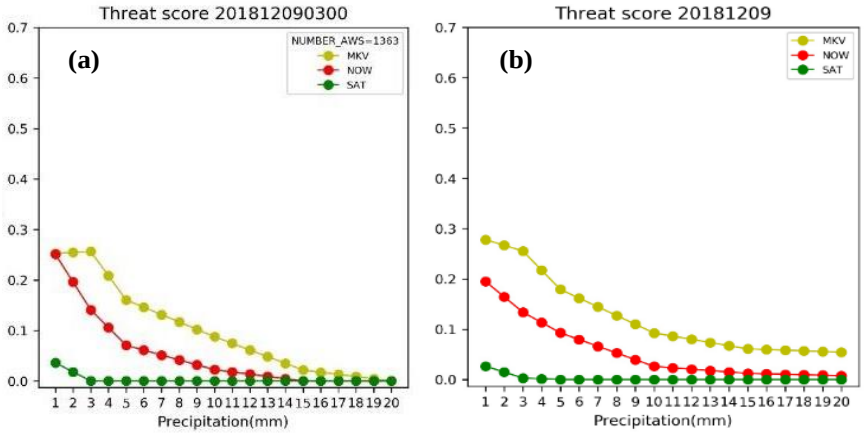

Figure 21. Threat scores of GSMaP_MVK (light green) GSMaP_NOW (red) and Himawari–8 (green) 3–hour precipitations for 00–03 UTC against AWS observation: **(a)** For 3–hour precipitations on 9 December 2018 (00–03 UTC); **(b)** Same as in (a) but for 00–24 UTC.

6. Summary and concluding remarks

We checked the quality of the operational precipitation analysis at VNMHA for the case of a heavy rainfall event in central Viet Nam in December 2018. The precipitation analysis was modified by revision of the use of observation data from AWS and additional radar data at Vinh, and application of GSMaP data. The revised precipitation analysis showed much better representation of the heavy precipitation system.

Comparison and verification of GSMaP data and Himawari-8 estimated rains against AWS observation were conducted. GSMaP distinctively outperforms precipitation estimates by Himawari-8, though their real time version (GSMaP_NOW) is inferior to the standard product (GSMaP_MVK). It is recommended to use GSMaP_NOW for real time operation for disaster prevention and to use GSMaP_MVK for verification of NWP to cover a shortage of AWS and radar data.

NCHMF started operational use of GSMaP data for their precipitation analysis in October 2019. Validation of the operational application of GSMaP is given by a separate paper [8].

Author Contributions: Conceptualization, K. Saito; methodology, K. Saito, M.K. Hung and N.V. Hung; validation, M.K. Hung, N.V. Hung and K. Saito; AWS data curation, M.K. Hung and K. Saito; Radar data curation, N.Q. Vinh and K. Saito; Satellite data curation, N.V. Hung and K. Saito; writing–original draft preparation, K. Saito; writing–review and editing, D.D. Tien and M.K. Hung; supervision, D.D. Tien; project administration, K. Saito and D.D. Tien; All authors have read and agreed to the published version of the manuscript.

Acknowledgments: The authors thank to Cuong Nguyen Minh of the Viet Nam Meteorological and Hydrological Administration, Kenji Akaeda, leader of JICA team, and other JICA team members (Michihiko Tonouchi, Kiichi Sasaki, and Hiroyuki Ichijo of the Japan Meteorological Business Support Center and Chiho Kimpara of the Japan Weather Association) for their support. Thanks are extended to Moeka Yamaji and Takushi Kubota of the Japan Aerospace Exploration Agency for their comments and help on GSMaP data.

Conflicts of Interest: The authors declare no conflict of interest.

References

1. Tonouchi, M.; Kasuya, Y.; Tanaka, Y.; Akatsu, K.; Akaeda, K.; Nguyen, V.T. Activities of JICA on disaster prevention and achievement of JICA project in Period 1. *VN J. Hydrometeorol.* **2020**, *5*, 1–12.
2. Kimpara, C.; Tonouchi, M.; Hoa, B.T.K.; Hung, N.V.; Cuong N.M.; Akaeda, K. Quantitative precipitation estimation by combining rain gauge and meteorological radar network in Vietnam. *VN J. Hydrometeorol.* **2020**, *5*, 36–50.
3. Marshall, J.S.; Palmer, W.M. The Distribution of raindrops with size. *J. Meteor.* **1948**, 5, 165–166. doi: 10.1175/1520–0469(1948)005<0165:TDORWS>2.0.CO;2
4. Vicente, G.; Scofield, R.A.; Mensel, W.P. The operational GOES infrared rainfall estimation technique. *Bull. Amer. Meteor. Soc.* **1998**, *79*, 1881–1898. doi: 10.1175/1520–0477(1998)079<1883:TOGIRE>2.0.CO;2
5. Aonashi, K.; Awaka, J.; Hirose, M.; Kozu, T.; Kubota, T.; Liu, G.; Shige, S.; Kida, S.; Seto, S.; Takahashi, N.; Takayabu, Y.N. GSMaP passive, microwave precipitation retrieval algorithm: Algorithm description and validation. *J. Meteor. Soc. Japan* **2009**, *87A*, 119–136. doi: 10.2151/jmsj.87A.119
6. Kubota, T.; Aonashi, K.; Ushio, T.; Shige, S.; Takayabu, Y.; Arai, Y.; Tashima, T.; Kachi, M.; Oki, R. Recent progress in global satellite mapping of precipitation (GSMAP) product. Proc. 2017 IGARSS, Fort Worth, TX **2017**, 2712–2715. doi: 10.1109/IGARSS.2017.8127556

7. Ushio, T. Structure and concept of high resolution GSMaP algorithms. JAXA/EORC workshop on water cycle, **2017**. Available online: http://www.eorc.jaxa.jp/event/2016/pdf/04_ushio.pdf
8. Hung, M.K.; Saito, K.; Khiem, M.V.; Tien, D.D.; Hung, N.V. Verification of GSMaP data in precipitation nowcasting at Vietnamese National Center for Hydro–Meteorological Forecasting. *VN J. Hydrometeorol.* **2020**, *5*, 80–94.

VIETNAM JOURNAL OF HYDROMETEOROLOGY

Research Article

Application of GSMaP Satellite data in precipitation estimation and nowcasting: evaluations for October 2019 to January 2020 period for Vietnam

Mai Khanh Hung[1*], Kazuo Saito[2,3,4], Mai Van Khiem[1], Du Duc Tien[1], Nguyen Viet Hung[5]

[1] National Center for Hydro–Meteorological Forecasting; maikhanhhung18988@gmail.com; maikhiem77@gmail.com; duductien@gmail.com
[2] Japan Meteorological Business Support Center, Japan; k–saito@jmbsc.or.jp
[3] Atmosphere and Ocean Research Institute, University of Tokyo, Japan; k_saito@aori.u.tokyo.ac.jp
[4] Meteorological Research Institute, Japan Meteorological Agency, Japan; ksaito@mri–jam.go.jp
[5] Aero Meteorological Observatory; truongphi115@gmail.com
* Correspondence: maikhanhhung18988@gmail.com; Tel.: +84916400000

Received: 05 June 2020; Accepted: 20 August 2020; Published: 25 August 2020

Abstract: The GSMaP Rainfall (Global Satellite Mapping of Precipitation) data (GSMaP_NOW and GSMaP_MVK) have been used for precipitation analysis at Vietnamese National Center for Hydro–Meteorological Forecasting (NCHMF) since October 2019. This study verified the quality of rainfall estimates of GSMaP_NOW, GSMaP _MVK and Himawari–8 based on 6 hourly rain gauge data from 184 SYNOP stations for a 4–month period from October 2019 to January 2020. The results show that GSMaP_MVK has the best rainfall estimate among the three data types in terms of RMSE, correlation and other categorical statistics except the probabilty of detection (POD). GSMaP_NOW was better than Himawari–8 for RMSE, correlation, and flase alarm rate, whilethe threat scores of GSMaP_NOW and Himawari–8 were in the same level. Himawari–8 tended to overestimate intense rains, and its bias scores were very large. This overestimation is significant when the cloud top temperature of prerecipitation system is very low. GSMaP_NOW can be used in parallel with Himawari–8 rainfall estimates to provide realtime information to the forecasters in forecasting and warning on the heavy rainfall, flash flood and landslide.

Keywords: Satellite precipitation estimates; GSMaP_NOW; GSMaP_MVK; Himawari–8; Precipitation nowcasting; Verification of rainall.

1. Introduction

Vietnam is one of the countries that suffers from many natural disasters every year [1]. In particular, disasters by heavy rains often cause the greatest damage in Vietnam. Therefore, monitoring, forecasting and warning of heavy rainfall, flash floods, landslides, and land subsidence due to floods are necessary and also the most important tasks of the Vietnamese National Center for Hydro–Meteorological Forecasting (NCHMF). In the past, forecasters carried out these works mainly based on rain gauge data and radar precipitation estimates. However, the density of observatories and radar stations is sparse. This makes it difficult for forecasters in heavy rainfall monitoring, forecasting and floods and landslides warning,

especially in areas where rainfall observations are limited. Rainfall estimates from satellites have been used to compensate this problem. In the world, there are many studies showing the effectiveness of satellite precipitation estimates in forecasting heavy rainfall landslides and flash floods [2–3].

Currently, NCHMF is receiving satellite Himawari–8 precipitation estimates from Aero Meteorological Observatory (AMO) operationally. These data provide precipitation information for areas where rain gauge observation stations and radar–estimated rainfall are insufficient. Himawari–8 rainfall estimates are used by forecasters to monitor cloud systems and update rainfall level to give timely forecastings and to warn heavy rain, flash flood and landslide. However, there are limitations in Himawari–8 data to accurately estimate precipitation, because it observes cloud systems by the brightness temperature [4–5]. These are difficulties for forecasters in monitoring, forecasting and warning heavy rain. An additional satellite rainfall estimate is needed to continuously provide rainfall information to forecasters. The GSMaP (Global Satellite Mapping of Precipitation) rainfall data is a useful solution. There are many studies proving the role of GSMaP in operational forecasts and research. GSMaP precipitation data is high–resolution estimates of rainfall based on satellite microwave radiometers provided by the Japan Science and Technology Agency (JST) and the Japan Space Exploration Agency (JAXA). GSMaP data have been evaluated and applied in many parts of the world [6–7]. In Vietnam, Ngo Duc Thanh et al. examined performance of GSMaP in central Vietnam for long–term rain [8].

Recently, Saito et al. [5] tested GSMaP data to improve the precipitation analysis at NCHMF. They compared the accuracy of precipitation estimates by GSMaP_NOW, GSMaP_MVK and Himawari–8 against AWS precipitation for a heavy rainfall case in central Vietnam in December 2018. Since October 2019, GSMaP has been used for operation at NCHMF. In order to confirm that GSMaP_NOW and MVK data are suitable for the operation, it is necessary to validate them for a long–term period. Based on that reason, this study carried out the evaluation of GSMaP_NOW and MKV in the period from October 2019 to the end of January 2020 as a foundation for applying this data in business.

2. Materials and Methods

2.1. Framework of Research

The aim of this research is to verify the 6–hour rainfall estimates from Himawari–8, GSMaP_NOW and GSMaP_MVK against rain gauge data. The data series used for this verification is four months from October 2019 to January 2020. Himawari–8 satellite estimates of rainfall are provided hourly from AMO to NCHMF with a horizontal resolution of 5km (0.045 degree). In this study, the 6–hour rainfall amount was calculated as the sum of six consecutive hourly rainfall estimates data. GSMAP_MKV is high–resolution (0.1 degree) global rain estimate with short time steps (1 hour) using passive microwave radiation measurement data by GPM satellites. This data was smoothed out based on the Kalman filter model, which is based on analysis of atmospheric motion vectors obtained from two consecutive infrared images by geostationary satellites [9–10]. JAXA develops a near real–time version of GSMAP products (GSMaP_NRT) for the monitored area of the Himawari–8 to create rainfall estimates in real time. After that, the next 0.5hours data is extrapolated by atmospheric motion vectors to create the GSMAP_NOW rain product at the present time with available satellite microwave data [11–12].

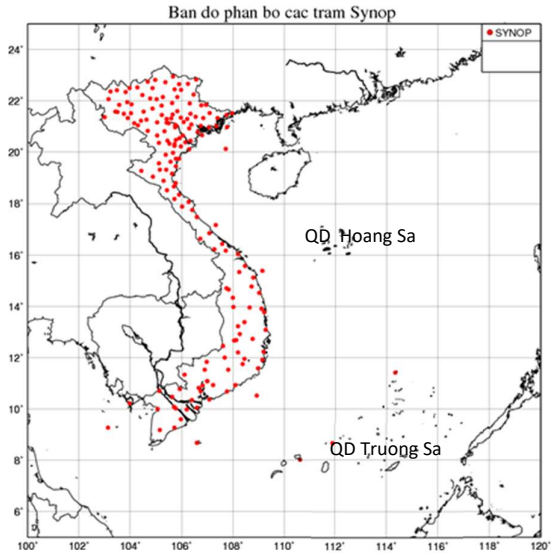

Figure 1. Distribution of 184 SYNOP rain gauges in Vietnam.

Table 1. Detailed GSMaP products.

	Resolution	**Latency**	**Update interval**
MVK	Horizontal: 0.1x0.1 deg.lat/lon Temporal: 01 hour	3 day(s)	01 hour (s)
NOW		0 hour(s)	0.5 hour(s)

There are 184 SYNOP rain gauge stations available in Vietnam and the distribution of rainfall stations is shown in Figure1 and Table 2. Rain gauge data which represent the rainfall at these points were used as reference in comparison of study. The rain gauge data were monitored and evaluated to control the quality processes to eliminate errors. Himawari–8, GSMaP_NOW and GSMaP_MVK grid rainfall estimates data were interpolated to these 184 positions of rain gauge stations. In this study, the nearest neighbor interpolation method was chosen. Due to the high localization rain, the nearest interpolation method reduces the influence of the terrain during interpolation. In this interpolation method, the distances from the positions of rain gauge stations to the grid nodes of the rainfall estimates data are calculated, and the value at the nearest grid point is assigned to the rain gauge point. Note that in Saito et al. (2020) [5], GSMaP and Himawari–8 3–hour rainfall estimates were verified against AWS data with interpolated verification grids of 5 km horizontal resolution.

Table 2. SYNOP rain gauge stations.

Name	**Lat**	**Lon**	**Name**	**Lat**	**Lon**	**Name**	**Lat**	**Lon**	**Name**	**Lat**	**Lon**	**Name**	**Lat**	**Lon**
Muong Te	22.4	102.8	Chiem Hoa	22.2	105.3	Son Tay	21.2	105.5	Ba Don	17.8	106.4	Lak	12.2	108.2
Sin Ho	22.4	103.2	Cho Ra	22.5	105.7	Lang	21	105.8	Con Co	17.2	107.4	Dac Mil	12.5	107.6
am Duong	22.4	103.5	Ngan Son	22.4	105.7	Hoai Duc	21.1	105.8	Dong Ha	16.8	107.1	Dak Nong	12	107.7
Than Uyen	22	103.9	Bac Can	22.2	105	Ha Dong	21	105.8	Khe Sanh	16.6	106.7	Da Lat	12	108.5
Muong Lay	22.1	103.2	Thai Nguyen	21.6	105.8	Chi Linh	21.1	106.4	Hue	16.4	107.6	Lien Khuong	11.7	108.4
Tuan Giao	21.6	103.4	Dinh Hoa	21.9	105.6	Hai Duong	21	106.3	A Luoi	16.2	107.3	Bao Loc	11.5	107.8
Pha Din	21.6	103.5	Minh Dai	21	105.1	Hung Yen	20.7	106.1	Nam Dong	16.2	107.7	Cat Tien	11.6	107.4
Dien Bien	21.4	103	Phu Ho	21.5	105.2	Nam Dinh	20.4	106.2	Da Nang	16.1	108.4	Phuoc Long	11.8	107

Name	Lat	Lon	Name	Lat	Lon	Name	Lat	Lon	Name	Lat	Lon	Name	Lat	Lon
Phieng Lanh	21.9	103.6	Viet Tri	21.3	105.4	Van Ly	20.1	106.3	Tam Ky	15.6	108.5	Dong Phu	11.5	106.9
Muong La	21.9	104.1	Vinh Yen	21.3	105.6	Phu Ly	20.5	105.9	Tra My	15.4	108.2	Tay Ninh	11.3	106.1
Son La	21.3	103.9	Tam Dao	21.5	105.7	Nho Quan	20.3	105.8	Ly Son	15.4	109.2	Tri An	11.1	107
Song Ma	21.1	103.8	Cao Bang	22.7	106.3	Ninh Binh	20.3	106	Q.Ngai	15.1	108.8	Bien Hoa	10.9	106.8
Co Noi	21.1	104.2	Bao Lac	23	105.7	C.Phuong	20.3	105.7	BaTo	14.8	108.7	Ta Lai	11.4	107.4
Yen Chau	21.1	103.3	Nguyen Binh	22.7	106	Thai Binh	20.4	106.4	Hoai Nhon	14.1	109	Long Khanh	10.9	107.2
Bac Yen	21.2	104.4	T.Khanh	22.8	106.5	Hoi Xuan	20.4	105.1	An Nhon	13.9	109.1	Thu Dau Mot	11	106.6
Phu Yen	21.3	104.6	That Khe	22.3	106.5	Yen Dinh	20	105.7	Quy Nhon	13.8	109.2	Nha Be	10.8	106.7
Moc Chau	20.8	104.7	Lang Son	21.8	106.8	SamSon	19.8	105.9	Son Hoa	13.1	109	Vung Tau	10.4	107.1
Mai Chau	20.7	105.1	Mau Son	21.9	107	Bai Thuong	19.9	105.9	Tuy Hoa	13.1	109.3	Con Dao	8.7	106.6
Kim Boi	20.7	105.5	Bac Son	21.9	106.3	Thanh Hoa	19.8	105.8	Nha Trang	12.3	109.1	Huyen Tran	8	110.6
Chi Ne	20.5	105.8	Huu Lung	21.8	106.6	Nhu Xuan	19.6	105.6	Cam Ranh	11.9	109.2	Moc Hoa	10.8	105.9
Lac Son	20.5	105.5	Dinh Lap	21.5	107.1	Tinh Gia	19.5	105.8	SongTTay	11.4	114.3	My Tho	10.4	106.4
Hoa Binh	20.8	105.3	Mong Cai	21.5	108	Quy Chau	19.4	105.1	Phan Rang	11.6	109	Vinh Long	10.3	106
Lao Cai	22.5	104	Quang Ha	21.5	107.8	Tuong Duong	19.3	104.5	Phan Thiet	10.9	108.1	Ben Tre	10.2	106.4
Bac Ha	22.5	104.3	TienYen	21.3	107.4	Quy Hop	19.5	105.3	LaGi	10.7	107.8	Ba Tri	10.1	106.6
SaPa	22.4	103.8	CoTo	21	107.8	Tay Hieu	19.3	105.4	Phu Quy	10.5	108.9	Cao Lanh	8	106.6
Pho Rang	22.2	104.5	CuaOng	21	107.4	Con Cuong	19.1	104.9	Phan Ri	11.2	108.5	Cang Long	10	106.2
Mu.C.Chai	21.9	104.1	BaiChay	21	107.1	Quynh Luu	19.1	105.6	Dak To	14.7	107.8	ChauDoc	10.7	105.1
Yen Bai	21.7	104.4	UongBi	21	106.8	Do Luong	18.8	105.3	Kon Tum	14.4	108	Tra Noc	10.1	105.7
Van Chan	21.6	104.5	HiepHoa	21.4	106	Hon Ngu	18.8	105.8	Playcu	14	108	Can Tho	10	105.8
Luc Yen	22.1	104.7	LucNgan	21.4	106.6	Vinh	18.7	105.7	An Khe	14	108.7	Vi Thanh	9.8	105.5
Ha Giang	22.8	105	SonDong	21.3	106.8	Huong Son	18.9	105.7	Yaly	14.7	107.8	Soc Trang	9.6	106
Hoang SPhi	22.8	104.7	BacGiang	21.3	106.2	Ha Tinh	18.4	105.9	Ayunpa	13.4	108.5	Rach Gia	10	105.1
Bac Me	22.7	105.4	BacNinh	21.2	106.1	Huong Khe	18.2	105.7	EaHleo	13.4	108.3	Phu Quoc	10.2	104
Bac Quang	22.5	104.9	PhuLien	20.8	106.6	Hoanh Son	18	106.5	Buon Ho	12.9	108.3	Tho Chu	9.3	103.5
Dong Van	23.3	105.3	HonDau	20.7	106.8	Ky Anh	18.1	106.3	MDrak	12.7	108.8	Bac Lieu	9.3	105.7
T.Quang	21.8	105.2	Bach.L.Vi	20.1	107.7	Tuyen Hoa	17.9	106	B.MThuot	12.7	108.1	Ca Mau	9.2	105.2
Ham Yen	22.1	105	BaVi	21.2	105.4	Dong Hoi	17.5	106.6	EaKmat	12.7	108.1			

2.2. Verification method

2.2.1. Continuous statistical verifications

The main aim of this method was to measure the correspondence between the estimated rainfall and the observation. To quantify this correspondence value, the following three statistical indices were used the mean error (ME), the root mean square (RMSE) and the correlation coefficient (CORR) [13].

$$ME = \frac{1}{N}\sum_{i=1}^{N}(F_i - O_i) \quad (1)$$

$$RMSE = \sqrt{\frac{1}{N}\sum_{i=1}^{N}(F_i - O_i)^2} \quad (2)$$

$$CORR = \frac{\sum_{i=1}^{N}(F_i - \bar{F})(O_i - \bar{O})}{\sqrt{\frac{1}{N}\sum_{i=1}^{N}(F_i - \bar{F})^2}\sqrt{\frac{1}{N}\sum_{i=1}^{N}(O_i - \bar{O})^2}} \quad (3)$$

where F_i is the satellite estimates, O_i is rain gauge values, $\bar{F}$ is mean of the satellite estimates, $\bar{O}$ is mean of the rain gauge values and *n* is total number of rain gauge (rainfall estimated data).

2.2.2. Categorical statistical verifications

In this study, the correspondence between the estimated and observed occurrence of events is measured by categorical statistics. Table 3 summarizes the contingency to verify satellite rainfall detection capability with rain or no rain events following thresholds from 1mm/6h to 100mm/6h.

Table 3. Contingency table of yes or no events with rain or no rain.

		Observed rainfall	
		Yes	No
Estimated Rainfall	Yes	hits	false alarms
	No	misses	correct negative

In Table 3, "hits" shows correctly estimated rain events, "misses" means when the rain is not estimated but in fact the rain occurs, "false alarm" describes when rain events is estimated but actual rain events do not occur, and "correct negative" correctly shows no rain events occur. Five categorical statistics indices used are the frequency bias (BIAS), probability of detection (POD), the false alarm ratio (FAR), the threat score (TS) and equitable threat score (ETS). BIAS, POD, FAR, TS and ETS indices are calculated as [13]:

$$\text{BIAS} = \frac{\text{hits+false alarm}}{\text{hits+misses}} \quad (4)$$

$$\text{POD} = \frac{\text{hits}}{\text{hits+misses}} \quad (5)$$

$$\text{FAR} = \frac{\text{false alarm}}{\text{hits+false alarm}} \quad (6)$$

$$\text{TS} = \frac{\text{hits}}{\text{hits+misses+false alarm}} \quad (7)$$

$$\text{ETS} = \frac{\text{hits - hits}_{random}}{\text{hits+misses+false alarm-hits}_{random}} \quad (8)$$

$$\text{Where } \text{hits}_{random} = P_c(\text{hits+false alarm}) \quad (9)$$

$$\text{And} \quad P_c = \frac{\text{hits+misses}}{\text{hits+misses} + \text{false alarm+correct negative}} \tag{10}$$

BIAS measures the ratio of the frequency of forecast events to the frequency of observed events. The forecast system tends to underforecast (BIAS<1) or overforecast (BIAS>1) events, and BIAS does not measure how well the forecast corresponds to the observations, but only measures relative frequencies. POD describes how often the estimate detected correctly the occurrence of rain events. Range of POD is from 0 to 1 and perfect score is 1. FAR shows the fraction of diagnosed events that turned out to be wrong. Range of FAR value is from 0 to 1. The perfect score is 0. TS shows how well the estimate implied "yes" events to correspond with the observed "yes" events. It measures the fraction of observed and/or estimated events that were correct. It can be thought of as the accuracy when correct negatives have been removed from consideration, which means that TS is only concerned with estimates that count. Sensitive to hits, penalizes both misses and false alarms. ETS is like TS, but it removes the contribution from hits by chance in the random forecast.

3. Results

3.1. Continuous Statistical verifications

Figures 2–4 are scatter plots which describe the correspondence between the 6–hour rainfall estimates from Himawari–8(HWM), GSMaP_NOW(NOW), GSMaP_MVK(MVK) and the 6–hour rains at SYNOP stations. In these scatter plots, the dashed blue line is the linear regression line between estimated rainfall and observed rainfall. The correlation coefficient (CORR), RMSE and ME values are displayed in the lower right corner. The solid blue diagonal line is the ideal regression or "45–degree line", if all pairs of estimated and observed points lie entirely on this line, then the estimates are perfect.

The three types of 6–hour rainfall estimates data from HMW, NOW and MKV are all positively correlated with the 6–hours observed rainfall. MVK has the strongest correlation, $Corr_{MVK}$= 0.45. HMW and NOW have similar correlation coefficient values with observed rain, while NOW was slightly better as $Corr_{HMW}$ = 0.35 and $Corr_{NOW}$ = 0.36. The ME value of HMW is positive and large (ME_{HMW} = 1.34). Conversely, the 6–hour rainfall estimates from NOW and MVK are lower than the actual measured rainfall as ME_{NOW}=–0.39 and ME_{MVK} =–0.35. This can also be seen through the linear regression lines for MVK and NOW are below the ideal regression line (Figures 2–3). In contrast, the linear regression line of HMW is above the ideal regression line.

Average error magnitude of three data types HMW, NOW and MVK are shown through RMSE values. Error magnitude of HMW is the biggest, $RMSE_{HMW}$ is 19.77. This value is 3.8 times greater than $RMSE_{NOW}$ ($RMSE_{NOW}$ = 5.16) and 4.0 times greater than $RMSE_{MVK}$ ($RMSE_{MVK}$ = 4.93).

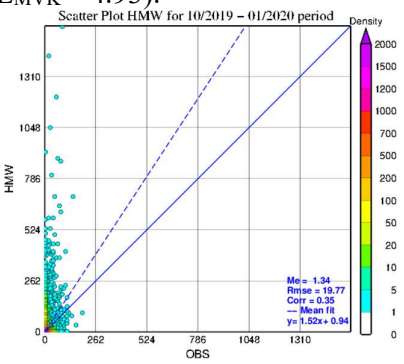

(a)

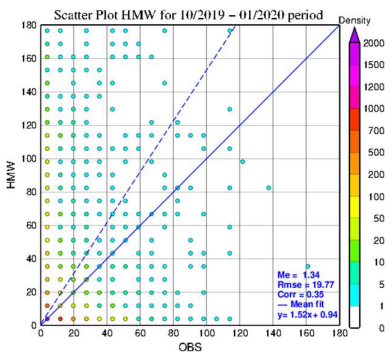

(b)

Figure 2. (**a)** Scatter plot diagram of 6–hour rain gauge observations and Himawari–8 6–hour rainfall estimates; (**b**) Same as in a) but enlarged view for the precipitation range 1–180 mm/6h.

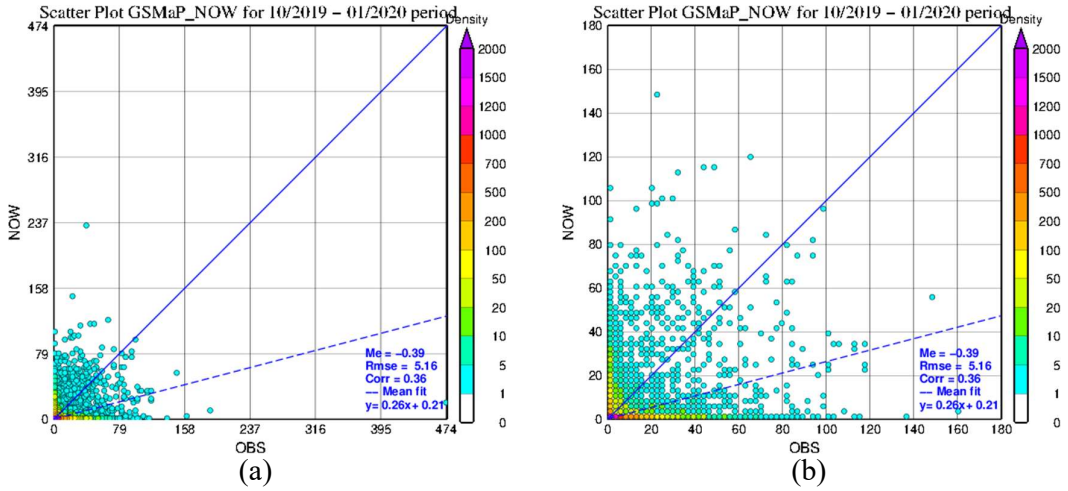

Figure 3. Same as Figure 2 except for GSMaP_NOW.

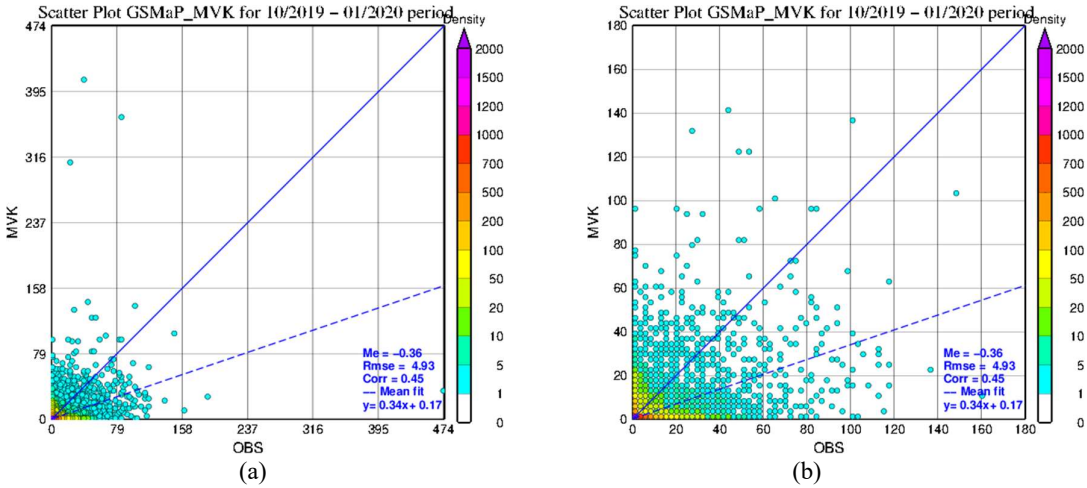

Figure 4. Same as Figure 2 except for GSMaP_MVK.

3.2. Categorical Statistical verifications

Details of the values of TS, POD, FAR, ETS and BIAS indices are shown in Figures.5a, 5b,5c, 5d, and 5e with the event numbers of the contingency table (Table 4). As shown in Figure 5, TS_{HMW}, TS_{NOW}, TS_{MVK} tend to decrease with increasing rainfall thresholds. At all 06h accumulated rainfalls, the values of TS_{MVK} (green) are larger than those of TS_{NOW}(red) and TS_{HMW}(orange).

Table 4. Contingency table by each threshold.

		Hits (FO)	**False alarms (FX)**	**Misses (XO)**	**Correct negative (XX)**	**BIAS**	**POD**	**FAR**	**TS**	**ETS**
	HMW	2170	3152	4772	73243	0.767	0.313	0.592	0.215	0.179
1mm/06h	NOW	1846	1330	5785	79670	0.416	0.242	0.419	0.206	0.181
	MVK	2384	1305	4645	75729	0.525	0.339	0.354	0.286	0.259
10mm/06h	HMW	688	1649	1089	79911	1.315	0.387	0.706	0.201	0.189

		Hits (FO)	False alarms (FX)	Misses (XO)	Correct negative (XX)	BIAS	POD	FAR	TS	ETS
	NOW	398	602	1594	86037	0.502	0.2	0.602	0.153	0.146
	MVK	541	482	1312	81728	0.552	0.292	0.471	0.232	0.224
	HMW	366	1257	505	81209	1.863	0.42	0.774	0.172	0.165
20mm/06h	NOW	202	332	788	87309	0.539	0.204	0.622	0.153	0.149
	MVK	226	230	706	82901	0.489	0.242	0.504	0.195	0.191
	HMW	206	1063	274	81794	2.644	0.429	0.838	0.134	0.129
30mm/06h	NOW	104	226	442	87859	0.604	0.191	0.685	0.135	0.132
	MVK	99	150	424	83390	0.476	0.189	0.602	0.147	0.145
	HMW	126	912	175	82124	3.449	0.419	0.879	0.104	0.101
40mm/06h	NOW	52	155	282	88142	0.62	0.156	0.749	0.106	0.105
	MVK	49	84	270	83660	0.417	0.154	0.632	0.122	0.12
	HMW	81	789	105	82362	4.677	0.435	0.907	0.083	0.081
50mm/06h	NOW	23	101	189	88318	0.585	0.108	0.815	0.073	0.073
	MVK	23	42	176	83822	0.327	0.116	0.646	0.095	0.095
	HMW	50	698	66	82523	6.448	0.431	0.933	0.061	0.06
60mm/06h	NOW	11	60	120	88440	0.542	0.084	0.845	0.058	0.057
	MVK	12	29	111	83911	0.333	0.098	0.707	0.079	0.079
	HMW	37	607	43	82650	8.05	0.463	0.943	0.054	0.053
70mm/06h	NOW	6	33	82	88510	0.443	0.068	0.846	0.05	0.049
	MVK	7	20	78	83958	0.318	0.082	0.741	0.067	0.066
	HMW	25	537	30	82745	10.218	0.455	0.956	0.042	0.042
80mm/06h	NOW	3	19	58	88551	0.361	0.049	0.864	0.037	0.037
	MVK	5	16	53	83989	0.362	0.086	0.762	0.068	0.067
	HMW	14	493	19	82811	15.364	0.424	0.972	0.027	0.026
90mm/06h	NOW	1	14	36	88580	0.405	0.027	0.933	0.02	0.019
	MVK	2	16	34	84011	0.5	0.056	0.889	0.038	0.038
	HMW	6	457	14	82860	23.15	0.3	0.987	0.013	0.012
100mm/06h	NOW	0	10	23	88598	0.435	0	1	0	0
	MVK	2	8	20	84033	0.455	0.091	0.8	0.067	0.067

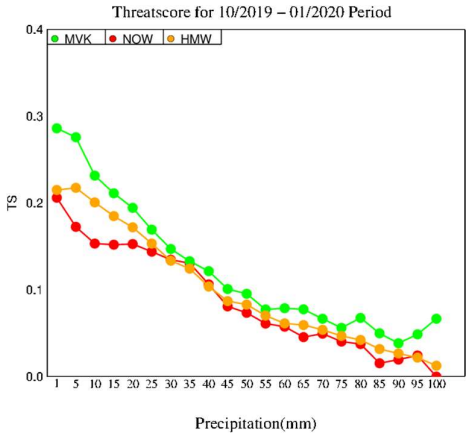

(a)

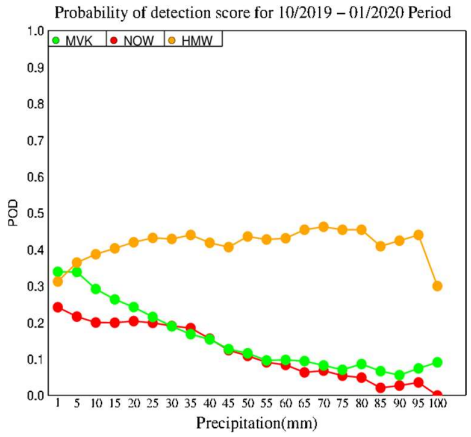

(b)

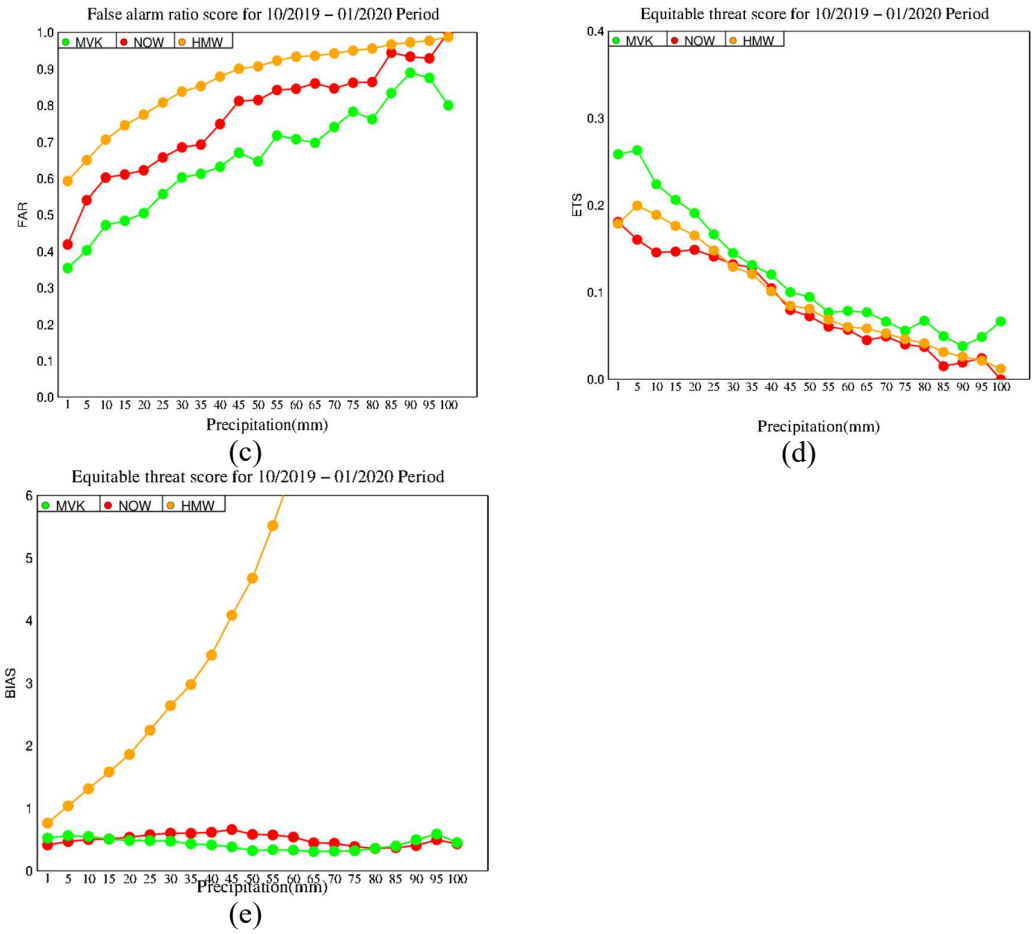

Figure 5. (**a**) Threat scores (TS); (**b**) Probability of detection (POD); (**c**) False alarm rate (FAR); (**d**) Equitable threat score (ETS); (**e**) BIAS of GSMaP_MVK (MVK; green), GSMaP_NOW (NOW; red) and Himawari–8 (HMW; orange).

The values of TS_{HMW} are close to TS_{NOW} but slightly larger than TS_{NOW} at most thresholds except for 30 to 40 mm/06h thresholds. Figure 6 shows POD. POD_{HMW} is larger than POD_{NOW} and POD_{MVK} at most thresholds except for 1 mm/6h. POD of MVK is larger than NOW except for 30 and 40 mm/6h thresholds. When precipitation is overestimated, the value of POD tends to be large, but it does not mean that the estimate is good. Therefore, POD should be checked with FAR. As seen in Figure 5c, FAR_{HMW} is the largest for thresholds from 1 to 95 mm/6h. This is consistent with the results on ME_{HMW} and $RMSE_{HMW}$ where ME_{HMW} is positive and $RMSE_{HMW}$ is the largest (19.77 mm).

In FAR (Figure 5c), FAR_{HMW} (orange) is always the largest except for 100 mm/6h threshold, suggesting its overestimation of rains. NOW has the second largest false alarm, and the red line is between the green and orange lines. FAR_{MVK} is the smallest at all thresholds. The overall trend of ETS_{MVK}, ETS_{NOW} and ETS_{HMW} (Figure 5d) is like those of TS (Figure 5a), as ETS_{MVK} is the largest at all thresholds, and the values of ETS_{HMW} and ETS_{NOW} are similar. The relationship between the ETS_{HMW} and ETS_{NOW} is also almost the same as in TS, but at the threshold of 01 mm/06h ETS_{NOW} is larger than ETS_{HMW}, and around 30 to 40 mm/06h superiority of ETS_{NOW} against ETS_{HMW} is more distinct in ETS (Table 4). Generally, ETS has a merit to offset the false gain by overestimation in TS, but in our case, the merit was not large due to the smallness of hit_{random} (Eq. 9). Calculation results of BIAS values of NOW, MVK and HMW are shown in Figure.5e. The $BIAS_{NOW}$ and $BIAS_{MVK}$ are less than 1 at all rainfall thresholds. This is consistent with ME_{NOW} and ME_{MVK}. In contrast,

$BIAS_{HMW}$ is less than 1 at only 01 mm/06h threshold then increases rapidly with rainfall thresholds. $BIAS_{HMW}$ is extremely large for intense rains as shown in Table 4 (e.g., 24 at 100 mm/06h threshold).

Here we show an example of rainfall overestimation by HMW on October 7–8, 2019 in Thai Binh province, the northeast coastal area of Vietnam. Thai Binh Rain gauge station has coordinates of 20.4ºN and 106.4ºE (Table 2). At the station location, HMW 6–hour rainfall estimation from 18 UTC 07 October 2019 to 00UTC 08 October 2019 was 324.6 mm. This value is 12 times larger than the actual observed value (27 mm). Estimated rainfall from MVK and NOW are 46.8 mm and 54.2 mm, respectively (Figure 6).

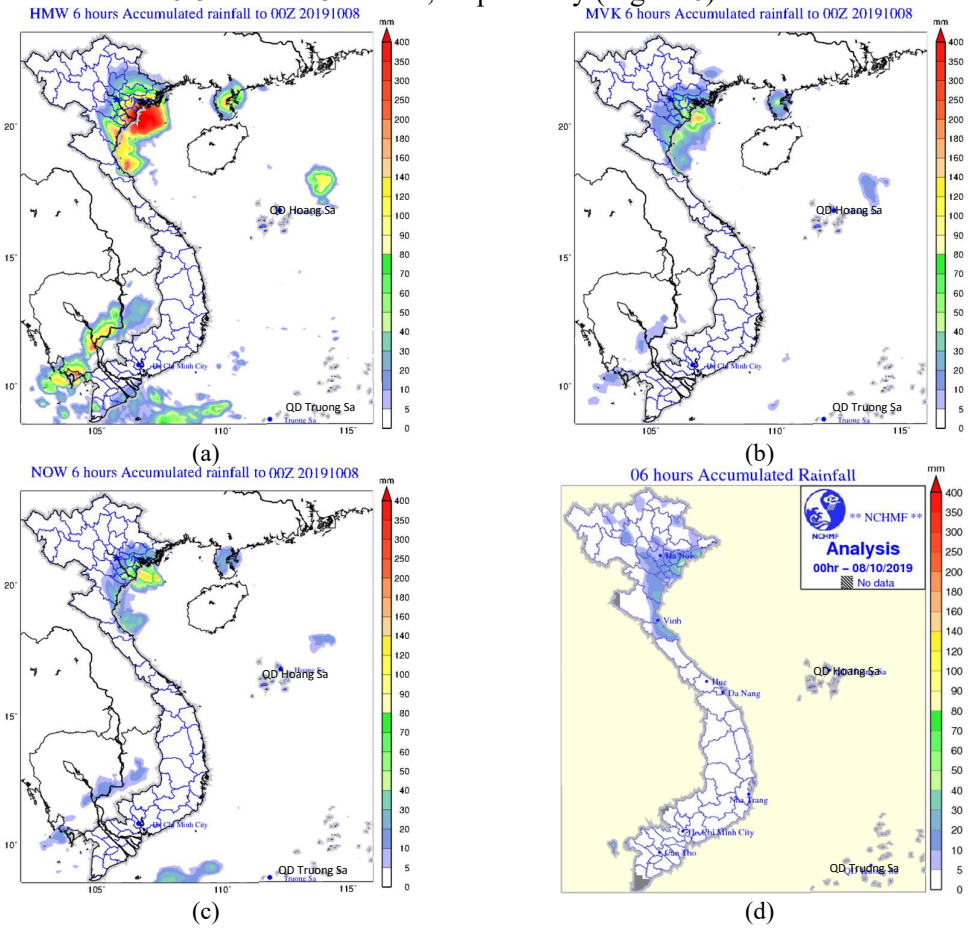

Figure 6. Six–hour estimated rainfall from 18 UTC 07 October 2019 to 00 UTC 08 October 2019: (a) Himawari–8; (b) GSMaP_MVK; (c) GSMaP_NOW; (d) SYNOP rain gauges.

Figure 7 is Himawari–8 IR images at 19 UTC 7 October 2019, and Figure 9 indicates the time sequence of the brightness temperatures (T_{BB}) around Thai Binh station and corresponding rainfall estimates by Himawari-8 (HMW). T_{BB} around Thai Binh at 19 and 20 UTC were –75.3 ºC and –70.1 ºC, respectively, and in these two times HMW recorded the largest values as 70.75 mm/h and 85.96 mm/h. As discussed in [5], to give rainfall estimation from Himawari–8, AMO uses relationship between T_{BB} and rainfall intensity R:

$$R = 1.1183*10^{11} exp(-3.6382*10^{-2} T_{BB}^{1.2}) \quad (11)$$

This relationship (Figure 8) is based on statistics between T_{BB} observed by GOES satellite and radar–estimated rainfall over north America [4].

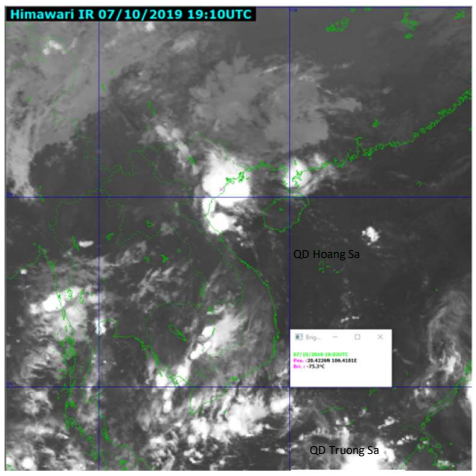

Figure 7. Infrared image by geostationary satellite (Himawari–8) at 19z 7 October 2019.

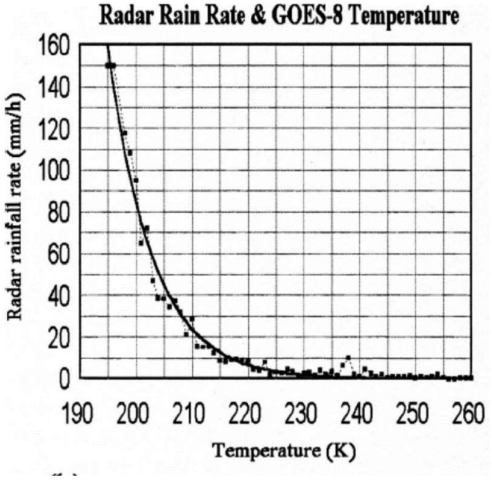

Figure 8. Relationship between TBB and rainfall rate [4].

Figure 9. Horizontal distribution of Himawari–8 6–hour precipitation estimate at Thai Binh station.

Figure 10 is the time variation of 06 hours accumulated rainfall from NOW (red line), MVK (green line), HMW (orange line) and 06h rain gauge (black line) in 5 heavy rainfalls in Vietnam from October 2019 to the end of January 2020. In general, the rainfall estimated from NOW, MVK and HMW show precipitation changes. The shapes of yellow, red, orange

lines are quite like black line. However, specifically in each rain, rainfall estimates from NOW, MVK and HMW also have differences.

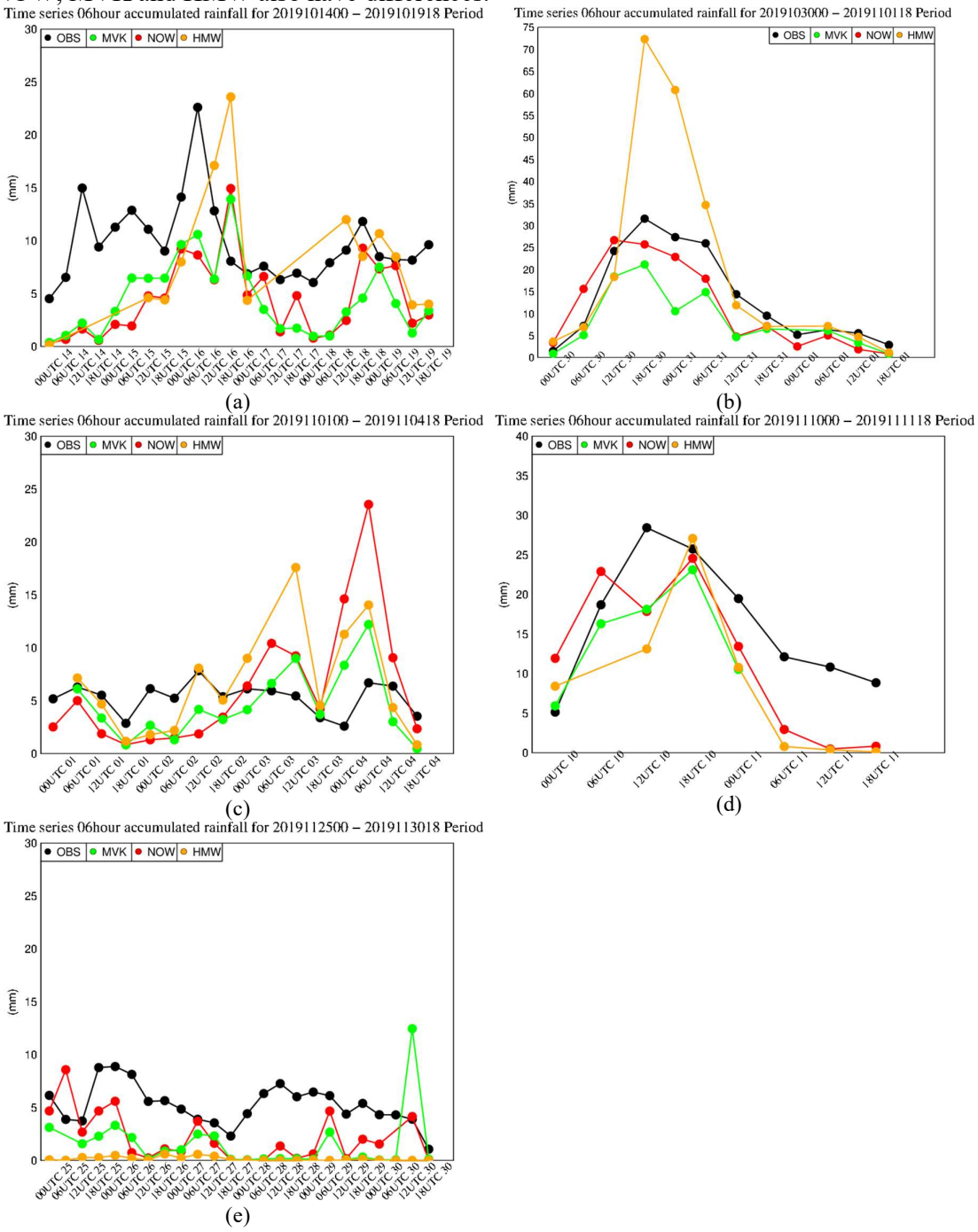

Figure 10. variation of 06 hours accumulated rainfall from NOW (red line), MVK (green line), HMW (orange line) and 06h rain gauge (black line) in 5 heavy rainfalls in Vietnam from October 2019 to the end of January 2020.

From 14th to 19th Oct (Figure 10a), rainfall estimated from NOW and MVK tend to be lower than observed. The black line is above the red line and the blue line. The rainfall estimated from HMW is higher than NOW and MVK and quite like the observed. From 30th Oct to 01st Nov (Figure 10b), rainfall estimated from NOW, MVK showed the variation of rainfall. Rainfall increased gradually and peaked during the 12UTC 30th to 00UTC on 31st

October period, then it dropped. Estimation of rain from HMW also shows this trend, however, the maximum rainfall of HMW is too large compared to the observed. Maximum value of HMW is 73mm. In fact, the maximum of rain gauge is just over 30mm. From 01st to 04th Nov (Figure 10c), before 12UTC 02nd NOV, the rainfall estimates from NOW, MVK and HMW all tended to be lower than rain gauge. After this point of time, the precipitation estimated from them tend to overestimate the rainfall which observed. From 12UTC 02nd Nov to 12UTC 03rd Nov, HMW gave the highest rainfall estimate. NOW has the highest rainfall estimate in the remaining period. Figure 10d shows the NOW, MVK, HMW estimated rainfall reflect actual precipitation patterns. The rainfall increased and decreased rapidly before and after the 06UTC–12UTC 10th Nov. However, the rainfall estimates are lower than reality. The most obvious low rainfall estimations occurred from 00UTC to 18UTC 25th Nov (Figure 10e). Most of the time, the 06h accumulated rainfall estimations are smaller than observed. In particular, the rainfall from the HMW is very small during this rain period.

4. Summary and concluding remarks

This study verified the quality of three rainfall estimates by GSMaP_NOW, GSMaP_MVK and Himawari–8 against 6–hour rain gauge data from 184 SYNOP stations for a 4–month period from October 2019 to January 2020. The three types of data were positively correlated with the observed rainfall. In particular, GSMaP_MVK has the highest correlation. The rainfall estimated from Himawari–8 was excessive compared with the actual data and has the largest RMSE. GSMaP_NOW and GSMaP_MVK rainfall estimates were slightly lower than actual ones. The RMSE of GSMaP_MVK was the smallest among the three estimates. GSMaP_MVK has the best rainfall estimation skills of the three data types in FAR, TS and ETS in all thresholds. TS_{HMW} was slightly larger than TS_{NOW} except from 30to 40mm/6h thresholds. POD_{HMW} was the largest, but this is derived from HWM's excessive rainfall estimates, because FAR_{HMW} value was the largest. The POD_{MVK} was larger than POD_{NOW} and the FAR_{MVK} was smaller than FAR_{NOW}.

The excessive rainfall estimates by Himawari–8 seen in this study is very different from the results in Saito et al. (2020) [5], which verified the three rainfall estimates against AWS 3–h rains for the case of the Da Nang heavy rainfall event in December 2018. Targeted rainfall in Saito et al. (2020) [5] was mainly brought by a precipitation system whose cloud top was not high, and warm rain process was likely dominant. In the Da Nang heavy rainfall event, Himawari–8 drastically underestimated intense rains. Contrary, Himawari–8 tends to overestimate intense rains if could top brightness temperature is extremely low. Such the cases easily occur not only by deep convection but by dense cirrus and anvil overcast.

In conclusion, GSMaP_MVKwasthe best rainfall estimate amongthe three data, but due to a delay of 3–4 days, it is not applicable to the operational forecasting and warning. Consequently, itis recommended to use GSMaP_MVK mainly for verification of NWP rainfall. GSMaP_NOW has a relatively good rainfall estimate, which can be used in parallel with Himawari–8 rainfall estimates to provide realtime information to the forecasters in forecasting and warning on the heavy rainfall, flash flood andlandslide.

Author Contributions: Author Contributions: Conceptualization, M.K. Hung; methodology, M.K. Hung, K. Saito, and D.D. Tien; validation, M.K. Hung, D.D. Tien; Rain gauge data curation, M.K. Hung, Satellite data curation, N.V. Hung, M.K. Hung, writing–original draft preparation, M.K. Hung; writing–review and editing, M.K. Hung, K. Saito, M.V. Khiem, D.D. Tien; supervision, K. Saito; All authors have read and agreed to the published version of the manuscript.

Funding: This study was supported by a project from the Ministry of Agriculture and Rural Development: “A study to forecast flood situation on Bac Nam Ha irrigation system to

support decision making of drainage pumps water in real time" coordinated implementation between the Institute of Water Resources Planning and the National Center for Hydro–Meteorological Forecasting.

Acknowledgments: We would like to thank Project of the Ministry of Agriculture and Rural Development: "A study to forecast flood situation on Bac Nam Ha irrigation system to support decision making of drainage pumps water in real time" for financial supports. We also thank AMO for satellite estimated rainfall data and JAXA on GSMaP data.

Conflicts of Interest: The authors declare no conflict of interest.

References

1. Eckstein, D.; Hutfils M.L.; Winges, M. Global Climate Risk Index. **2019**. Available online: https://germanwatch.org/files/Global%20Climate%20Risk%20Index%202019_2.pdf
2. Artan, G. Adequacy of satellite derived rainfall data for stream. *Nat. Hazard* **2007**, *43*, 167–185.
3. Hossain, F.; Katiyar, N.; Hong, Y.; Wolf, A. The emerging role of satellite rainfall data in improving the hydro–political situation of flood monitoring in the under–developed regions of the world. *Nat. Hazards* **2007**, *43*, 199 – 210.
4. Vicente, G.R.; Scofield, A.; Mensel, W.P. The operational GOES infrared rainfall estimation technique. Bull. *Amer. Meteor. Soc*. **1998**, *79*, 1881–1898.
5. Saito, K.; Hung, M.K.; Hung, N.V.; Vinh, N.Q.; Tien, D.D. Heavy rainfall in central Viet Nam in December 2018 and modification of precipitation nowcasting at VNMHA. *VN J. Hydrometeorol.* **2020**, *5*, 65–79.
6. Kim, H.; Kubota, T.; Utsumi, N.; Ishitsuka, Y.; Yoshimura, K.; Oki, R.; Oki, T. Development and Applications of the GSMaP: Overview & Lessons learned in a real–world case for Hydrological Status and Outlook System. 2017. Available online: http://www.wmo.int/pages/prog/hwrp/chy/hydrosos/documents/presentations/day2/Session3–Hyungjun_Kim–GSMaP.pdf
7. Hieu, B.T.; Ishidaira, H.; Shaowei, N. Evaluation of the use of global satellite–gauge and satellite only precipitation products in stream flow simulations. *Appl. Water Sci.* **2019**, *9,* 53.
8. Thanh, N.D.; Matsumoto, J.; Kamimera, H.; Hai, B. Monthly adjustment of Global Satellite Mapping of Precipitation (GSMaP) data over the Vu Gia–Thu Bon River Basin in Central Vietnam using an artificial neural network. *Hydrol. Res. Lett*. **2013**, *7*, 85–90.
9. Joyce, R,J.; Janowiak, J.E.; Arkin, P.A.; Xie, P.P. Cmorph: a method that produces global precipitation estimates from passive microwave and infrared data at high spatial and temporal resolution. *VN J. Hydrometeorol.* **2004**, *5*, 487–503.
10. Ushio, T.; Kubota, T.; Shige, S.; Okamoto, K.; Aonashi, K.; Inoue, T.; Takahashi, N.; Iguchi, T.; Kachi, M.; Oki, R.; Morimoto, T.; Kawasaki, Z. A Kalman filter approach to the Global Satellite Mapping of Precipitation (GSMaP) from combined passive microwave and infrared radiometric data. *J. Meteor. Soc. Japan* **2009**, *87A*, 137–151.
11. Kachi, M.; Aonashi, K.; Kubota, T.; Shige, S.; Ushio, T.; Mega, T.; Yamamoto, M.; Hamada, A.; Seto, S.; Takayabu, Y. N.; Oki, R. Developments and applications of

the Global Satellite Mapping of Precipitation (GSMaP) for the Global Precipitation Measurement (GPM). *Geophys. Res. Abstracts* **2016**, *18*, EGU2016–11384–1.

12. Oki, R. GSMaP and its applications. 2017. Available online: http://www.wmo.int/pages/prog/sat/meetings/workshop_on_SWCEM/documents/7(1)_20160216_WMO%20WS_JAXA.pdf
13. Takeuchi. Outline of operational numerical weather prediction at the Japan Meteorological agency. 2013. Available online: http:// https://www.jma.go.jp/jma/jma–eng/jma–center/nwp/outline2013–nwp/index.htm

VIETNAM JOURNAL OF HYDROMETEOROLOGY

Research Article

Identifying of the start date of the active tropical cyclone season in the western North Pacific and East Sea

Nguyen Thi Diem Huong[1], Ta Huu Chinh[1*]

[1] National Center for Hydro–Meteorological Forecasting; huongdiem.nchmf@gmail.com; chinhth2010@gmail.com

[*] Correspondence: chinhth2010@gmail.com, Tel.: +84–868791281

Received: 5 July 2020; Accepted: 18 August 2020; Published: 25 August 2020

Abstract: This paper presents the way of identifying the start date of an active storm season in the western North Pacific (WNP) and East Sea (ES). The start (end) date for an active TC season in a year is identified at 5th (95th) percentile of data. Normal and empirical distributions are used to estimate climatological thresholds for the early and late start of the active TC season. Climatological early (late) start is under (over) the date at 33% (67%) of cumulative probability function. Climatological early start is 24 April (20 May) while climatological late start is 28 May (20 June) for the WNP (ES). In the WNP, the start date of storm season tends to be in early and normal (normal and late) phase in post–La Niña (post–El Niño) years. The relationship is not really clear in ES.

Keywords: Start of TC season; Climatological start date of TC season.

1. Introduction

The western North Pacific (WNP) is the most active tropical cyclone basin in the world [1]. Normally, there are about 25 to 30 storms annually. TCs activating in the WNP tend to attack many countries in East Asia (Japan, Korea, China) and Southeast Asia (the Philippines, Vietnam), causing significant damage to people and properties. Being a part of the WNP, East Sea (ES) has about 10–12 TCs each year, which accounts for roughly one third of the total number of TCs in the WNP; about 5–7 of them either making landfall or having direct impact on Vietnam. The damage caused by TCs in ES may be very serious due to its shorter warning time before landfall. For instance, the Haiyan typhoon directly affected the Philippines, Vietnam and China in November 2013, causing $ 4.55 billion in damage and 6300 deaths [2,3]. Thus, it is essential to identify and forecast the start of storm season in WNP and ES.

Many studies have mentioned different characteristics of TC activity, such as, genesis, intensity, landfall and track as well [1,4,5]. Especially, TC features in relation to ENSO, intra–seasonal oscillation (ISO), Pacific Decadal Oscillation (PDO), Indian Ocean Dipole (IOD) were intensively understood by meteorologists over the world. For instance, ENSO modulates monsoon trough in WNP. Consequently, in El Niño (La Niña) years, TC genesis location expands southeastward (retreats northwestward). Li and Zhou (2013a,b) [4,5] demonstrated effects of ISO on genesis, intensity and track of TC in WNP. In particular, increase (decrease) of genesis in active (non–active) phases of ISO is associated with strengthening (weakening) of monsoon trough. Kubota and Chan (2009) [6] found that, during low PDO phase, TC landfall in Philippines decreases (increases) significantly in El Niño (La Niña) years. During high PDO phase, difference in TC landfall between ENSO phases is u

nclear. However, inter–annual variation of start date of TC receives less attention by scientists. A few studies mentioned this issue. Kim et al. (2017) [7] and Zhao et al. (2019) [8] illustrated relationship between ENSO and inter–annual variation of start date of TC season in WNP. Although start date of TC season in ES has not understood well yet. More studies relating to this issue should be conducted to enhance our understanding. For purpose of operational forecast, National Center for Hydro–Meteorological Forecasting, Vietnam (NCHMF) is responsible for providing information of start date of TC season for community in seasonal forecast bulletins. Meanwhile, currently, NCHMF has no objective criteria to evaluate start date of TC season in both WNP and ES. Thus, goal of this paper is to document the way of identifying. Hopefully, this paper will provide useful information for operational forecast. In this paper, Section 2 describes data, methodology. Section 3 presents results and discussions. Section 4 is the conclusion.

2. Methodology

Climatology of tropical cyclone

In this study, Japan Meteorology Agency (JMA) TC data is used. After 1980s, data quality was more reliable due to contribution of satellite measures. Thus, the analysis is performed in period 1980 – 2019. Only TCs having maximum wind speed is above 17.2 m s^{-1} retained to analyze. Figure 1 shows the monthly climatology of TC numbers in twelve months in the WNP and ES. February has the lowest TC numbers, while the most active period of TC over WNP and ES is from July to November. A similar trend of TC numbers is also exhibited in the ES, but, the number of TC is lower than that in WNP. Thus, the concept of "TC year" in the WNP and ES is defined as starting on 1 February and ending on 31 January of the coming year.

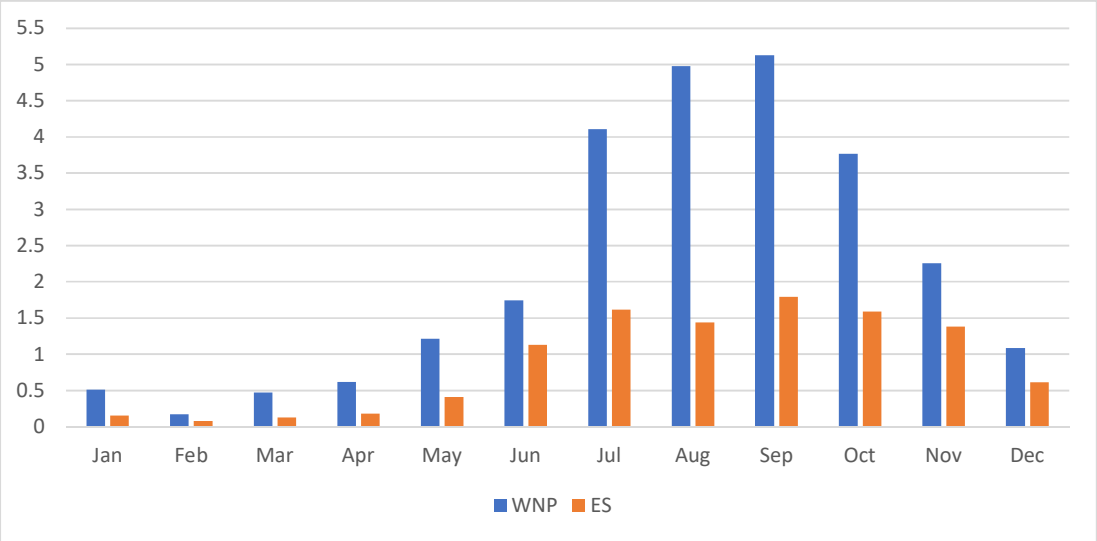

Figure 1. Monthly mean TC numbers in the WNP during 1980–2019.

Identification of the start of storm season

In this study, start dates were identified by percentile which is a common concept in statistical science. Normal distribution with two parameters: mean (μ) and standard deviation (σ) were used to estimate climatological early and late starts. The general form of its probability density function as below:

$$f(x) = \frac{1}{\sigma\sqrt{2\pi}} e^{-\frac{1}{2}\left(\frac{x-\mu}{\sigma}\right)^2} \quad (1)$$

Kernel (empirical) distribution was also employed. It is a non–parametric function and is estimated from a sample of data. While normal distribution function is built from two parameters of mean and standard deviation. Thus, it is useful if data estimated by normal distribution is compared with that estimated by empirical distribution. The goal is to identify whether normal distribution is appropriate to apply or not. More detail of the methods can be found in Wilks (2011) [9].

We define the TC season in the WNP (ES) as the period from the 5th percentile to the 95th percentile of TC formation dates in each TC year. This definition, based on the percentiles, thus, the TC season occupies 90% of total TC numbers of TC year. Based on this definition, the start date of the active TC season is identified for each year from 1980–2019. Then, the empirical distribution functions of the start date for the WNP and ES are built (Figure 2) and are compared with the normal distributions. The figure 2 shows that the empirical distributions of start date in the WNP which have similar shapes with the normal distributions. Thus, the normal distribution can be applied to estimate the start date of the active TC season. Meanwhile, in ES, empirical distribution of start date skews to right side of normal distribution. It implies that normal distribution should not be utilized. More specifically, Table 1 shows terciles of start dates (early, normal, and late) identified by normal and empirical distributions. In WNP, for normal distribution, the point of 24 Apr (28 May) representing 33% (67%) data of cumulative distribution function separates early and normal (normal and late) stages of start dates. The results received from normal and empirical are relatively same for WNP. But, they are much different for ES (Table 1). It suggests that, for ES, empirical distribution should be used to estimate early, normal and late stages of start date instead of normal distribution. The results in Figure 3 illustrate that the climatological start date in ES is later than that in WNP, which is consistent with distribution of start dates in Figure 2. The median of start date in ES (WNP) is nearly 160 (nearly 140). First and third quartiles of whisker–box–plot in ES are also later than those in WNP. The results will be discussed in more details in next Section (Figure 4 and Table 2).

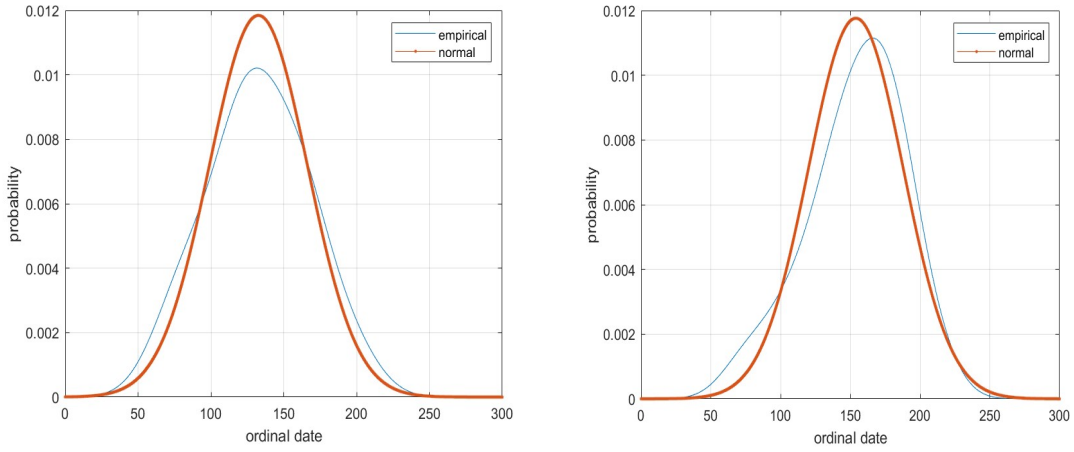

Figure 2. Empirical and normal distributions of the start date of the TC season during 1980 – 2019 for WNP (left) and ES (right).

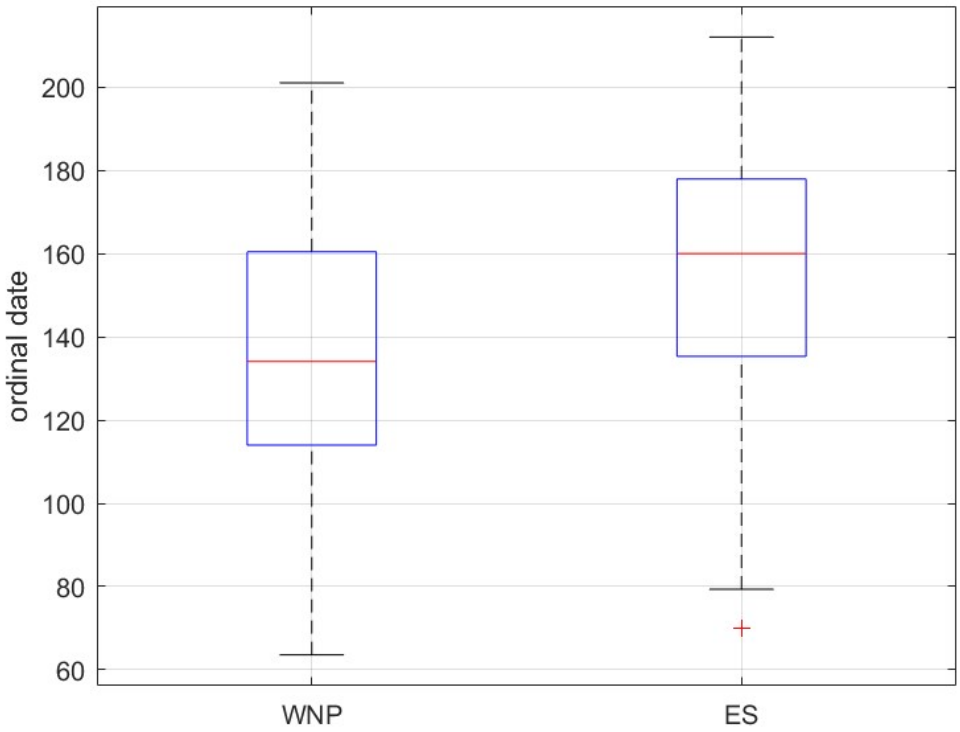

Figure 3. Box plots of start dates during 1980–2019 for the ES and WNP. Vertical axis is ordinal start dates. Red lines in center of boxes are median. Red cross in ES is outlier.

Table 1. Definition of early, normal, and late start date of storm season

Early	Normal	Late
For the WNP (Normal)		
date < 24 Apr	24 Apr =< date =< 28 May	date > 28 May
For the WNP (Empirical)		
date < 28 Apr	28 Apr =< date =< 24 May	date > 24 May
For the ES (Normal)		
date < 16 May	16 May =< date =< 18 June	date > 18 June
For the ES (Empirical)		
date < 20 May	20 May =< date =< 20 June	date > 20 June

3. Results and discussions

Figure 4 shows interannual variation of start dates for both WNP and ES. The correlation between two timeseries is 0.17. It implies that, although ES is a part of WNP, interannual variation of start date in ES is not completely dependent on that in WNP. In particular, in some years (e.g., 1982–1985, 1998, 1999, 2016), the start dates come early/late in WNP, they are also similar in ES. Inversely, start dates are not coincident in some other years (e.g., 1997, 2002, 2005, 2010, 2012, 2013, 2014, 2015). In fact, WNP is much larger than ES. If active storm area is in eastern part of WNP far away from ES and Philippines Sea, the start date in ES might not be related to that in WNP. Table 2 shows the start dates of both WNP and ES in relation to post–ENSO years. In WNP, in post–El Niño (post–La Niña) years, the start dates

tend to come later (earlier). The start dates are between June and July in post–El Niño years, while they stay around April and May in post–La Niña years. This trend also occurs in ES, but, it is not really clear as in WNP. The results for WNP, in this study, is consistent with the finding of Kim et al. (2017) [7]. Kim et al. (2017) documented that a strong El Niño in the previous winter can cause the late TC season in the coming year. It can be speculated that, ES is among interaction of monsoon systems, physical mechanism of TC formation can be more complicated and affect relationship of start date and ENSO. The results from this study suggest that it is feasible to use ENSO as a potential predictor to predict start date in WNP and ES. More studies need to be conducted to provide useful seasonal forecast.

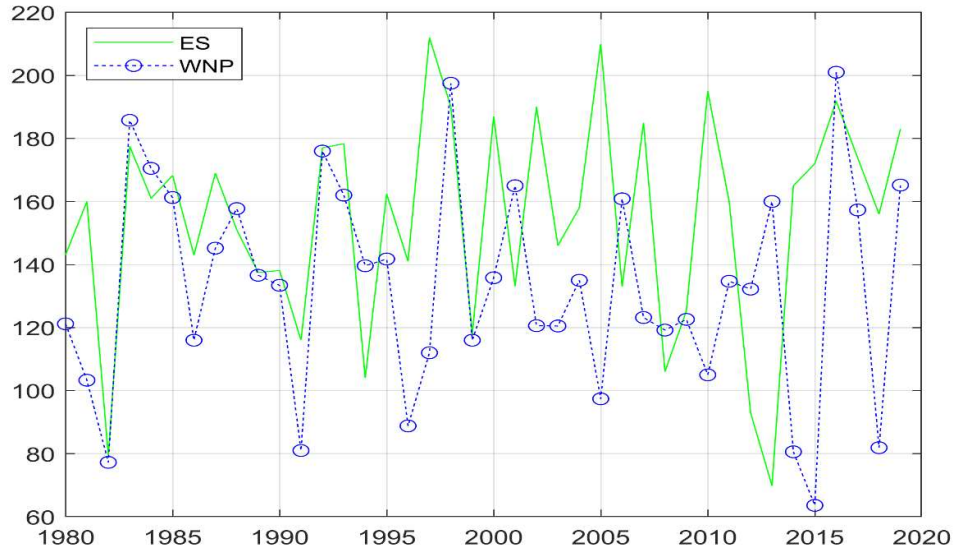

Figure 4. Interannual variation of start dates in WNP and ES during 1980–2019.

Table 2. The start date of the active TC season in post–ENSO years.

post–El Niño	**1983**	**1988**	**1998**	**2003**	**2016**
WNP	3–Jul	5–Jun	15–Jul	29–Apr	19–Jul
ES	25–Jun	3–May	8–Jul	25–May	9–Jul
post-La Niña	**1989**	**1999**	**2000**	**2008**	**2011**
WNP	15–May	25–Apr	14–May	28–Apr	13–May
ES	16–May	27–Apr	5–Jul	15–Apr	8–Jun

4. Conclusions

This paper examined inter–annual variation of start date in WNP and ES by using normal and empirical distributions. In WNP, the start dates built by normal and empirical distributions have the almost similar shapes. It suggests that it is feasible to apply normal distribution. Meanwhile, in ES, normal distribution is not really appropriate. Empirical should be used stead. The results found that, in WNP, if start date of a year comes among 24 April and 28 May (by normal distribution), it will be in normal class. In ES, normal class is identified as among 20 May and 20 June (empirical distribution). Thus, climatologically, active storm season seems to be later in ES than in WNP. In WNP, interannual variation of start date has relationship with ENSO (mentioned by Kim et al., 2017 [7]). However, it might

be not really clear in ES. The relationship between ENSO and start date in ES needs to be deepened in coming studies. The information from this paper can provide the useful way and criterion to identify start date of active storm season in WNP and ES for operational seasonal forecast.

Author Contributions: N.T.D. Huong supported to build draft of paper; T.H. Chinh; calculate and analyze data.

Acknowledgments: This paper is supported by the Ministry of Natural Resource and Environment through research project "Application of climate indices in seasonal forecast for Vietnam area" (code: TNMT.2020.05.01).

Conflicts of Interest: There is no conflicts.

References

1. Kim, H.K.; Seo, K.H. Cluster analysis of tropical cyclone tracks over the western North Pacific using a self-organizing map. *J. Clim.* **2016**, *29*, 3731–3751, doi.org/10.1175/JCLI-D-15-0380.1.
2. Dasallas, L.; Lee, S. Topographical Analysis of the 2013 Typhoon Haiyan Storm Surge Flooding by Combining the JMA Storm Surge Model and the FLO-2D Flood Inundation Model. *Water* **2019**, *11*, 144.
3. Lagmay, A.M.F.; Agaton, R.P.; Bahala, M.A.C.; Briones, J.B.L.T.; Cabacaba, K.M.C.; Caro, C.V.C.; Mungcal, M.T.F. Devastating storm surges of Typhoon Haiyan. *Int. J. Disaster risk reduct.* **2015**, *11*, 1-12.
4. Li, R.C.; Zhou, W. Modulation of western North Pacific tropical cyclone activity by the ISO. Part I: Genesis and intensity. *J. Clim.* **2013a**, *26*, 2904-2918.
5. Li, R. C.; Zhou, W. Modulation of western North Pacific tropical cyclone activity by the ISO. Part II: Tracks and landfalls. *J. Clim.* **2013b**, *26*, 2919-2930.
6. Kubota, H. ; Chan, J.C. Interdecadal variability of tropical cyclone landfall in the Philippines from 1902 to 2005. *Geophys. Res. Lett.* **2009**, *36*.
7. Kim, D.; Kim, H.S.; Park, D.S.R.; Park, M. S. Variation of the tropical cyclone season start in the Western North Pacific. *J. Clim.* **2017**, *30*, 3297-3302.
8. Zhao, H.; Wu, L.; Wang, C.; Klotzbach, P.J. Consistent late onset of the western North. Pacific tropical cyclone season following major El Niño events. *J. Meteor. Soc. Japan* **2019**, *97*, 673-688.
9. Wilks, D.S. *Statistical methods in the atmospheric sciences,* 3rd ed.; Academic press: Cambridge, Massachusetts, **2011**; Volume 100, ISBN: 9780123850225.

VIETNAM JOURNAL OF HYDROMETEOROLOGY

Research Article

Application of remote sensing techniques for analyzing operation of upstream reservoirs in transboundary river basins of Vietnam

Tran Anh Phuong[1*], Tran Manh Cuong[1], Nguyen Hoang Van[1], Pham Nhat Anh[1], Nguyen Anh Duc[1], Duong Hong Son[1]

[1] Water Resources Institute: phuongtran.monre@gmail.com; manhcuongkt11@gmail.com; vannh5nk@wru.vn; phamnhatanh2803@gmail.com; nganhduc@yahoo.com; dhson.monre@gmail.com.

***** Correspondence: phuongtran.monre@gmail.com; Tel.: +84961776683

Received: 12 June 2020; Accepted: 18 August 2020; Published: 25 August 2020

Abstract: Operation of upstream reservoirs in transboundary river basins strongly influences water resources in Vietnam**.** However, due to the lack of observation data, it is difficult to have sufficient information on their operation. In that context, remote sensing with a global coverage has a great potential to provide this information. This study estimated the time series of surface water area by processing Landsat images from the Google Earth Engine platform. Then, the area – volume – elevation relationship constructed from DEM was used to derived the water level and volume from the surface water area datasets. The results showed that remote sensing enables to monitor temporal variations of water level and volume of reservoirs. Remote sensing can also detect the wet and dry periods and determine the operation of reservoirs, which supports to improve inflow prediction to Vietnam, and therefore, improve the water resources management in the transboundary rivers.

Keywords: Transboundary river; Remote sensing; Reservoir operation; Water level.

1. Introduction

Water plays a crucial role for the sustainable development. In the context of population growth and climate change, water demand for domestic and socio–economic development will continue to increase in the foreseeable future while water resources tend to be exhausted [1]. This leads to aggressively serious disputes and conflicts over water resources amongst countries, especially in transboundary river basins [2]. Hence, ensuring water security for countries located at the downstream of transboundary rivers is a necessity.

Water resources in Vietnam are heavily influenced by the international waters. Approximately 61% of the total water in the territory of Vietnam comes from foreign countries. Six out of nine major rivers in Vietnam share the basins with other countries. In particular, the two largest rivers, the Mekong and Red River, have larger basin areas outside Vietnam's territory. The basin area of Mekong River in Vietnam's territory accounts for only 8.7% of the entire basin area. The annual flow in Vietnam's territory only contributes about 10% of the annual flow of the Mekong river basin. For the Red river, 50.7% of the basin area is located in China and Laos, while only 49.3% is in Vietnam. The total rainfall in the Red river basin in Vietnam only accounts for 57.8% of the total rainfall in the whole basin. The variation of water resources in Vietnam is, thus, strongly depends on changes in water resources originated from outside the country's boundary, influencing water security in Vietnam.

One of the most threats for water security of Vietnam is the construction of hydropower dams at the upstream of the Mekong and Red rivers. Located at the downstream, Vietnam has been largely influenced by the operation of these reservoirs. In order to reduce negative effects of these dams, water resources prediction and management in the Mekong and Red river basins are very important. However, the effectiveness of water resources prediction and management strongly depends on information about reservoir condition and operation. As a result, assessing conditions of water level and volume of reservoirs and determining their operation schedule in transboundary rivers are essential for better management and prediction of water resources.

Recently, remote sensing with its high spatial coverage has been widely used in hydrology and water resources [3]. Remote sensing not only helps in generating topography and land cover maps, and serving for hydrological parameter estimation but also provides important inputs such as data on precipitation, temperature, evaporation and soil moisture for flood and drought prediction. Particularly, application of remote sensing for water resources monitoring in transboundary rivers has attracted the attention of researchers over the world. For example, in Bangladesh, Biancamaria et al. [4] used Topex/Poseidon satellite altitude to measure water levels in India to increase forecasting time in the transboundary rivers located both in Bangladesh and India. Nishat and Rahman [5] used remote sensed images of topography, land cover and water level to calibrate and validate hydrodynamic model in Hang–Brahmaputra–Meghna (GBM) international river basin. Zhang et al. [6] used water surface areas estimated from MODIS satellite images and the elevation–water surface area relationship to monitor the storage variation of reservoirs in South Asia. In Vietnam, the project on "Supporting the cooperation program between the two governments of Vietnam and the Netherlands" on Water and Climate Services for Transboundary Water and Disaster Risk Management focuses on using geographic and remote sensing information systems to improve monitoring and modelling of transboundary water sources in the Da River basin. The National Remote Sensing Department (Ministry of Environment and Natural Resources) has implemented the project named "Monitoring water resources variation, water exploitation and water consumption in foreign territories of the Red and Mekong river basins", which assessed the exploitation and consumption of water resources in the upstream foreign parts of the Red and Mekong river basins as well as their impacts on flow regime in these rivers in Vietnam. However, so far there have been only few studies that use remote sensing for monitoring reservoirs in transboundary river basins. However, so far using remote sensing techniques to investigate the reservoir operation in the transboundary river basins has not been intensively studied.

The objective of this study is to explore the capability of remote sensing to investigate the temporal variations of reservoirs and analyze their operation schedule in the Mekong and Red rivers. To do that, we process the Landsat–8 data on the Google Earth Engine (GEE) platform to estimate the water surface area. After that, based on the area–elevation–volume relationship developed from the DEM topography map, we quantify the reservoir water level and volume. Finally, the temporal variations of water level and volume are analyzed to determine the reservoir operations. The reliability of this approach was proved by our previous study which compared the water level obtained by the Landsat images with the observed data at the Ka Nak reservoir in Kon–Ha Thanh River basin [7].

2. Methodology and data

2.1. Methodology

Figure 1 presents the approach that we used to analyze the spatiotemporal variations of reservoir water levels and volumes as well as explore their operation rules. As can be seen in

the figure, the input data for this approach is the Landsat images and topography of reservoirs. While the Landsat images were used to estimate the surface water areas of reservoirs, the topography data were used to construct the surface water area–water level–water volume relationship. The water level and water volume of each reservoir were obtained from the Landsat-derived water surface areas using the surface water area–water level–water volume relationship. Finally, we analyzed the spatiotemporal variations of the water surface area, water level and water volume of reservoirs and study the operation rules of these reservoirs. In order to perform this approach, we used two main tool including GEE platform and ArcGIS software, which are presented as below.

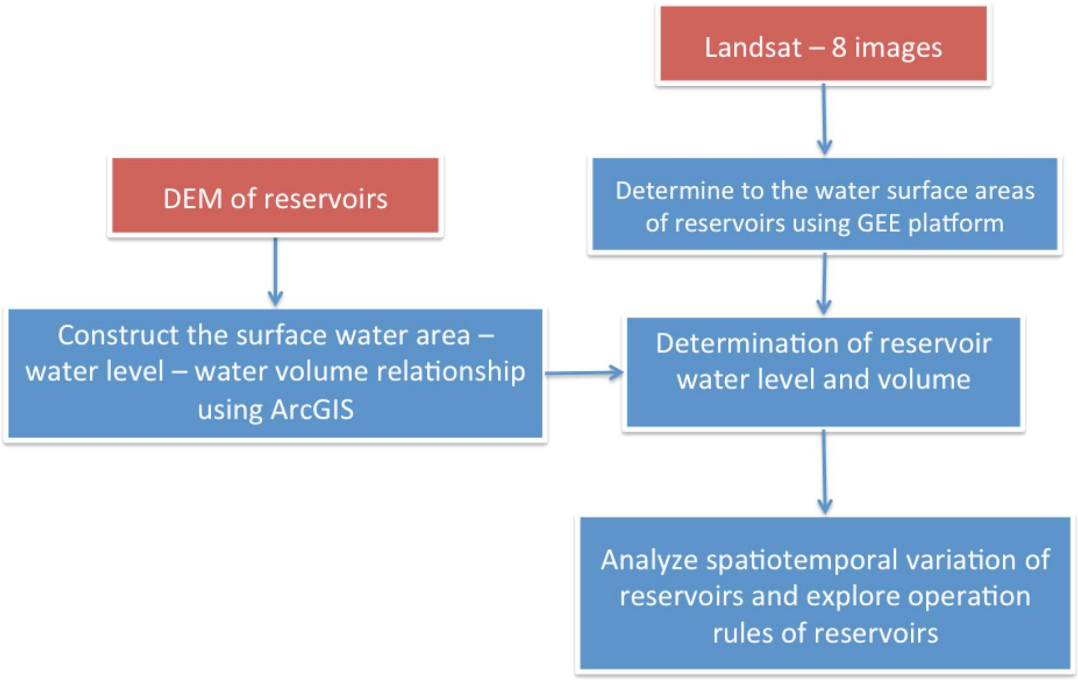

Figure 1. Flowchart that using remote sensing technique to investigate the spatiotemporal variation of reservoirs and their operation rules in the Mekong and Red river.

Google Earth Engine platform: This platform is developed by Google Inc. GEE combines satellite images and geospatial datasets with analyzing capabilities to allow users to detect changes, map trends, and quantify differences on the Earth's surface over a period of time (**Figure 2**). Cloud–based GEE platform can process a large data volumes with much shorter time and higher accuracy comparing to the conventional approach. Instead of downloading and processing each satellite image as in the conventional approach, GEE platform allows users to simultaneously process multiple images on Google's servers, which significantly saves computer resources and computation time. Another advantage of using this platform is that it permits to delineate the study area and perform spatio–temporal analysis on this area using build–in functions or user–developed scripts in JavaScript or Python.

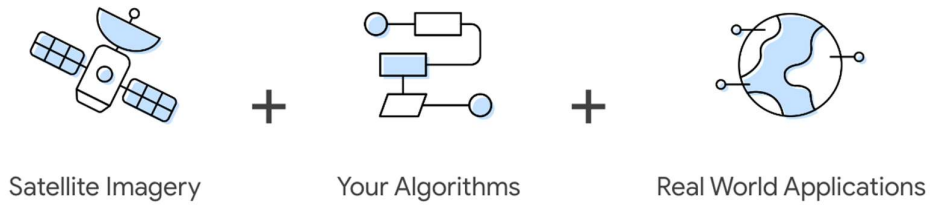

Figure 2. Structure of the GEE [8].

In this study, a JavaScript program was written to differentiate water object from other land surface objects (e.g., vegetation, bare soil) and extract it from the Landsat image using Normalized Difference Water Index (NDWI). In GEE, NDWI is calculated through "normalized Difference" function from image bands B3 (green) and B5 (NIR) as below:

$$NDWI = \frac{B3-B5}{B3+B5} \quad (1)$$

The *NDWI* is to highlight the reflectance ability of water in the green wavelength compared to the near–infrared NIR wavelength. Pixels with NDWI greater than zero representing water pixels on image.

The water surface area in each Landsat image were calculated as the total number of the water pixels multiplied by the image resolution, which is formulated by "ee.Image.pixel Area" function in the GEE. The above procedure was repeated for all Landsat images that meet the cloud cover requirement to obtain the time–series of surface water area for each reservoir.

ArcGIS: This software is a geographic information system (GIS) for working with maps and geographic data maintained by the Environmental Systems Research Institute (Esri). The software can be used for creating map and analyzing mapped information. It has been widely used for applications in natural resources and environment. In this study, ArcGIS was used to create the surface water area–water level–water volume relationship from topographic map DEM. To do that a region corresponding with maximum water level of a reservoir was specified. Then, using geographic calculation tools in ArcGIS, the water surface area–water level–water volume for each reservoir was constructed.

2.2. Landsat satellite data

The Landsat satellite system was launched into orbit in 1972. Until now, eight generations of Landsat have been launched. Each satellite is equipped with a MSS (multi–spectral scanner), a set of RBP television radios. In this study, we used observation data from Landsat–8 Operational Land Imager (OLI) and Thermal Infrared Sensor (TIRS). Landsat–8 was launched in 2013 and provides data with spatial resolution of 30m and temporal resolution of 16 days [9].

This study extracted and analyzed Landsat remote sensing images in order to study the variation of six hydropower reservoirs in the Chinese territory of the Mekong river including: Gongguoqiao Dam, Xiaowan Dam, Manwan Dam, Dachaoshan Dam, Nuozhadu Dam, Jinghong Dam and five other hydroelectric reservoirs on the Da River (in Red river system) including Yayangshan Dam, Shimenkan Dam, Longma Dam, Jufudu Dam, Gelantan (Figure 3). Study period is from January 1st, 2015 to February 29th, 2020. Landsat–8 images were collected from GEE's database. For removing the cloud impact, only images with a cloud cover lower than 10% were selected.

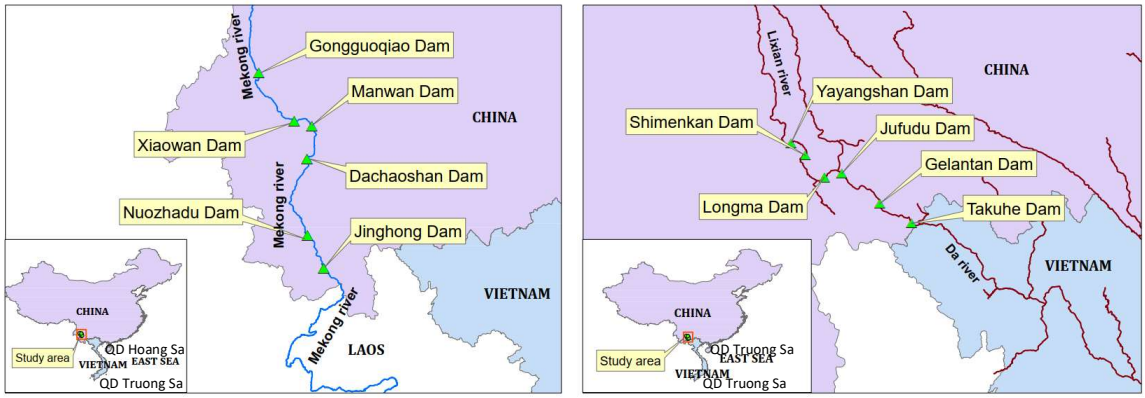

Figure 3. Locations of reservoirs on the Mekong (left) and Da River (right) in Chinese territory.

3. Results

3.1. Variations of reservoir water level and volume on the Mekong River

The variations of water level and volume of Xiaowan, Nouzhadou and Jinghong reservoirs during 2015–2020 period in the Chinese territory of the Mekong river basin from the upstream to downstream are shown in Figure 3–5. Xiaowan and Nouzhadou are the two largest reservoirs and Jinghong is the lowest reservoir in the cascade system of reservoirs in the Chinese territory. It can be seen that the Chinese reservoirs usually begin releasing water at the end of January and most of the reservoirs reach the lowest water level by the end of May. The sharp reduction of water level and volume of reservoirs from January to March indicates that the releasing flow is much larger than the inflow in this period.

From June to August, the reservoirs slowly store up water, which implied that the inflow to the reservoirs is slightly higher than outflow. From August to January, the reservoirs quickly fill up water. The reservoirs are full around the end of November to early January. It is worth noting that the water level of reservoirs in mid–February 2020 is lower than the water level at the same time of the other years, which indicates that the 2020 dry season is the driest in the 2015–2020 period. The similar trend was also found in the other reservoirs which are not shown here.

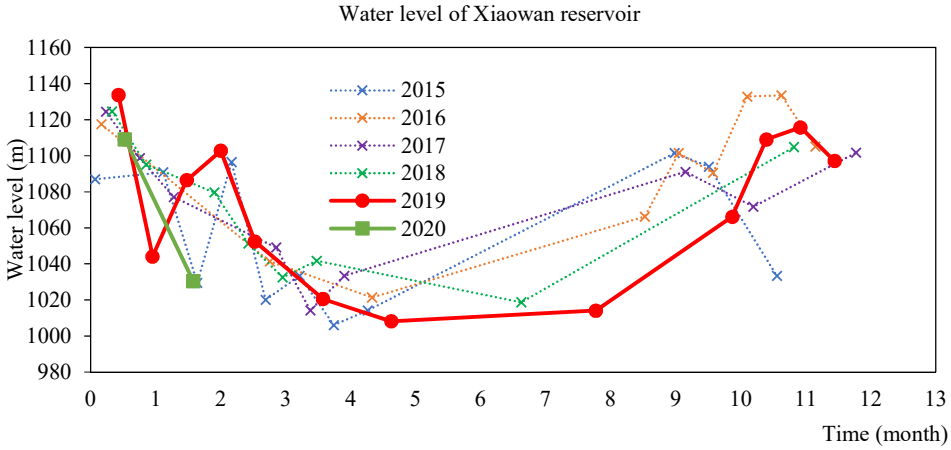

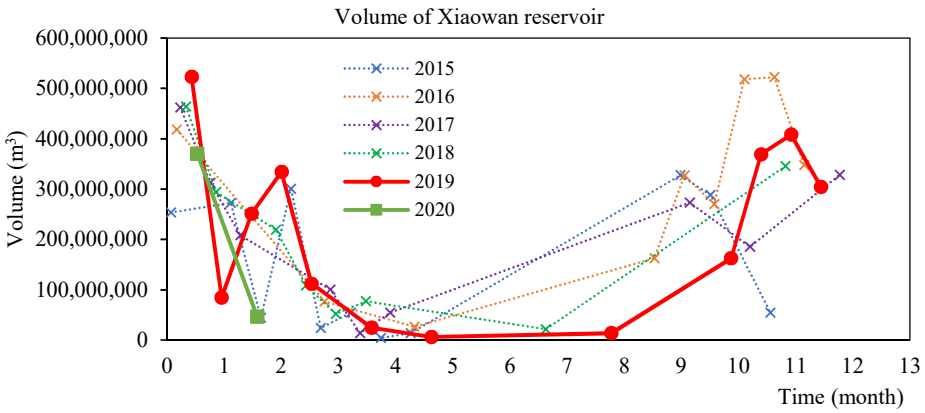

Figure 4. Changes in water volume and level of Xiaowan reservoir on Mekong river.

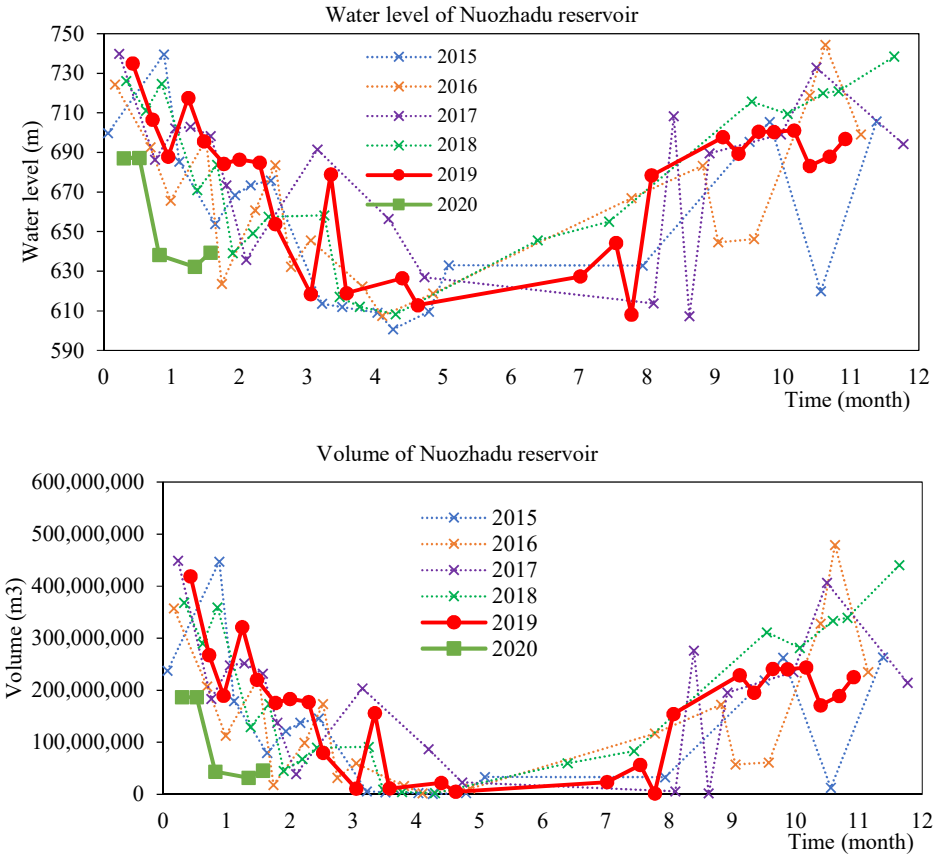

Figure 5. Changes in water volume and level of Nouzhadu reservoir on Mekong river.

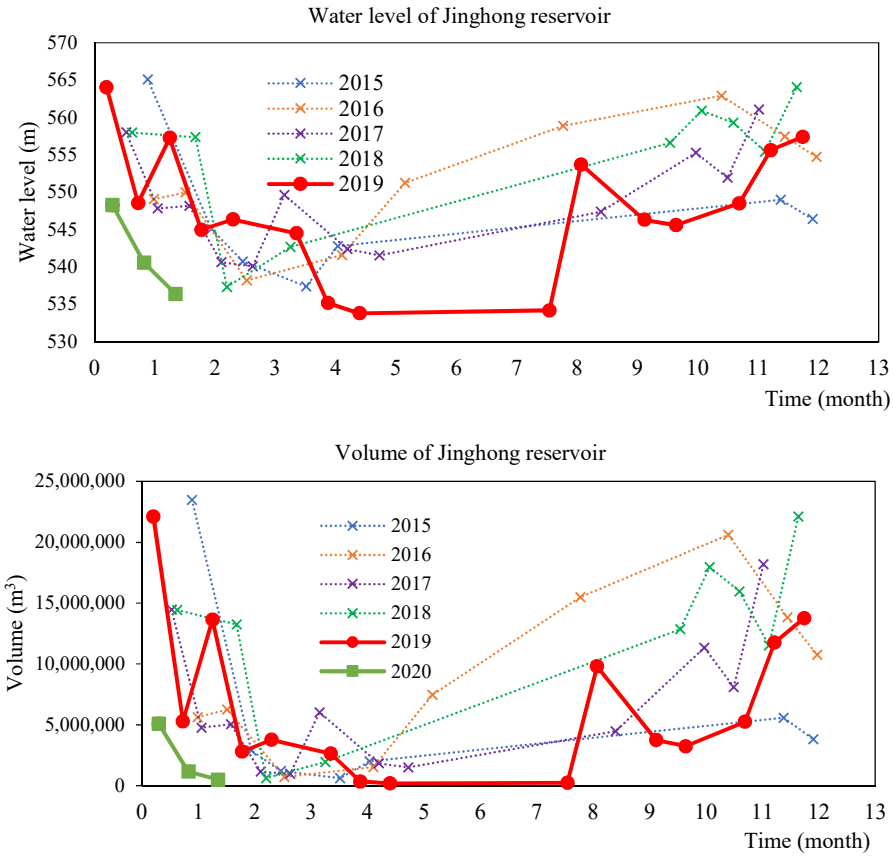

Figure 6. Changes in water volume and level of Jinghong reservoir on Mekong river.

3.2. Variations of reservoir water level and volume on the Red River

Due to the large reservoirs in the Red River basin outside the Vietnamese territory located on the Da river, the study concentrated on reservoirs in the Da river. Figures 6–8 present the variations of water level and volume of three reservoirs in the 2015–2020 period. From December, the outflow is larger than the inflow. By the end of March or early April, the reservoir volume reaches the lowest value of the year. From early May to mid–August, the reservoirs gradually fill up water. From mid–August to November, the reservoirs stores up water rapidly and the reservoirs usually reach the highest water level by November. This indicates that reservoirs in the Da river is one month earlier than those in the Mekong river.

It is worth noting that the water level of reservoirs in 2019 was quite different from the previous years due to the small amount of precipitation in the wet season. The reservoirs were not fully filled until the end of December. By the end of December, while reservoirs usually begin to release water in the other years, it is still on the progress of filling up in 2019. This leads to low amount of water released from these reservoirs to Vietnam in the dry season of 2019–2020.

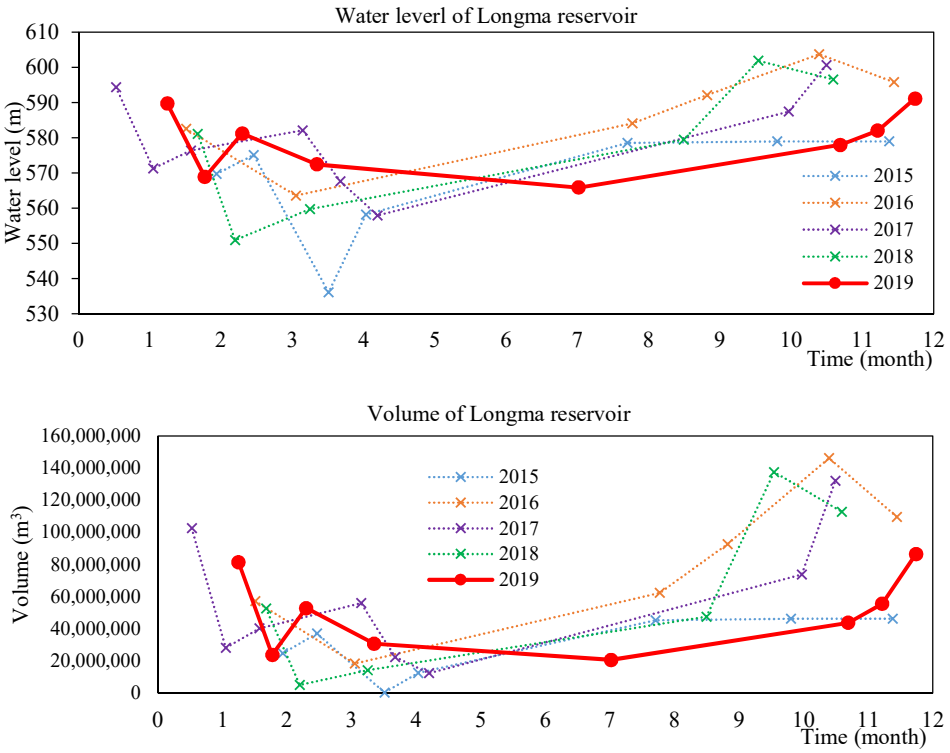

Figure 7. Changes in water level and volume of Longma reservoir on Da river.

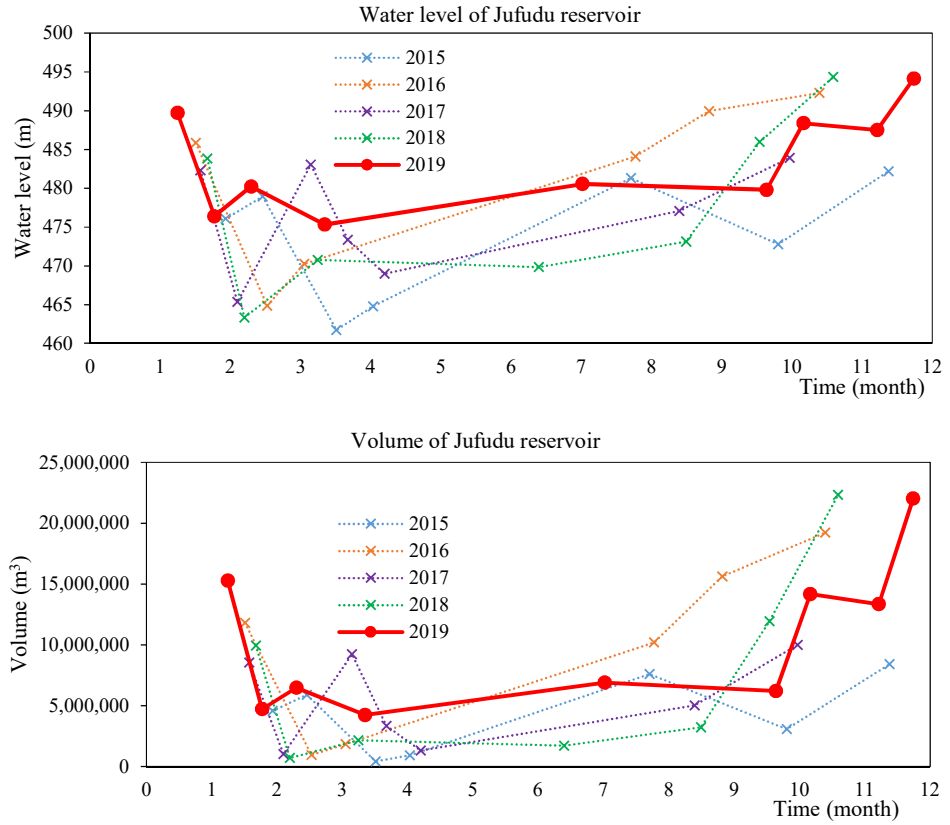

Figure 8. Changes in water level and volume of Jufudu reservoir on Da river.

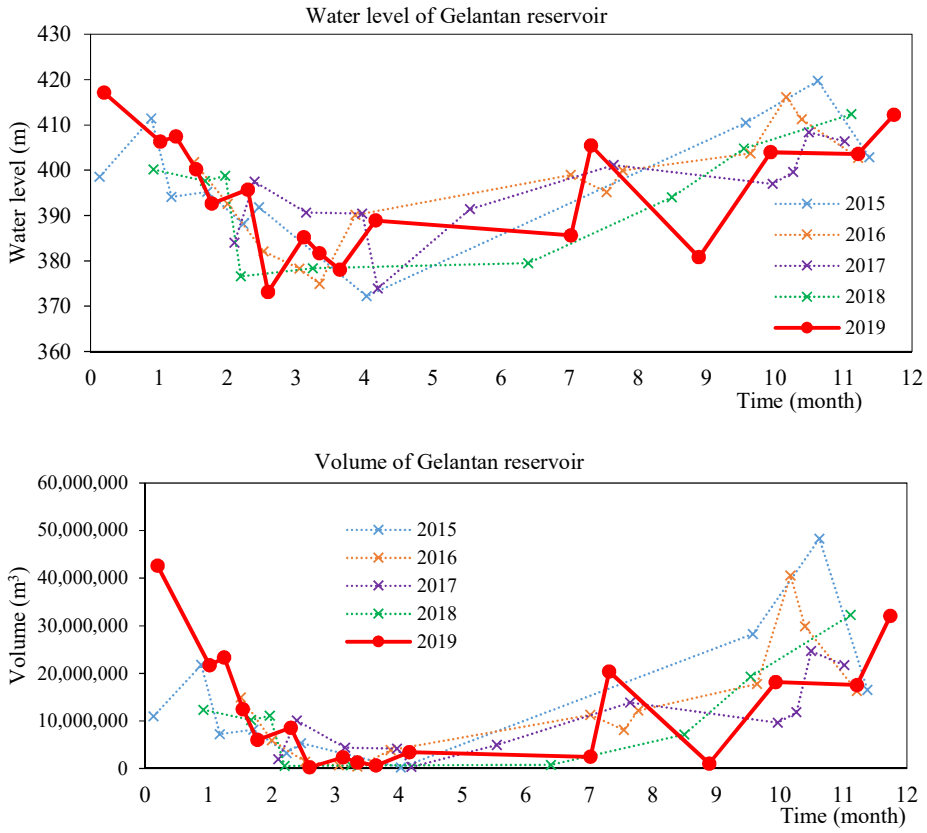

Figure 9. Changes in water level and volume of Gelantan reservoir on Da River.

4. Conclusion

One of the most challenging tasks for water resources forecasting and management in transboundary river basins is the shortage of observed data in foreign territories. This greatly reduces the accuracy of flow forecasting and limits the effectiveness of water resources management. While it is unfeasible to use conventional observation methods, remote sensing with its large coverage has a great potential to monitor water resources in foreign territories. However, so far there have been a few studies in Vietnam that evaluate the applicability of the remote sensing in water resources monitoring. This study focused on monitoring the temporal variations of water level and volume in the reservoirs in Mekong and Red river basins. While the GEE platform was used to quickly process a large amount of Landsat data to produce the time–series of water surface area, ArcGIS was employed to construct the water surface area–water level–water volume for each reservoir, which then was used to derive the time–series of water level and volume from the water surface area data. By combing the GEE platform and ArcGIS, we can observe the variations of water level and volume of reservoirs as well as analyze the reservoir operation schedules.

The water level and volume of reservoirs in the Mekong and Red rivers derived from the Landsat–8 data collected during the 2015–2020 period were analyzed. The results indicated that Landsat–8 can well monitor the temporal variations of reservoir water level and volume as well as reconstruct the operation schedules of reservoirs. The results also showed that the

reservoir water volume in the 2020 dry season is lower than the other years in the 2015–2020 period due to lack of rainfall in both wet and dry season. These findings are valuable information that can be used for the water resources forecasting and management in the Red and Mekong rivers. However, due to low spatial and temporal resolution of the Landsat data, the changes in water surface area below 30 m and shorter than 16 days cannot be detected. In the next study, the remote sensing datasets with higher spatio–temporal resolution will be used to better monitor the variations of reservoir water level and volume.

Author Contributions: Conceptualization, D.H.S., N.A.D. and T.A.P.; methodology, T.M.C., T.A.P.; data analysis, T.M.C., T.A.P.; data curation, T.M.C., T.A.P.; writing–original draft preparation, T.A.P., T.M.C.; writing–review and editing, T.A.P., P.N.A., N.H.V.; visualization, T.M.C.; supervision, N.A.D., D.H.S. All authors have read and agreed to the published version of the manuscript.

Acknowledgments: We thank our colleagues from the Water Resources Institute who provided insight and expertise that greatly assisted the research. We also thank reviewers for their insight comments and suggestions that significantly improved the quality of this paper.

Conflict of interest: The authors declare no conflict of interest.

References

1. Vörösmarty, C.J.; Green, P.; Salisbury, J.; & Lammers, R.B. Global water resources: vulnerability from climate change and population growth. *Sci.* **2000**, *289*, 284–288.
2. Munia, H.; Guillaume, J.H.A.; Mirumachi, N.; Porkka, M.; Wada, Y.; Kummu, M. Water stress in global transboundary river basins: significance of upstream water use on downstream stress. *Environ. Res. Lett.* **2016**, *11*, 1–12.
3. Kham, D.V. Research on remote sensing technology (RS) and geographic information system (GIS) in meteorology. Vietnam Institute of Meteorology, Hydrology and Climate Change, 2008.
4. Biancamaria, S.; Hossain, F.; Lettenmaier, D.P. Forecasting transboundary river water elevations from space. *Geophys. Res. Lett.* **2011**, *38*, 1–5.
5. Nishat, B.; Rahman, S.M. Water Resources Modeling of the Ganges–Brahmaputra–Meghna River Basins Using Satellite Remote Sensing Data. JAWRA *J. Am. Water Resour. Assoc.* **2009**, *45*, 1313–1327.
6. Zhang, S.; Gao, H.; Naz, B.S. Monitoring reservoir storage in South Asia from multisatellite remote sensing. *Water Resour. Res.* **2014**, *50*, 8927–8943.
7. Le, H.H.; Tran, A.P.; Pham, N.A.; Cao, H.H.; Thai, Q.N. Application of remote sensing to monitor water level fluctuations in Kanak reservoir in Vietnam. Proceeding of VACCI, **2019,** 132.
8. Gorelick, N.; Hancher, M.; Dixon, M.; Ilyushchenko, S.; Thau, D.; Moore, R. Google Earth Engine: Planetary–scale geospatial analysis for everyone. *Remote Sens. Environ.* **2017**, *202*, 18–27.

9. Roy, D.P.; Wulder, M.A.; Loveland, T.R.; Woodcock, C.E.; Allen, R.G.; Anderson, M.C.; Helder, D.; Irons, J.R.; Johnson, D.M.; Kennedy, R.; Scambos, T.A. Landsat–8: Science and product vision for terrestrial global change research. *Remote Sens. Environ.* **2014**, *145*, 154–172.